The Development and Application of Novel Drug Delivery System Targeting Human Dectin-1 with SPG/DNA Complexes

Author

2021DAB001　Kazuki Sumiya

(March 2024)

Under the supervision of

Prof. Kazuo Sakurai

Table of Contents

Chapter1. General Introduction

1-1 Importance of Pharmaceuticals

As we enter an era of 100-year life spans, the critical role of pharmaceuticals has become more important today than ever before. In modern society, pharmaceuticals are indispensable for both the prevention and treatment of disease and play an essential role in supporting people's health and long-term longevity. In addition, the pharmaceutical sector is actively engaged in the development of new drugs, expanding treatment options and making the fight against disease more efficient.[2, 3]

In the pharmaceutical field, progress is increasingly taking place in the discovery of new therapeutics and new uses for existing drugs. These advances have contributed to enhancing the success rate of treatments and reducing the risk of side effects. In addition, it has been reported that advances in modern research methods and technologies have facilitated the sharing of information and collaboration among researchers, accelerating the drug development process.[4]

These developments have allowed new drugs and therapies to quickly reach the market and play a vital role in achieving health and longevity in the age of 100 years of life. Pharmaceuticals are an important pillar of health maintenance and disease treatment in today's society, and their evolution and innovation are essential to shaping for our future.[5]

1-2. Drugs under development

The development of small molecule drugs confronts many challenges, including the chemical structural intricacy, limited efficacy and side effects, efficiency of the development process, and the ever-changing needs of the market and patients. As the chemical structures of these compounds become increasingly intricate, they tend to be more difficult to synthesize, analyze, and optimize, requiring new synthetic methods and analytical techniques. This trend also leads to increased time and cost in the development process.[6]

Furthermore, most small molecule drugs show only limited efficacy in the treatment of their target diseases and often cause unwanted side effects due to their nonspecific mechanism of action. This phenomenon is particularly noticeable in complex diseases such as chronic diseases and cancer. In addition, the overuse of small molecule drugs exacerbates the problem of resistance to agents, making the development of new drugs more difficult and posing a serious threat to public health.[6]

The drug discovery process is characterized by high costs, long trial durations, and low response rates, all of which contribute to the failure of many candidate compounds at the clinical trial stage.[7] Moreover, the pharmaceutical market and patient needs are always changing, especially the demand for personalized medicine and treatments that address the root causes of disease. Therefore,

small molecule drugs alone are unlikely to be able to keep pace with these changes.[7]

These are important issues in the development of small molecule drugs, and their solution requires the introduction of new approaches and technologies. Research designed to overcome the limitations of small molecule drugs and to develop more effective and secure therapies is expected to play an increasingly valuable role in modern medicine.

1-3. Nucleic Acid Drugs

Nucleic acid drugs, including DNA and RNA therapeutics, have the potential to fundamentally change the treatment of genetic diseases, infectious diseases, and cancer. However, they are fraught with challenges in stability and delivery, typically reaching target cells in an active state at less than 1% of the injection dose. This low efficiency is due to obstacles such as enzymatic degradation and activation of unexpected biological responses such as activation of the immune system.[8,9]

Drug delivery system (DDS) technologies are emerging to enhance the stability and targetability of nucleic acid drugs, which play an important role in the commercialization of nucleic acid drugs because they provide several advantages to the system, including protection against degradation by biological enzymes, improved cellular uptake, and better intracellular transport

and localization.[8,9] Among the many materials available, nanomaterials are particularly promising for nucleic acid delivery because their properties enable them to be designed to overcome these disadvantages.[10]

Various DDS technologies are being investigated to improve the delivery of nucleic acid drugs to target tissues or cells. These include lipid nanoparticles such as liposomes, polymeric micelles and lipoplexes, and even inorganic materials. These systems are designed to overcome the challenge of inhibiting degradation of nucleic acid drugs, which is critical to achieving the desired therapeutic effect. [1,9] (Figure 1-1)

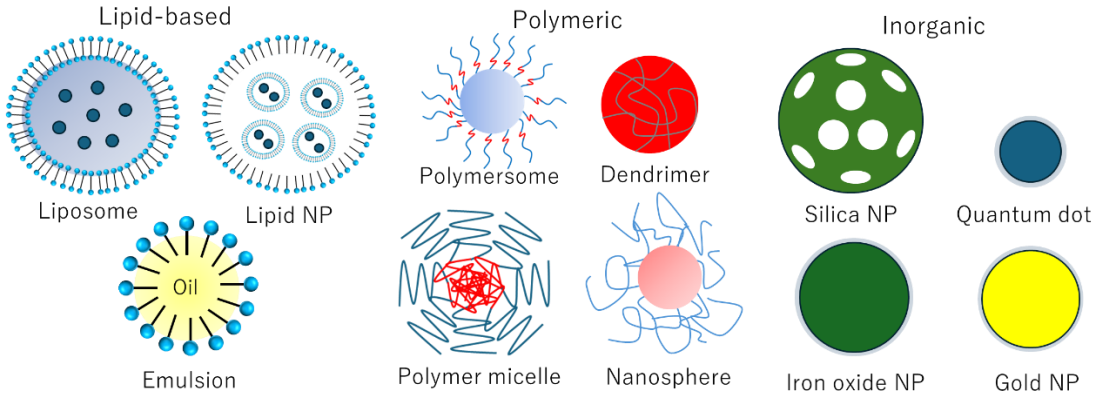

Figure 1-1. The representative nanoparticles used in DDS technology.[1]

However, challenges remain in the areas of immune response control, toxicity, and specific delivery to target cells. These are significant barriers that must be addressed to fully realize the therapeutic potential of nucleic acid drugs.[10]

1-4. Regarding our technology and its targets

It is known that β-1,3-glucan, a type of polysaccharide, has a triple-helix structure in neutral aqueous solutions and becomes a single chain in alkaline solutions.[11-13] According to previous studies, the single chain can revert to the triple helix by changing the solvent from alkaline to neutral, and around 2000 we showed that in the presence of certain single-chain homopolypolynucleotides, such as poly(dA) (or dA_X, where X represents the base number) and poly(C), as shown in Figure 2, β-1,3 -glucan to form quantitative complexes.[14] This complexation phenomenon is due to a combination of hydrogen bonding and hydrophobic interactions between glucose and dA bases.[15]

Our research group has been using this complex to specifically deliver nucleic acid drugs. Our methodology involves binding dA_X to a therapeutic hetero-oligonucleotide sequence and forming a complex between the resulting dA_X hetero sequence and β-1,3-glucan. We primarily use schizophyllan (SPG, a type of β-1,3-glucan) with three main chain glucoses and one side chain glucose, as shown in Figure 1-2.[15] This complex is henceforth referred to as the SPG complex; the SPG complex makes the therapeutic oligonucleotide more resistant to hydrolysis by deoxyribonuclease. When dA_X thioate phosphate (s-dA_X) is used instead of the natural form of dA_X phosphate diester, the resulting s- dA_X /SPG complex is more stable than the dA_X /SPG complex.[16]

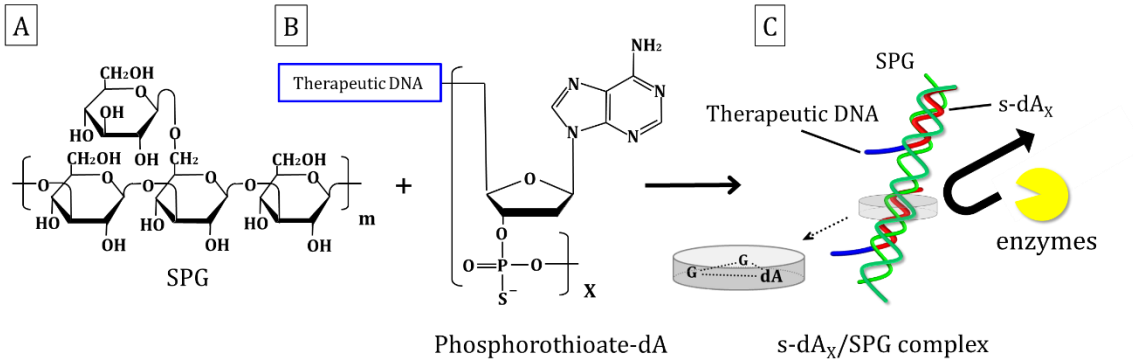

Figure 1-2. A novel complex formed from β-1,3-glucan schizophyllan (SPG) and a single chain of DNA (A) Repeating unit of SPG, (B) phosphorothioate poly(deoxyadenylic acid)(dA_X), and (C) a complex made from SPG and dA_X. The stoichiometric structure made from two main-chain glucoses and one dA

Dendritic cell-associated C-type lectin-1 (Dectin-1) binds to β-1,3-glucan, a major cell wall component of fungi and bacteria.[17] We hypothesized that the complex would be recognized by Dectin-1 because the complex is composed of β-1,3-glucan. After various investigations, we found that the SPG complex is recognized by Dectin-1 and taken up by the cell, resulting in the delivery of the therapeutic oligonucleotide into the cell. Interestingly, the binding constant between the s-dA_X/SPG complex and dectin-1 is about 6 times higher than that of the dA_X/SPG complex.[18] In a previous study, we demonstrated that the SPG complex can deliver antisense oligonucleotides (AS-ODNs) silencing Y-box binding protein 1 (YB-1)[19] and small interfering RNA (siRNA) silencing CD40 to cells expressing dectin-1 and suppress protein expression.[20] The SPG complexes are also used for immunological applications. In addition, SPG complexes can be used to deliver immunostimulatory CpG-ODNs and peptides

to induce antigen-specific immune responses and exert superior antitumor effects.[21]

1-5. Purpose and Structure of this Paper

Previous studies have shown that SPG complex-based drug delivery systems (DDS) are highly targeted and thereby highly pharmacologically effective. [18 21 20] However, these studies have been conducted primarily in mice. To advance the development of new drugs using the complex, it is important to clarify whether the same high targetability can be achieved in human cells as well as in mice. Therefore, in each chapter of this study, we examine the issues of polysaccharide-nucleic acid complexes and consider the establishment of DDS techniques for new and effective human applications.

Structural analysis in solution is important in drug development. The structure of polymers is directly related to their physical properties and provides clues for predicting and controlling solubility, viscosity, and in vivo kinetics. The in vivo efficacy of a drug depends on its interaction with biomolecules, and structural analysis is necessary to elucidate this. The stability of macromolecular drugs, the design of delivery systems, distribution and metabolism in the body, and the prediction of solution properties in the manufacturing process are also influenced by the structure in solution. For these reasons, structural analysis in solution is essential to support effective

and safe drug development. Therefore, Chapter 2 focuses on the structure of polysaccharide-nucleic acid complexes in solution.

In Chapter 3, we focused on affinity differences among variants of human Dectin-1 to identify the variants targeted by specific complexes. This suggests that the complexes may be tied to specific variants, which may lead to more effective therapeutic effects.

In Chapter 4, we examined how these complexes function in human-derived cells. Based on the results of our studies in mouse cells, we gained a better understanding of the efficiency and mechanisms of nucleic acid drug delivery to human cells. This brings us one step closer to developing an effective delivery method for nucleic acid drugs that transcends interspecies differences.

Chapter 5 summarizes this thesis.

1-6 Reference

1. Mitchell, M. J.; Billingsley, M. M.; Haley, R. M.; Wechsler, M. E.; Peppas, N. A.; Langer, R., Engineering precision nanoparticles for drug delivery. *Nat Rev Drug Discov* **2021,** *20* (2), 101-124.

2. Burke, H., Why are pharmaceutical companies so important? https://www.proclinical.com/blogs/2020-8/why-are-pharmaceutical-companies-important

3. Family, human body, religion, and care for longevity society. https://www.titech.ac.jp/english/public-relations/outreach/stories/dlab-future-techscapers02.

4. Kiriiri, G. K.; Njogu, P. M.; Mwangi, A. N., Exploring different approaches to improve the success of drug discovery and development projects: a review. *Future Journal of Pharmaceutical Sciences* **2020,** *6* (1), 27.

5. Medicines in Development. https://phrma.org/Scientific-Innovation/In-The-Pipeline/Medicines-in-Development.

6. Zhong, L.; Li, Y.; Xiong, L.; Wang, W.; Wu, M.; Yuan, T.; Yang, W.; Tian, C.; Miao, Z.; Wang, T.; Yang, S., Small molecules in targeted cancer therapy: advances, challenges, and future perspectives. *Signal Transduction and Targeted Therapy* **2021,** *6* (1), 201.

7. Grant, H., Challenges in Drug Discovery and Development. https://techbullion.com/challenges-in-drug-discovery-and-development/

8. Jiang, X.; Wang, N.; Liu, C.; Zhuo, Y.; Liang, L.; Gan, Y.; Yu, M., Oral delivery of nucleic acid therapeutics: Challenges, strategies, and opportunities. *Drug Discov Today* **2023,** *28* (4), 103507.

9. Lu, Z. R.; Shi, G. H., Nucleic Acid Delivery. *Pharm Res* **2023,** *40* (1), 1-2.

10. Mendes, B. B.; Conniot, J.; Avital, A.; Yao, D.; Jiang, X.; Zhou, X.; Sharf-Pauker, N.; Xiao, Y.; Adir, O.; Liang, H.; Shi, J.; Schroeder, A.; Conde, J., Nanodelivery of nucleic acids. *Nat Rev Methods Primers* **2022,** *2*.

11. McIntire, T. M.; Brant, D. A., Observations of the (1→3)-β-d-Glucan Linear Triple Helix to Macrocycle Interconversion Using Noncontact Atomic Force Microscopy. *Journal of the American Chemical Society* **1998,** *120* (28), 6909-6919.

12. Stokke, B. T.; Elgsaeter, A.; Brant, D. A.; Kuge, T.; Kitamura, S., Macromolecular cyclization of (1 → 6)-branched-(1 → 3)-β-D-glucans observed after denaturation–renaturation of the triple-helical structure. *Biopolymers* **1993,** *33* (1), 193-198.

13. Sato, T.; Sakurai, K.; Norisuye, T.; Fujita, H., Collapse of Randomly Coiled Schizophyllan in Mixtures of Water and Dimethylsulfoxide. *Polymer Journal* **1983,** *15* (1), 87-96.

14. Sakurai, K.; Shinkai, S., Molecular Recognition of Adenine, Cytosine, and Uracil in a Single-Stranded RNA by a Natural Polysaccharide: Schizophyllan. *Journal of the American Chemical Society* **2000,** *122* (18), 4520-4521.

15. Sakurai, K.; Mizu, M.; Shinkai, S., Polysaccharide--polynucleotide complexes. 2. Complementary polynucleotide mimic behavior of the natural polysaccharide schizophyllan in the macromolecular complex with single-stranded RNA and DNA. *Biomacromolecules* **2001,** *2* (3), 641-50.

16. Mochizuki, S.; Sakurai, K., β-1,3-Glucan/antisense oligonucleotide complex stabilized with phosphorothioation and its gene suppression. *Bioorg Chem* **2010,** *38* (6), 260-4.

17. Brown, G. D.; Gordon, S., A new receptor for β-glucans. *Nature* **2001,** *413* (6851), 36-37.

18. Mochizuki, S.; Morishita, H.; Kobiyama, K.; Aoshi, T.; Ishii, K. J.; Sakurai, K., Immunization with antigenic peptides complexed with β-glucan induces potent cytotoxic T-lymphocyte activity in combination with CpG-ODNs. *J Control Release* **2015,** *220* (Pt A), 495-502.

19. Izumi, H.; Nagao, S.; Mochizuki, S.; Fujiwara, N.; Sakurai, K.; Morimoto, Y., Optimal sequence of antisense DNA to silence YB-1 in lung cancer by use of a novel polysaccharide drug delivery system. *Int J Oncol* **2016,** *48* (6), 2472-8.

20. Zhang, Q.; Ichimaru, N.; Higuchi, S.; Cai, S.; Hou, J.; Fujino, M.; Nonomura, N.; Kobayashi, M.; Ando, H.; Uno, A.; Sakurai, K.; Mochizuki, S.; Adachi, Y.; Ohno, N.; Zou, H.; Xu, J.; Li, X. K.; Takahara, S., Permanent acceptance of mouse cardiac allografts with CD40 siRNA to induce regulatory myeloid cells by use of a novel polysaccharide siRNA delivery system. *Gene Ther* **2015,** *22* (3), 217-26.

21. Kobiyama, K.; Aoshi, T.; Narita, H.; Kuroda, E.; Hayashi, M.; Tetsutani, K.; Koyama, S.; Mochizuki, S.; Sakurai, K.; Katakai, Y.; Yasutomi, Y.; Saijo, S.; Iwakura, Y.; Akira, S.; Coban, C.; Ishii, K. J., Nonagonistic Dectin-1 ligand transforms CpG into a multitask nanoparticulate TLR9 agonist. *Proc Natl Acad Sci U S A* **2014,** *111* (8), 3086-3091.

CHAPTER 2. structural analysis of SPG/DNA complexes in solution

2-1. Purpose of this chapter

The key role of research in DDS technology is because the structure of nanoparticles (specifically, their shape and size) profoundly affects how drugs are distributed in the body and how they behave within cells. Evidence gathered to date indicates that these physical properties of nanoparticles greatly influence the efficiency and effectiveness of DDS. Therefore, in order to optimize the pharmacological effects of polysaccharide-nucleic acid complexes and to realize their full potential, it is essential to understand the exact structure of these complexes.

To achieve this goal, this chapter adopts a two-step approach. First, a detailed structural analysis of schizophyllan, the major component that builds these complexes, is performed. Because the unique chemical structure of schizophyllan greatly influences the physical properties of the overall complex, a deep understanding of its properties is essential for predicting the behavior of the overall complex. This information is then used to unravel the structure of SPG/DNA complexes in solution. This allows us to understand exactly how the complex will function in vivo and what physical form it will take. Through these steps, we aim to ultimately develop effective DDS using SPG/DNA complexes.

2-2 Experimental Section

2-2-1 Materials

Three low-molecular-weight tSPG samples (denoted as S-1m, S-2k, and S-3n) were kindly provided by Mitsui Sugar Co., Ltd (Tokyo, Japan) or Prof Seiji Shinkai (Kyushu University) and were employed along with a previously used sample (L-1). They were prepared as follows: After isolating "native SPG" with an ultra-high molecular weight (>10^{6-7}) from the culture filtrate of *Schizophyllum commune* Fries,[1] the native SPG was treated with ultrasonic irradiation and/or shear stress to reduce the molecular weight.[1, 2] The obtained samples were dissolved in distilled water and re-precipitated into acetone or methanol. After repeating this treatment several times, the sample purity was determined by using elemental analysis and ^{13}C NMR.[3] The molecular weights of tSPG were estimated by measuring the intrinsic viscosity in water and determined to be almost the same, in the range of 5-6 $\times$ 10^5, although there was a difference in the number of times or the extent (shear rate itself, concentration, or temperature) in applying shear stress and sonication. For these samples, we measured the weight-averaged molecular weight (M_w) in 0.01 N (tSPG) and 0.25 N (sSPG) NaOH as well as in DMSO (sSPG). Phosphorothioate dA_{30}, dA_{40}, and dA_{60} were synthesized at FASMAC Co., Ltd. (Kanagawa, Japan) and the molar masses (M) of these samples were 9850 (dA_{30}), 13100 (dA_{40}), 19700 (dA_{60}). Hereinafter, dA_X stands for phosphorothioate deoxyadenylic acid oligomer.

2-2-2 ^{13}C quantitative NMR.

SPG was dissolved in dimethyl sulfoxide-d_6 at a concentration of 50 mg/mL and the solution was enclosed in an NMR quartz cell. Quantitative ^{13}C NMR spectra were recorded using an inverse-gated ^{1}H decoupling method with a 13C flip angle of 30°, a repetition time of 30 s, and a scan number of 30 at 500 MHz by using JNM-ECP500 (JEOL).[4]

2-2-3 Circular dichroism

Circular dichroism (CD) in the wavelength range of 240–320 nm was measured on a Jasco J820 with a 1.0 cm quartz cell equipped with a water-jacket. From the temperature dependence of CD data upon heating, we determined the dissociation temperature (T_m) for the complex. The DNA concentration was 0.1 mg/mL.

2-2-4 Complexation and definition of the molar ratio of $[\mathbf{mG}]/[\mathbf{dA}]$

The typical procedure for the complex formulation is as follows. A fixed amount of SPG was dissolved in 0.25 N NaOH aqueous solution for about 1 h to obtain an sSPG solution. An appropriate amount of sSPG/NaOH solution, dA_X in water, and a phosphate buffer solution (330 mM NaH_2PO_4, pH 4.7) were mixed together. After mixing, the pH was controlled to around 7 and the solutions were stored at 4 °C overnight. The final mixture contained the complex (denoted dA_X-SPG) as well as unreacted or naked dA and SPG, depending on the feeding composition.

In the complex, two main-chain glucoses bind to one dA, as presented in Figure 1-2. We prepared several solutions with various mixing compositions including this stoichiometry of 2:1. We express the dA_X and sSPG mixing ratio in two different ways. One is the repeating unit mixing molar ratio defined by $([\mathrm{mG}]/[\mathrm{dA}])_{\mathrm{mix}}$, where $[\mathrm{mG}]$ and $[\mathrm{dA}]$ are the molar concentrations of the main-chain glucose and of dA, respectively. The other is the weight ratio of sSPG to dA_X. For example, when we used an sSPG with $M = 10^5$ and dA_{60} with $M = 19700$, the mixing weight ratio at $[\mathrm{mG}]/[\mathrm{dA}] = 2.0$ (at the stoichiometry) would be SPG:dA=0.56:0.43. Note that the resultant complex does not always form the stoichiometric complex. It has been observed that the complex normally contains more SPG than expected from the stoichiometry. In other words, the real $[\mathrm{mG}]/[\mathrm{dA}]$ of the complex would be larger than 2.0 even when we mix SPG and dA_X at $([\mathrm{mG}]/[\mathrm{dA}])_{\mathrm{mix}} = 2.0$.

2-2-5 Gel permeation chromatography coupled with multi-angle light scattering

Fractionation of tSPG, sSPG, and dA_X/SPG was carried out using a Prominence 501 system coupled with Dawn-Heleos-A (Wyatt). A total of 100 μL of solution with concentrations ranging from 1.0 to 3.3 mg/mL was injected into a system consisting of a Shodex HPLC pump (DU-H2130) equipped with a Shodex degassing unit (ERC-3125S). The chromatogram was obtained with an RI-501 interferometric differential refractive-index (RI) detector (Shodex) and a UV absorbance detector (SPD-20A; Shimadzu). These detectors were connected in tandem, with the refractometer located at the end because of back-pressure;

RI detectors cannot withstand pressure > 100 psi. For tSPG, the tandem-connected columns of SB-806MHQ and LB-803 in this order from upstream were used. The mobile phase was a 50 mM phosphate buffer containing 0.5 M KCl (pH 7.4) and ethylenediaminetetraacetic acid (EDTA) and the flow rate was 0.6 mL/min. For sSPG, we used two set-ups: One included the same columns and the same mobile phase with tSPG, but we injected 100 μL of sSPG in 0.25N NaOH into the mobile phase, assuming that the renaturation toward tSPG would take place immediately after 0.25 NaOH was neutralized by diluting with the mobile phase and that the renaturation might occur only intramolecularly due to the dilute condition. The other set-up used DMSO/LiCl as a mobile phase and a KD-806M column.[5] For dA_X-SPG, the columns were tandemly connecting GF7M and GF510 and the mobile phase was 50 mM phosphate buffer containing 0.5 M KCl and EDTA. Here, EDTA was added to avoid unfavorable adsorption of phosphorothioate DNA by the GPC columns.

The excess Rayleigh ratio, $R_\theta(c)$, was measured as a function of the scattering angle (θ) in the range of 14°–163° by using a Dawn-Heleos-A (Wyatt). The incident light with a wavelength of 633 nm in a vacuum was created by a HeNe laser source and the detectors were calibrated with toluene. Data acquisition and manipulation were performed using Wyatt's ASTRA for Windows software (V. 7.3.2.19). The angular dependence of $R_\theta(c)$ was analyzed by using Eq 1 to determine the z-averaged radius of gyration [$\langle S^2 \rangle_z^{1/2}$] and the weight-averaged molecular mass (M_w), where scattering angle θ is related to the magnitude of the scattering vector q through $q = 4\pi/\lambda \sin(\theta/2)$.

$$\frac{Kc}{R_\theta(c)} = \frac{1}{M_w}\left[1 + \frac{1}{3}q^2\langle S^2\rangle_z + 0(q^4)\right] \quad (1)$$

Here, c and K are the mass concentration and the optical constant, respectively, and K is given by $(4\pi^2 n^2)/(N_A\,\lambda_0^4)(\partial n/\partial c)^2$ with the refractive index of the solvent n, the wave length of the incident light in a vacuum λ_0, and Avogadro's number N_A, and $(\partial n/\partial c)$ is the specific refractive index increment of the solute. Because of the very dilute conditions, we can assume that there is no concentration dependence in $Kc/R_\theta(c)$. $(\partial n/\partial c)$ was calculated from the following relation:

$$\left(\frac{\partial n}{\partial c}\right)_{\mathrm{co}} = w_{\mathrm{SPG}}\left(\frac{\partial n}{\partial c}\right)_{\mathrm{SPG}} + (1 - w_{\mathrm{SPG}})\left(\frac{\partial n}{\partial c}\right)_{\mathrm{dA}} \quad (2)$$

where w_{SPG} is the weight fraction of SPG and $(\partial n\,/\,\partial c)_{\mathrm{dA}} = 0.164$ and $(\partial n/\partial c)_{\mathrm{SPG}} = 0.142$ cm^3 g^{-1} was used.

In our chromatography, we measured UV absorbance (Abs) at 260 nm and the refractive index (RI) at 633 nm as a function of the elution time (t). Only dA_X absorbs this UV light and RI is related to the concentration of dA_X-SPG. Therefore, at each fraction, we may evaluate $[\mathrm{mG}]/[\mathrm{dA}]$ as a function of the elution time (t).

$$\left(\frac{[\mathrm{mG}]}{[\mathrm{dA}]}\right)_f(t) = \left[\frac{3}{M_{\mathrm{SPG}}}\left(\frac{\mathrm{RI}(t)}{\left(\frac{\partial n}{\partial c}\right)_{\mathrm{co}}} - \frac{Abs(t)}{\varepsilon_w}\right)\right] \div \left(X\,\frac{Abs(t)}{\varepsilon_m}\right) \quad (3)$$

Here ε_m and ε_w are the molar and weight-metric extinction absorption coefficients of complexed phosphorothioate dA_X, respectively, which are known to be 3.01×10^5 $\ell mol^{-1}cm^{-1}$ and 2.30×10^4 $m\ell g^{-1}cm^{-1}$, respectively. M_{SPG} is the molar mass of the SPG repeating unit (666.58) and X is the number of dA. There is a hypochromic effect observed due to the complexation,[6] meaning that ε differs between the naked and complexed states. As shown in Figure S1 in List of Publications #1, this difference between dA_X and dA_X-SPG is 7.4%. Therefore, in the case that the naked and complexed dA_x show overlapping elution times, there is a certain error in the result. Furthermore, $(\partial n/\partial c)_{\mathrm{co}}$ depends on the SPG vs. dA_X composition in the complex and it may change from 0.142 to 0.164. In the calculation of $(\partial n/\partial c)_{\mathrm{co}}$, we assumed that the complex always takes the stoichiometry, that is $(\partial n/\partial c)_{\mathrm{co}} = 0.151\ \mathrm{cm^3\ g^{-1}}$ with $w_{\mathrm{SPG}} = 0.57$. However, there is no guarantee of this assumption. In this regard, the value obtained by Eq. 3 may not always be accurate.

To differentiate the mixing (or feeding) $[\mathrm{mG}]/[\mathrm{dA}]$, we denote the former mixing molar ratio as $[\mathrm{mG}]/[\mathrm{dA}]_{\mathrm{m}}$ and the latter observed ratio as $[\mathrm{mG}]/[\mathrm{dA}]_{\mathrm{f}}$. From $[\mathrm{mG}]/[\mathrm{dA}]_{\mathrm{f}}$, we can calculate the averaged molar ratio defined by $\mathrm{av.}\,(\partial n/\partial c)_f = \int [\mathrm{mG}]/[\mathrm{dA}]_{\mathrm{m}}\, f\mathrm{d}t / \int f\ \mathrm{d}t$, with f and t being the fractional molar concentration and time, respectively.

2-2-6 Collecting fractionated sSPG or complex

S-3n was dissolved in 0.25N NaOH solution and the low-molecular-weight fraction was obtained by filtrating through a 100 kDa ultrafiltration membrane (Merck; UFC510096, Amicon Ultra), followed by dialysis with a 3.5 kDa membrane (Idea Trading Corporation; Standard RC Tubing, MWCO:3.5kDa G235029). By using the obtained fraction, we prepared the complex with dA_X at a mixing ratio of $([\mathrm{mG}]/[\mathrm{dA}])_{\mathrm{mix}} = 4.0$ and this mixture was fractionated by collecting an appropriate elution time range. For example, we collected 24.3–24.6, 23.2–23.7, and 21.8–22.3 min for dA_{60}-SPG complex.

2-2-7 Synchrotron SAXS measurements.

SAXS measurements were performed at BL-40B2 of SPring-8, Japan, for the fractionated sample. A Pilatus 100K detector was placed 4.3 m away from the sample position. The wavelength of the incident beam was 0.100 nm. The 4.3 m set-up provided a q range of 0.02–2.00 nm^{-1}. Approximately 0.1 mL of dA_{60}-SPG complex with a concentration of about 1.0 mg/mL was sealed in a quartz tube cell with a diameter of 2.0 mm (Hilgenberg GmbH, Malsfeld, Germany) and the X-ray transmittance of the samples was determined with an ion chamber located in front of the sample and a Si photodiode for X-rays (Hamamatsu Photonics; S8193) behind the sample. The exposure time was 300 s. Owing to the very limited amount of sample, we measured only one concentration and analyzed the data without extrapolating to the zero concentration, assuming that the inter-particle interference factor was negligible.

2-2-8 Wormlike chain and rigid-rod models

The worm-like cylinder model envisions a continuously flexible and isotropic rod, particularly suited to describe semiflexible polymer chains in solution, such as tSPG and the double helix of DNA.[7, 8] The physical parameters to characterize the model are the persistence length (p) determined by the bending energy divided by the Boltzmann factor and the molar mass per unit length (M_L). The persistence length is an indication of the chain's stiffness; it goes to zero for the Gaussian chain and to infinity for the rigid-rod limit. The value of M_L is well related to the molecular dimensions and the chemical structures.[8] The radius of gyration of a worm-like chain with a contour length of L and a persistence length of p can be written with the Benoit-Doty equation in the case that L is much larger than the cross-sectional size of the molecule.[9]

$$\langle S^2 \rangle = \frac{qL}{3} - q^2 + \frac{2q^3}{L}\left[1 - \frac{q}{L}\left(1 - e^{-\frac{L}{q}}\right)\right] \quad (4)$$

The contour length is related to the molecular weight (M) of the chain by $L = M/M_L$.

Scattering amplitude $A(\mathbf{q})$ from the short rigid rod with hemispherical end-caps (see the inset of Figure 2-8) can be given by Eq. 5,[10, 11] where $A(\mathbf{q})$ is related to the form factor scattering intensity $I(q)$ by $I(q) = \langle |A(\mathbf{q})|^2 \rangle$; here, $\langle \omega \rangle$ represents the averaging over all orientations of the rod relative to the scattering vector $\mathbf{q}$.

$$A(\mathbf{q}) = \pi R^2 L \frac{\sin\left(\frac{qL}{2}\cos\omega\right)}{\frac{qL}{2}\cos\omega} \frac{2\,J_1(qR\sin\omega)}{qR\sin\omega}$$
$$+4\pi R^3 \int_0^1 dt \cos\left[q\cos\left(Rt+\frac{L}{2}\right)\right](1-t^2)\frac{J_1\left[qR\sin\omega\,(1-t^2)^{\frac{1}{2}}\right]}{qR\sin\omega\,(1-t^2)^{\frac{1}{2}}} \quad (5)$$

Here, ω is the angle between $\mathbf{q}$ and the cylindrical axis and J_1(x) is the first order Bessel function.

2-3 Results

2-3-1 Chromatography and SLS: comparison of the three SPG samples

Figure 2-1 presents GPC chromatograms for three SPG samples at different solvents and mobile phases: (A) SPG solution was prepared in 0.01N NaOH, in which SPG takes triple helix (tSPG) and the mobile phase was a neutral PBS buffer, (B) SPG was dissolved in 0.25N NaOH, where tSPG dissociates into single chains of SPG (sSPG) and the mobile phase was the same as in A, and (C) SPG was dissolved in DMSO as sSPG and the mobile phase was DMSO/LiCl. Panel A3 compares the RI chromatograms for three samples in 0.01N NaOH. As expected, the three samples showed almost the same chromatogram and the values of M_w and $\langle S^2 \rangle_z$ were calculated from Eq. 1 and plotted against the elution time in A1 and A2. Although the RI chromatogram showed that S-3n exhibited a slightly lower molecular weight than the others, M_w and $\langle S^2 \rangle_z$ almost overlapped. The upper three rows in Table 2-1 summarize the obtained values. Comparing the values of M_w in 0.01N NaOH as tSPG, it can be concluded that the three samples did not differ markedly, although S-3n had the lowest. B3 shows the RI chromatograms when the samples were dissolved in 0.25N NaOH and injected into the neutral buffer. It has been reported that tSPG dissociates into sSPG in 0.2N NaOH. On the other hand, after injecting these solutions into the GPC channel, its neutral mobile phase of PBS was considered to make SPG re-form tSPG. We presumed that this triple-helix formation mainly occurred intra-molecularly instead of inter-molecularly. This is because the pH change was so rapid when the SPG/0.25N NaOH solution was injected into the mobile

phase and more importantly the SPG concentration was very low; after injection, the SPG concentration became about 1/500 of the cross-over concentration; where the cross-over concentration is the critical concentration above which inter-molecular interactions between polymer chains in solution become dominant. Therefore, we could regard the obtained M_w in this procedure as $M_w$of individual sSPG chains constituting tSPG. To confirm this assumption, S-n3 was dissolved in DMSO, which is known to dissociate tSPG to sSPG, and measured M_w (C1–C3). The RI peak in C3 was unimodal, while those in B3 were bimodal because the gel column for DMSO was not as good in fractionation as that of water. Apart from this, the molecular weights were almost the same as shown in B2 and C2 and in Table 2-1. We determined $M_w$foreach peak (or shoulder) top in B3 and the values are summarized in Table 2-1 in the lower rows. The averaged M_w over the two peaks in 0.25N was 1.35 $\times 10^5$, which is close to that of 1.31×10^5 in DMSO, confirming our above assumption: M_w in 0.25N gives M_w of sSPG in tSPG.

B3 in Figure 2-1 shows that all samples exhibited a bimodal pattern. We read the M_w values at the top (or shoulder) of the 1st and 2nd peaks and denoted these values by 1st-$M_{w,\mathrm{sSPG}}$ and 2nd-$M_{w,\mathrm{sSPG}}$, respectively. In B2 and B3, for example, the dotted lines show how to read them. We took a ratio with $M_{w,\mathrm{tSPG}}$ and the resultant values are compared in the second and third lows in Table 2-2. It was shown that $M_{w,\mathrm{tSPG}}$/2nd-$M_{w,\mathrm{sSPG}}$ was around 6, while $M_{w,\mathrm{tSPG}}$/1st-$M_{w,\mathrm{sSPG}}$ was around 2.5. These results may be explained as follows (referring

Figure 2-2): Some of the components in tSPG may adopt the form of a perfect triplex, in which all of the three sSPG chains have the same length, but the others do not (compare A and B in Figure 2-2). The others may have some defects that might have been created during the process of molecular-weight reduction, namely, applying ultra-sonic sounds and/or shear-stress to tSPG in solutions. Furthermore, secondary aggregation of the tSPG (or bundle of tSPG) illustrated in C is inevitably present in a certain percentage.[7, 12] The observed $M_{\mathrm{w,tSPG}}$ is essentially averaged over the three species of A–C. After dissociation into 0.25N NaOH, all tSPG chains are molecularly dispersed to form sSPG due to the breaking of hydrogen bonds. In this situation, we can expect that the solution contains sSPG that has the same length as tSPG (D) and shorter sSPG (E). The shorter chains are created from B. This can explain the bimodal peak in 0.25N NaOH and the 1st and 2nd peaks in Panel B3 in Figure 2-1 correspond to D and E. In this context, the following question would arise: Why was the relation of $M_{w,\mathrm{tSPG}}$/2nd-$M_{w,\mathrm{sSPG}}$=3 not observed? This is because the tSPG sample always contain a certain amount of the bundles, which makes the averaged $M_{\mathrm{w,tSPG}}$ larger than 3 × D.

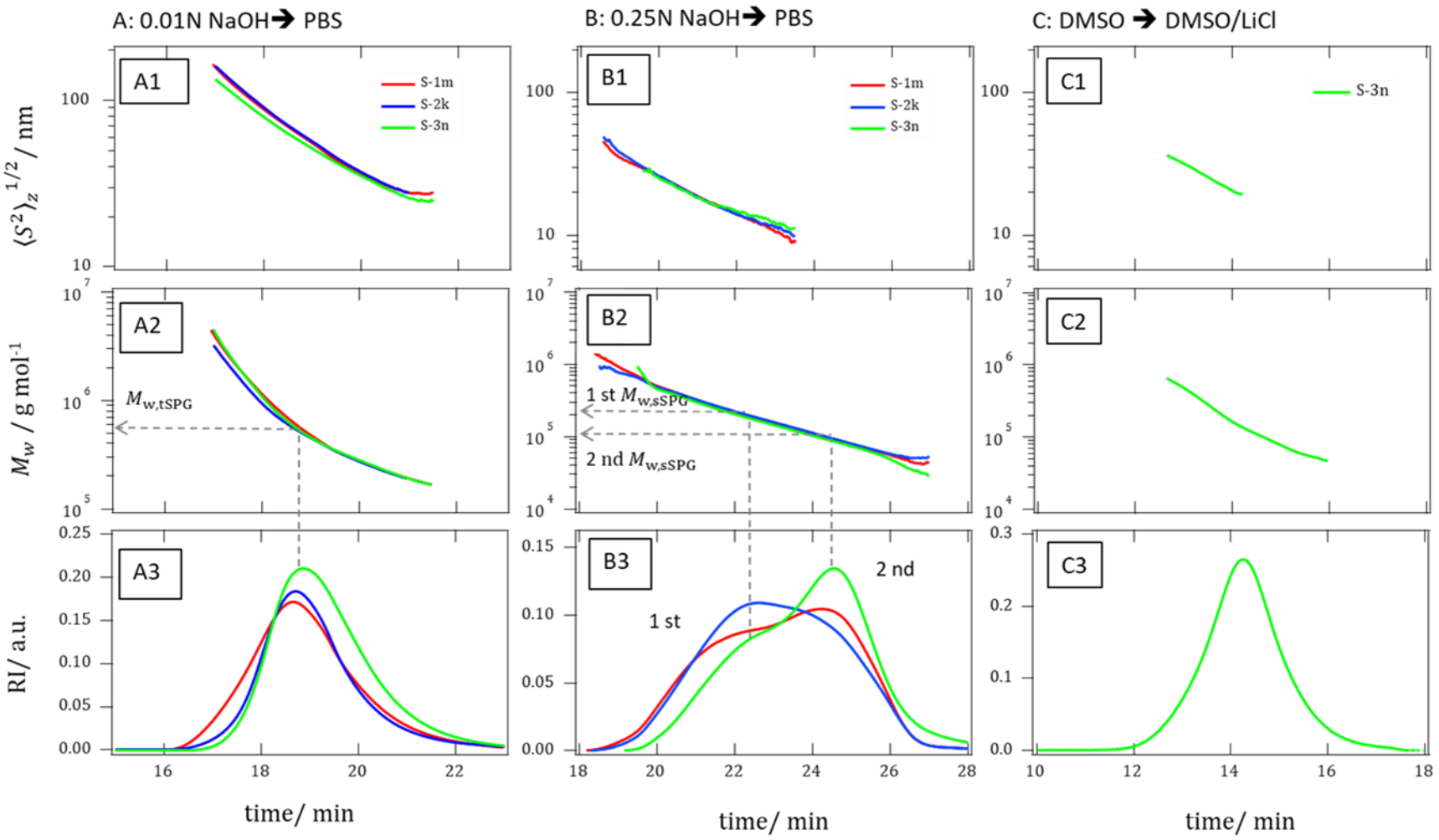

Figure 2-1. GPC chromatograms of RI (bottom) and the calculated M_w and $\langle S^2 \rangle_z$ plotted against the elution time in the three conditions, comparing the three samples, except for DMSO.

Table 2-1. Results of light scattering measurements to determine the molecular weight and radius of gyration in the three different solvent conditions.

solvent	Sample code	$10^{-5} \times M_w$ and M_w/M_z in ()				$\langle S^2 \rangle_z^{1/2}$ (nm)		
		Peak top	$\pm 0.5\sigma$	$\pm 1\sigma$		Peak top	$\pm 0.5\sigma$	$\pm 1\sigma$
0.01N NaOH	S-1m	6.25± 0.02	6.85 (1.09)	7.32 (1.28)	-	65.1± 0.1	71.1	79.7
	S-2k	5.42± 0.01	5.50 (1.06)	5.95 (1.22)	-	64.5± 0.2	67.9	78.3
	S-3n	5.02± 0.01	5.18 (1.13)	5.37 (1.24)	-	54.7± 0.1	58.8	69.0
	L-1	7.85± 0.01	9.97 (1.51)	12.6 (2.15)		73.4± 0.1	98.5	133.6
DMSO	S-3n	1.31± 0.03	1.39 (1.08)	1.61 (1.26)	-	17.3± 0.2	18.2	21.0
	L-1	1.50± 0.01	1.51 (1.05)	1.75 (1.12)		19.1± 1.3	19.5	22.4
0.25N NaOH		1st		2 nd		1st	2 nd	
	S-1m	2.84	-	0.986		14.5 ± 0.5	5.6± 0.6	
	S-2k	2.22	-	1.04		13.8 ± 0.6	5.4± 0.4	
	S-3n	1.87	-	0.868		14.9 ± 0.5	6.0± 0.6	
		Averaged 1 st and 2 nd peaks		1.35				

2-3-2 ^{13}C qNMR to confirm preservation of the chemical structure

One can suppose that the application of sonication or shear-stress may change the chemical structures. We thus carried out quantitative ^{13}C NMR, where the nuclear Overhauser effect of carbon, which enhances the signals from certain carbons disproportionately to their compositions, was minimized by inverse-gated decoupling. This method eventually caused a lower carbon signal and thus a longer acquisition time, but achieved the quantitative analysis of carbon. The quantitative ^{13}C NMR of SPG and other glucans has been performed by Kono et al., [4, 13] so we followed their procedure.

Figure 2-3 shows a typical ^{13}C NMR spectrum for S-3n; the other two samples showed the similar spectra. This sample had the largest 2nd peak and thus appeared to have more defects in tSPG; it probably underwent the most severe treatment in the molecular-weight reduction process. Each peak can be assigned to the indicated carbon in the inset,[4] here, the side-chain glucose is denoted by D, while the main-chain one bearing the side-chain is A, and the other main-chain glucoses without the side-chain are B and C. The area of each peak corresponds to the amount of the carbon. Some peaks, for example, (4) and (7), can be related to only one carbon [(4) is A5 and (7) is D4, respectively] because these carbons are in different effective magnetic fields due to different chemical atmospheres from the same carbons in the different glucoses. For the others such as (1), it was difficult to accurately deconvolute the peaks. The molar ratio of each glucose was determined by solving a simultaneous equation

as shown in Figure S3 in List of Publications #1; the result is shown in Table 2-3. The molar ratio of the-side chain to main-chain glucoses is 2.96 ± 0.02, agreeing with the original chemical structure. This result suggests no cleavage of the side chain during the molecular-weight reduction process. We suppose that this treatment causes cleavage of β-1,3-linkages between the main-chain glucoses, and the resultant defect caused the 2nd peak in GPC in 0.25N NaOH (Figure 2-1).

Table 2-2. Peak deconvolution of 0.25N NaOH GPC chromatogram and the molecular weight ratio of tSPG to sSPG.

	S-1m	**S-2k**	**S-3n**
Peak area ratio (1 st : 2 nd)	0.43 : 0.57	0.52 : 0.48	0.31 : 0.69
$M_{w,tSPG}$/1 st $M_{w,sSPG}$	2.2	2.4	2.7
$M_{w,tSPG}$/2 nd $M_{w,sSPG}$	6.3	5.2	5.8

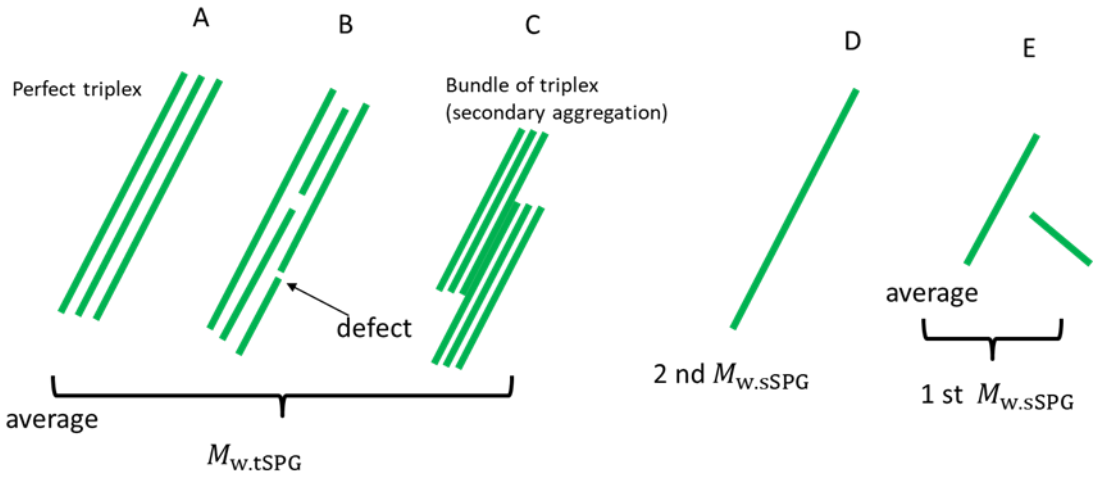

Figure 2-2. A schematic illustration to explain the bimodal peak in 0.25N NaOH solution (Figure 2-1) and the molecular weight ratio in Table 2.

Table 2-3. The molar ratio of the side-chain to main-chain glucoses in S-3n determined by ^{13}C NMR spectra. The definitions of A, B, C, and D are shown in Figure 2-3.

Residue	ratio
A	1.00
B or C	0.95 ± 0.09
D	0.98 ± 0.02
(A+2B)/D	2.96 ± 0.02

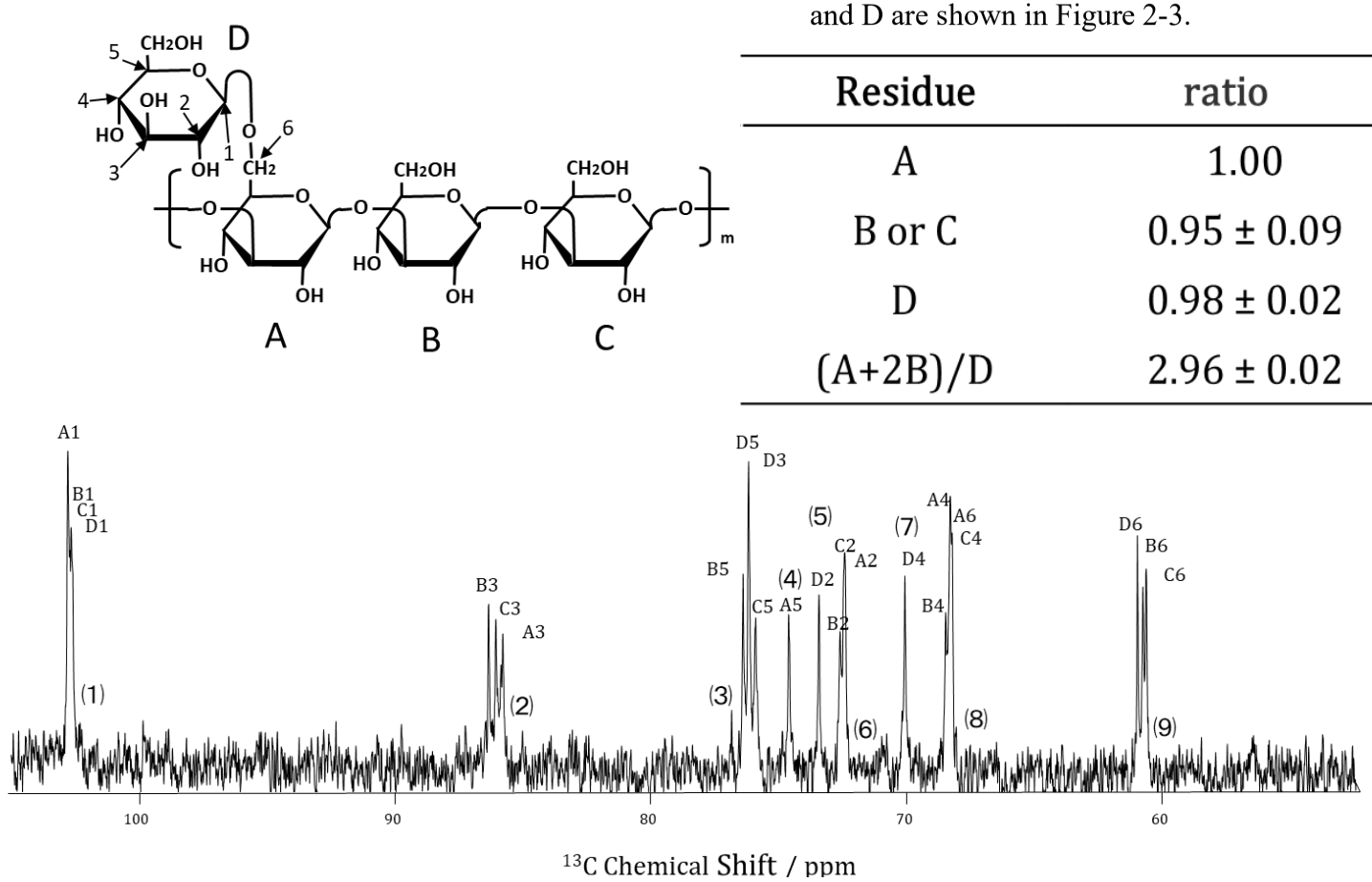

Figure 2-3. ^{13}C NMR spectra of SPG (sample S-3n) in DMSO-d_6 at 90 °C, obtained by the inverse-gated H-decoupling method. Chemical shifts of each carbon in the A, B, C, and D glucose residues of SPG (the chemical structure is shown in the inset) are marked accordingly.

2-3-3 Conformation analysis

Figure 2-4 plots $\langle S^2 \rangle_z$ against M_w for all of the samples as well as the values reported by Norisuye et al.[14-16] for comparison. The solid gray curve fitting to tSPG was calculated from Eq. 4 by using $q = 150\ \mathrm{nm}$ and $M_L = 2000\ \mathrm{nm}^{-1}$. sSPG was fitted by a straight line with a slope of 0.58, which corresponds a random coil swollen by the excluded volume effect. Our tSPG and sSPG in DMSO data points nicely overlap with the previous results. The data points for 0.25N NaOH were shifted downward and appeared to maintain a slope similar to that of tSPG, except for the higher M_w of L-1. If, after injection into the neutral mobile phase, the rapid intramolecular renaturation had caused globular aggregates, the slope would have been around 0.3–0.4, as shown previously.[12] Brant et al.[11,17] reported that, when the renaturation was carried out at sufficiently low concentration, the resultant SPG took macrocycles with diameters that can reach several tens of nanometers. According to them, the cross-sectional size of the chain suggested that tSPG was locally retrieved. They proposed a possible model in which one single chain may form a cyclic triple helix through a “back-biting” reaction. In our case, we injected a 0.25N NaOH solution into the buffer to control a neutral pH in the GPC line and the concentration was quite low (about 0.01 mg/mL), far below than the cross-over concentration above where intermolecular interactions start. Therefore, we can expect the ring formation to occur during this process.

The molecular weight dependence of $\langle S^2 \rangle$ for rigid rods and rigid rings is simply calculated as follows:

$$\langle S^2 \rangle^{1/2} = \begin{cases} \dfrac{1}{\sqrt{12}} \dfrac{M}{M_L} & \text{rod} \\ \dfrac{1}{2\pi} \dfrac{M}{M_L} & \text{ring} \end{cases} \tag{6}$$

Again, M/M_L equals the contour length of the chain, L. The values calculated from these two equations are shown in Figure 2-4 by using $M_L = 2000\ \mathrm{nm}^{-1}$. The rod model nicely fits the data points in the low-molecular-weight region. The 0.25N NaOH data points are almost fitted by the ring line, but deviated downward. This deviation may be ascribed to the chain flexibility. Shimada and Yamakawa[18] obtained an expression of $\langle S^2 \rangle$ for worm-like chains in the case of $L/(2q) < 1$ (Eq. 7) and the calculated values are shown by the solid line.

$$\langle S^2 \rangle = \frac{L^2}{4\pi^2} \left(1 - 0.1140 \frac{L}{2q} \right) \tag{7}$$

Agreement with the experimental data was improved to some extent, but failed to fit the data for the higher-molecular-weight region of L-1. The agreement between the data and the ring model supports the formation of the ring with $M_L = 2000\ \mathrm{nm}^{-1}$. This means that the local structure of the ring SPG may also be a triple helix of SPG, as mentioned by McIntire[11] and Brant. It should be mentioned what caused the derivation in the higher molecular weight of L-1 from the ring conformation. It may be due to the formation of imperfect ring-shapes and/or due to the inclusion of globular aggregates.

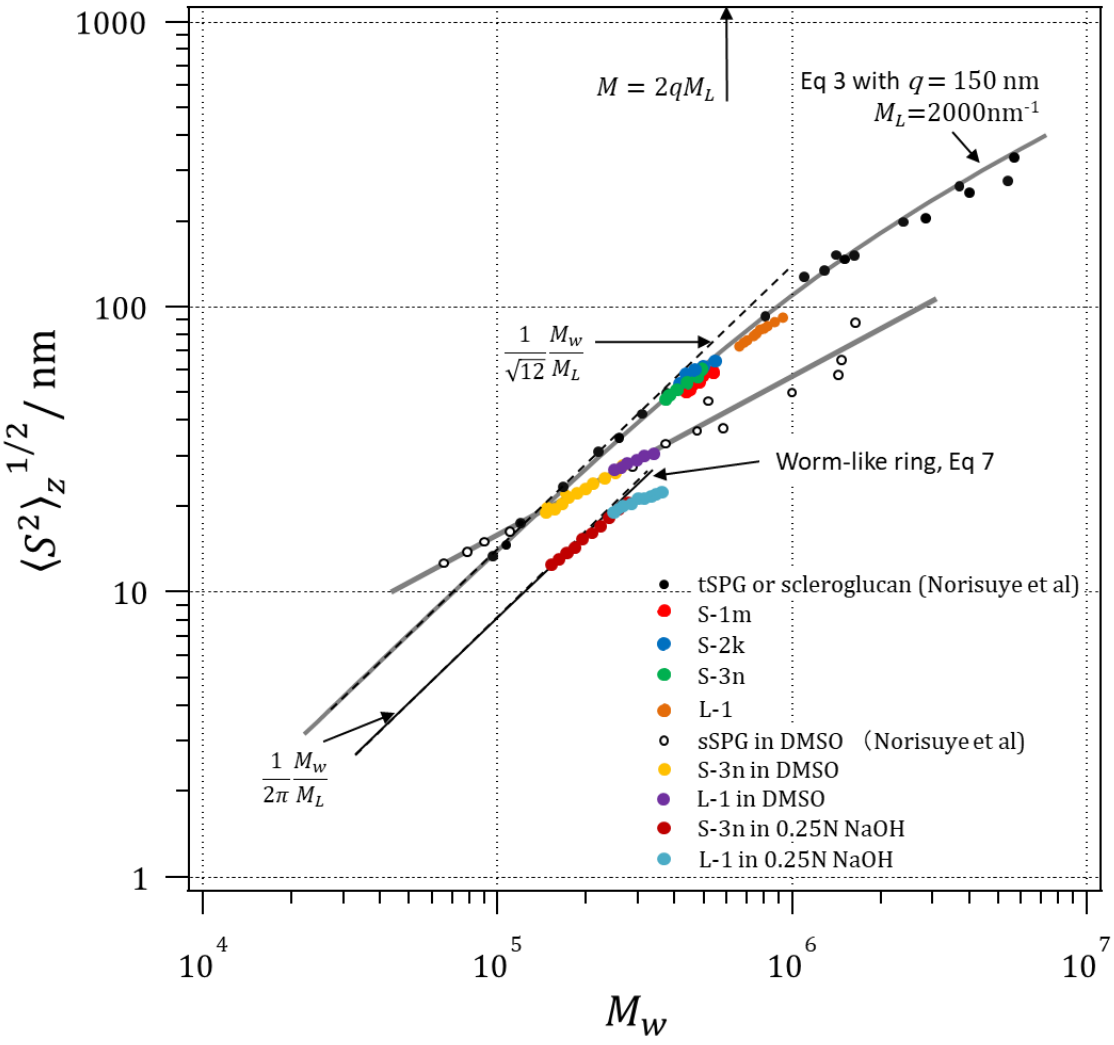

Figure 2-4. Double logarithmic plots of $\langle S^2 \rangle_z$ against M_w for the four samples in 0.01N and 0.25N NaOH and DMSO, comparing with the reported values of SPG and scleroglucan. The dotted straight lines indicate theoretical values for rigid rod or rings with $M_L = 2000\ \mathrm{nm}^{-1}$ and the solid curves were calculated from Eqs. 4 or 7 using the indicated parameters. The solid line fitted to the points in DMSO has a slope of 0.58, corresponding to a swollen random coil.

2-3-4 Complexation between dA_x and short sSPG

We reported the complex formation between tSPG with M_w= 1.1 × 10^6 or 4.5 × 10^5 and dA_{40} (both phosphodiester and phosphorothioate) in the previous papers.[12] The complex made from tSPG with M_w= 1.1 × 10^6 showed a unimodal peak (Figure 2 in the reference 12). Based on this result, we presumed an "SPG template model" for the complexation; that is, when long sSPG chains approach each other to re-form tSPG and start to form hydrogen bonds between their main-chains, short DNA chains are incorporated into the triple-helix formation. This is the reason why the molecular weight of the complex was close to that of the original tSPG. Contrary to this previous result, we observed multiple peaks appearing at the lower-molecular-weight side as shown in Figure 2-5.

We removed the higher-molecular-weight fraction from S-3n by using a 100 kDa ultrafiltration membrane (hereinafter, this sample is denoted as fractionated S-3n); its RI chromatogram is shown as "after" in Figure 2-5-A, indicating that the higher -molecular-weight components were indeed removed. By using this fractionated S-3n, we prepared the complex at the same $[\mathrm{mG}]/[\mathrm{dA}]_{\mathrm{m}}$ with "before" and measured GPC (Figure 2-5). As a result, three peaks became more obvious and the higher-molecular-weight fractions disappeared. To understand the cause of these peaks, we fractionated the complex and the resultant UV chromatogram clearly showed that three peaks were successfully isolated (2-5-C). M_w was evaluated by extrapolating at the zero angle (2-5-D) and the obtained values as well as their distributions are

summarized in Table 2-4. We carried out similar measurements for dA_{30} and dA_{40} by using fractionated S-3n and M_w was determined. All of the results are summarized in Table 2-4.

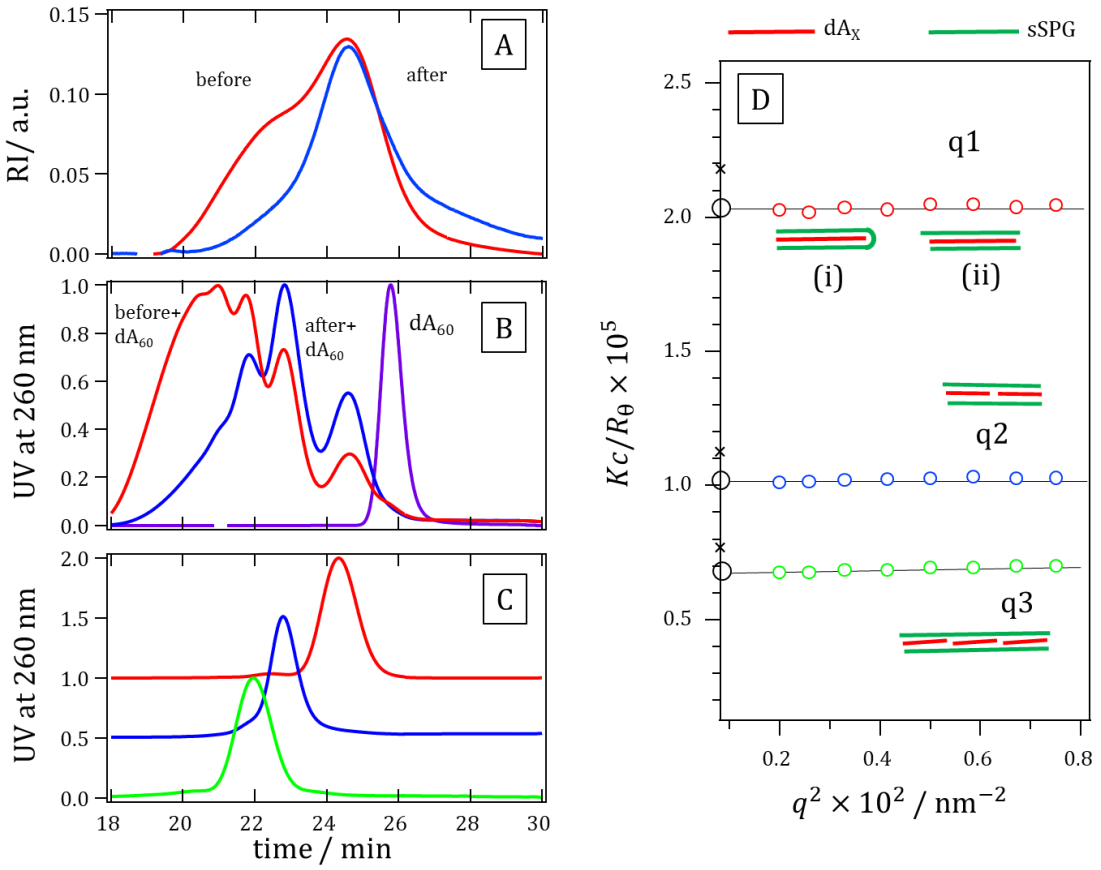

Figure 2-5. Complexation between dA60 and the low-molecular-weight SPG (S-3n). A: RI chromatograms of S-3n before and after fractionation. B: Comparison of the UV chromatograms of the complex between before and after fractionation as well as naked dA60. C: UV chromatograms after fractionation to isolate three peaks, where the baseline was shifted upward to facilitate easy comparison. D: The angular dependence of the light scattering intensity at each peak top in C to determine M_w. On the vertical axis, the cross marks show the molar masses calculated from the 1:2 stoichiometric model. The inset cartoons show the molecular models of q1, q2, and q3. (i) shows a 1:1 complex made from one sSPG chain and one dAx and (ii) shows a 2:1 complex made from two sSPG-chains and one dAx.

2-3-5 Proposing a new model for the complex formation: DNA-templated pathway

The obtained M_w values for the isolated complexes showed quite interesting relations as shown in Table 2-4. We denoted the lowest-molecular-weight isolation as q1, and the second and third ones as q2 and q3, respectively (see also Figure 2-5-C&D). Surprisingly, the dispersity indexes expressed by M_w/M_n were quite small, at around 1.01 ± 0.01, compared with those in the original SPG. When we took the ratio of M_w within the complex made from the same dA_X, for example, dividing M_w of q2-dA_{30}-SPG or q3-dA_{30}-SPG by that of q1-dA_{30}-SPG, it was always 2 or 3, respectively. These calculations are shown in the 5th column in Table 2-4 as $\mathrm{qx/q1}$. Even when we took the ratio of q1-dA_{30}-SPG to q1-dA_{60}-SPG, it was 2.0. These results indicate that dA_X preferentially collects the most suitable SPG in terms of chain length when forming the complex. When one dA_X molecule is involved, dA_X only collects the suitable short sSPG to form a complex of q1 (as shown in Panel D in Figure 2-5). When two dA_X molecules are involved, they collect sSPG twice as long as that of q1. When three dA_X molecules are involved, sSPG becomes three times the length. The observed relation in $\mathrm{qx/q1}$ indicates that such preferential selection occurred during the complexation. This can be referred as “dA-templated quantized complexation”. This is the reason we denoted the small complexes as q1, q2, or q3, by taking the initial letter of “quantization”. The complex is known to have a triple helix made from two SPG chains and one DNA chain (Figure 1-2); thus, we can calculate the number of main-chain glucoses (N_{mG}) from the measured molar mass of $M_{\mathrm{w.dA_X-SPG}}$ with the following relation:

$$N_{\mathrm{mG}} = 3\frac{1}{M_{\mathrm{SPG}}}\left(\frac{M_{\mathrm{w.dA_X SPG}} - NM_{\mathrm{w.dA_X}}}{2} - 18\right) \quad (8)$$

Here, M_{SPG} is the molar mass of the SPG repeating unit as shown in Figure 1-2-A, which is 666.58, and N and $M_{\mathrm{w.dA_X}}$ are the number of $\mathrm{dA_X}$ chains and the molar mass of $\mathrm{dA_X}$, respectively. The obtained N_{mG} is summarized in the last column in Table 2-4, as well as the one sSPG chain's molecular weight, that is, $(M_{\mathrm{w.dA_X SPG}} - NM_{\mathrm{w.dA_X}})/2$. It is quite astonishing that all of the N_{mG} values almost agreed with number of dA units. In our early report,[6] we determined the stoichiometric ratio to be $[\mathrm{mG}]/[\mathrm{dA}] = 2.0$. This value was also supported by a computer chemistry.[19] The present small complexes perfectly satisfy this stoichiometry.

It should be noted that N_{mG} always showed a slightly larger number than expected from the template $\mathrm{dA_X}$ (difference is shown in parentheses). The exact stoichiometric molecular weights expected from the number of $\mathrm{dA_X}$ are marked by crosses in Figure 2-5-D, showing that these differences appear to be beyond experimental error in the light scattering. At this moment, we are not sure why the complexation needs such extra glucoses. One possibility is that the complex is made from one sSPG chain and one $\mathrm{dA_X}$, as shown in inset (i) in Figure 2-5-D, where the sSPG chain forms a hairpin-like conformation. The U-shape portion needs extra glucoses. Another possibility is that this difference

is just due to experimental error caused by determination of $(\partial n/\partial c)$ of the complex.

Table 2-4. Molecular weights for the fractionated low-molecular-weight complexes and the radius of gyration.

		$10^{-4}M_w$	M_w/M_n $(\pm 0.5\sigma)$	qX/q1	av.$\left(\frac{[\mathrm{mG}]}{[\mathrm{dA}]}\right)_f$ $(\pm 0.5\sigma)$	$\langle S^2\rangle_z^{1/2}$ /nm	$10^{-4}M_w$ sSPG	N_{mG}[b]
dA_{30}-SPG	q1	2.51 ± 0.06	1.01	-	-	-[c]	0.77	35 (+5)
	q2	5.05 ± 0.07	1.02	2.01	-	-[c]	1.53	71 (+11)
	q3	7.69 ± 0.01	1.00	3.06	-	7.13 ± 1.8	2.37	109 (+19)
dA_{40}-SPG	q1	3.37 ± 0.01	1.01	-	-	-[c]	1.03	47 (+7)
	q2	6.59 ± 0.02	1.02	1.96	-	-[c]	1.98	91 (+11)
	q3	10.0 ± 0.05	1.00	2.97	-	9.23 ± 2.3	3.02	140 (+20)
dA_{60}-SPG	q1	4.95 ± 0.02	1.01	1.97[a]	1.9	4.96 (SAXS)	1.48	68 (+8)
	q2	9.90 ± 0.04	1.01	2.00	2.1	8.94 ± 1.6	2.98	137 (+17)
	q3	14.9 ± 0.04	1.02	3.01	2.2	12.5 ± 1.1	4.50	207 (+20)

(a) M_w of q1-dA_{60}-SPG is divided by M_w of q1-dA_{30}-SPG
(b) The number of the main chain glucoses calculated from Eq 8 and the differences from the number of dA are in the bracket
(c) Too small to be measured with SLS and we did not carried SAXS.

As changing the mixing molar ratio $([\mathrm{mG}]/[\mathrm{dA}])_{\mathrm{mix}}$ from 1.5 to 16 for dA_{60} and fractioned S-3n, the RI and UV chromatograms were measured (Figure 2-6-A and B). Here, we injected the samples so as to fix the same amount of dA_{60}. In the case of $([\mathrm{mG}]/[\mathrm{dA}])_{\mathrm{mix}}$ =1.5 and 2.0, there was uncomplexed dA_{60} observed at the elution time $t = 25.7$min. When $([\mathrm{mG}]/[\mathrm{dA}])_{\mathrm{mix}}$ exceeded 4, we did not observe uncomplexed dA_{60}. A further increase of SPG caused increases in the q1, q2, and q3 peaks simultaneously only in RI. Note that there was no large difference between $([\mathrm{mG}]/[\mathrm{dA}])_{\mathrm{mix}} = 8$ and 16 in UV. This is because UV detected only dA_{60}, while RI detected both dA_{60} and SPG. The increasing RI with

increase of $([\mathrm{mG}]/[\mathrm{dA}])_{\mathrm{mix}}$, such as 8 and 16, can be ascribed to increase in uncomplexed SPG.

Several interesting phenomena are presented in Figure 2-6. First, there is an isosbestic point observed in UV at the elution time of 24.9 min (Figure 2-6-B), providing an evidence of one-to-one interconversion of reactant and product. Second, the peak positions of q1, q2, and q3 do not change at all, indicating that the molecular weights of these complexes did not change with increasing SPG. This is in marked contrast in the complex with larger SPG (Figure S6 in List of Publications #1), where we observed a broad unimodal peak and the peak top position was shifted toward to the larger molecular side with increasing $([\mathrm{mG}]/[\mathrm{dA}])_{\mathrm{mix}}$. Third, there was unreacted dA_{60} even in SPG-rich compositions such as $([\mathrm{mG}]/[\mathrm{dA}])_{\mathrm{mix}}$ = 4. This means that dA_{60} did not form a complex with sSPG if the chain length of sSPG did not match with dA_X. This is quite surprising because our results indicate that dA_X meticulously selects only a suitable length of sSPG to bind, and if it runs out, dA_X does not form a complex. Figure 2-6-C shows that $([\mathrm{mG}]/[\mathrm{dA}])_f = 2.0$ is maintained for each fraction, as expected. Here, we omitted $[\mathrm{mG}]/[\mathrm{dA}]_{mix} = 16$ because a large amount of SPG left led to incorrect results.

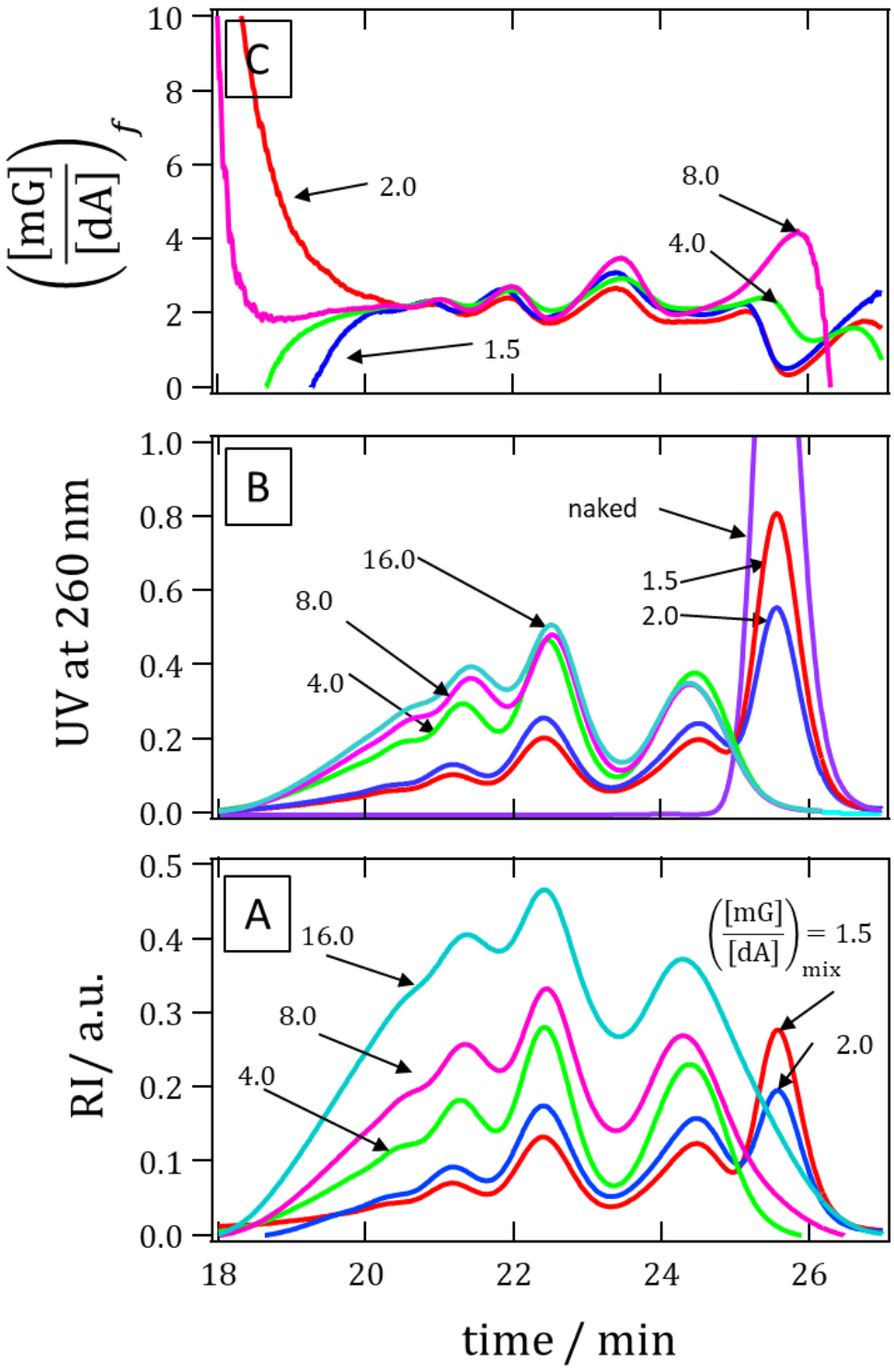

Figure 2-6. Mixing composition $([mG]/[dA])_{mix}$ dependence of RI (A), UV (B), and $([mG]/[dA])_f$ (C) for dA60 and sSPG (fractionated S-3n).

2-3-6 Characterization of q1 dA60-SPG complex

Figure 2-7-A compares the CD spectrums of q1-dA_{60}-SPG, dA_{60}-SPG(n), and dA_{60}. Here, dA_{60}-SPG (n) is a complex made from S-3n without any fractionation. The two spectra for the complexes were similar and very different from dA_{60}, although there was a slight difference in the two complexes at low wavelengths. This indicates that q1-dA_{60}-SPG and dA_{60}-SPG(n) adopt almost the same local structures. Figure 2-7-B plots CD at $\lambda = 280\ \mathrm{nm}$ upon heating, after dividing by that at room temperature. At 70 ℃, the complexes completely dissociated and their spectra agreed with that of dA_{60}. q1-dA_{60}-SPG dissociated at a lower temperature than dA_{60}-SPG(n). The dissociation temperatures (T_m) were determined as the temperature at which half of the complex was dissociated, as indicated by cross marks. Comparing with the reported T_m for DNAs, for example, poly(dA-dT) duplex is about 50–60 ℃,[20] it can be concluded that q1-dA_{60}-SPG shows comparable stability with DNAs.

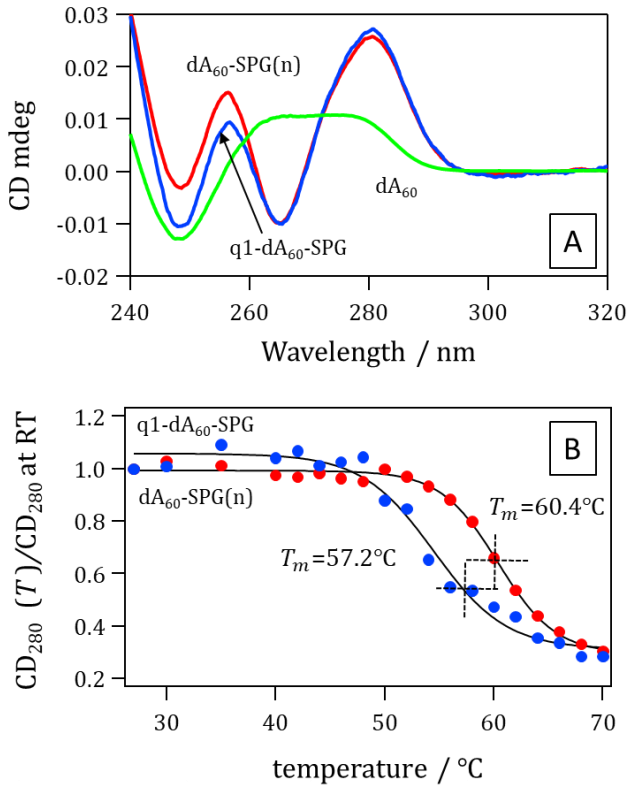

Figure 2-7. Comparison of CD spectra among q1-dA60-SPG, dA60-SPG(n), and dA60 (A) and their temperature dependence at $\lambda = 280$ nm.

Figure 2-8 shows SAXS profiles for q1-dA_{60}-SPG. The exponent (α) in the case of expressing $I(q) \propto q^{-\alpha}$ appeared to converge as $\alpha \to 0$ in the limit of the small-q, such as $q < 0.1\ \mathrm{nm}^{-1}$. This indicates that the present q-range was adequate to cover the entire size of the scattering objects. In the range of $0.2 < q < 1.0\ \mathrm{nm}^{-1}$, $\alpha \sim 1$, indicating the presence of a finite size of rod. There is a small peak at $q = 4.2\ \mathrm{nm}^{-1}$, indicating reasonably narrow dispersity in shape. We found the most well-fitted curve by using a capped cylinder model given by Eq 5 for which the parameters were $L = 17\ \mathrm{nm}$ and $R = 1.2\ \mathrm{nm}$. When we changed to $R = 1.2\ \mathrm{nm}$ or $L = 13\ \mathrm{nm}$, a certain deviation appeared, as shown

in the figure. It was found that the SAXS profile was quite sensitive to R, but not for L. We could determine $L = 17\ \text{nm} \pm 2\ \text{nm}$ and $R = 1.2 \pm 0.1\ \text{nm}$. dA_{60} takes a right-handed helix in aqueous solutions and the distance between the adjacent base molecules is 0.35 nm, and thus the contour length of dA_{60} is 21 nm. The obtained total length of q1-dA_{60}-SPG is 19.2 nm $(L + 2R)$, which reasonably agrees with the contour length of dA_{60}. By introducing an appropriate distribution in R, the intensity around q = 3.0 −4.5 nm^{-1} could be more nicely fitted as shown in Figure S8 in List of Publications #1.

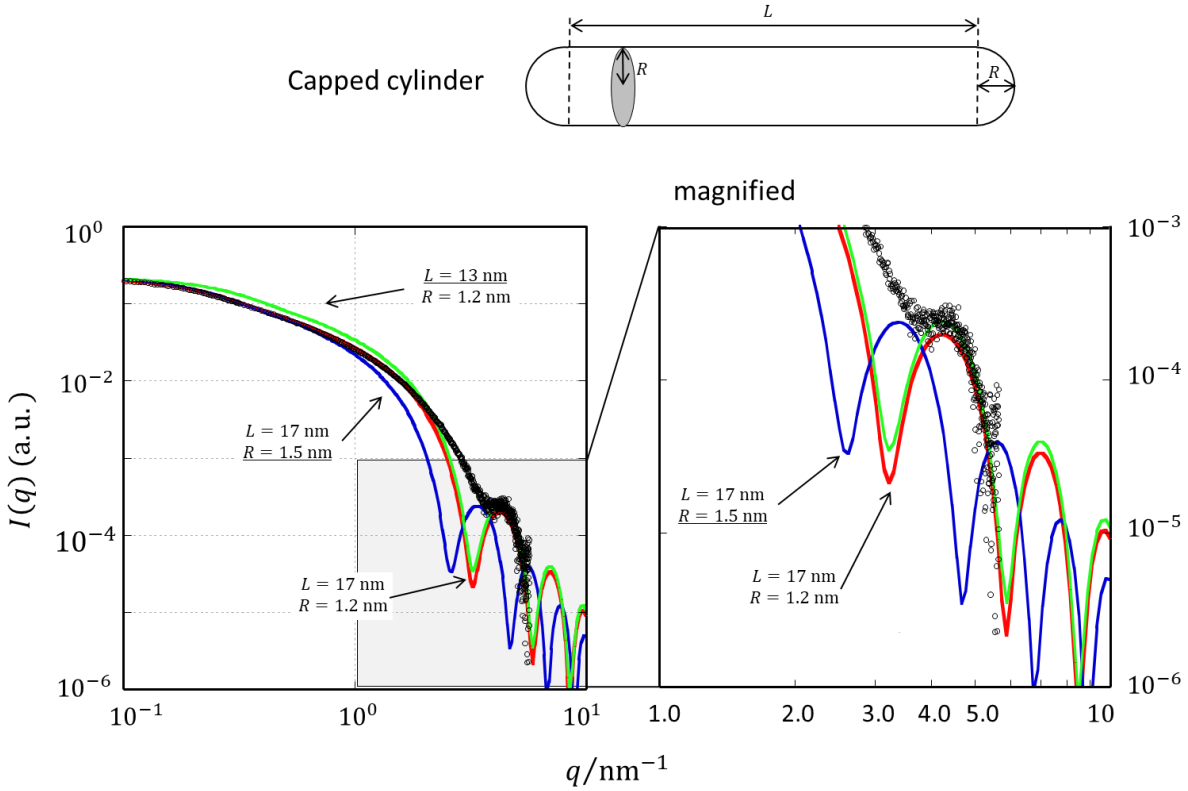

Figure 2-8. SAXS profile for q1-dA60-SPG comparing with theoretical values calculated from Eq 5 with three different parameter sets. A capped cylinder model is also presented. The best fitted curve was given by $L = 17$ nm and $R = 1.2$ nm.

Figure 2-9 plots $\langle S^2 \rangle_z$ obtained by MALS and SAXS against M_w. The three straight lines show the relations expected for rigid rods with $M_L = 2000,\ 2345,$ and $2840\ \mathrm{nm}^{-1}$, where $2000\ \mathrm{nm}^{-1}$ is for tSPG and $2345\ \mathrm{nm}^{-1}$ was calculated assuming that the one sSPG chain was replaced by a dA chain without changing the pitch, as illustrated in the figure. The data points were not fitted by this M_L. In order to fit the data, it appeared that $M_L = 2840\ \mathrm{nm}^{-1}$ was appropriate. This means that the molecular pitch became shorter by about 20% as the complex formed, as shown by the illustration. A similar result was obtained in our previous paper.[12] We have to admit that, in the previous paper, there was some miss-calculation or error in determining the M_w values (Figure S9 in List of Publications #1). We believe that this was mainly caused by the unfavorable adsorption of phosphorothioate dA_X by the GPC column. We found that this problem was overcome by adding EDTA in the elute solvent. The corrected $\langle S^2 \rangle_z$ values for dA_{60}-SPG(n) are also plotted in the figure as dA_{60}-SPG(n). The best fitting curve was obtained when we chose $q = 21 \pm 0.5\ \mathrm{nm}$ under the condition of fixed $M_L = 2840\ \mathrm{nm}^{-1}$. This value to express flexibility of the worm-like chain seems to be relatively small when we compare with other stiff chains, such as 150 nm (tSPG), 58–68 nm (double helix of DNAs), and 42 nm [poly(hexyl isocyanate)].[8] The right end column in Table 2-4 shows the number of main-chain glucoses in the complexed sSPG chain. They were always slightly larger than the number of dA. This feature suggests that there are some free glucoses between the complex, as illustrated by C in the figure and if these free

ones are present, they may act as a freely rotating joint and thus decreases the flexibility.

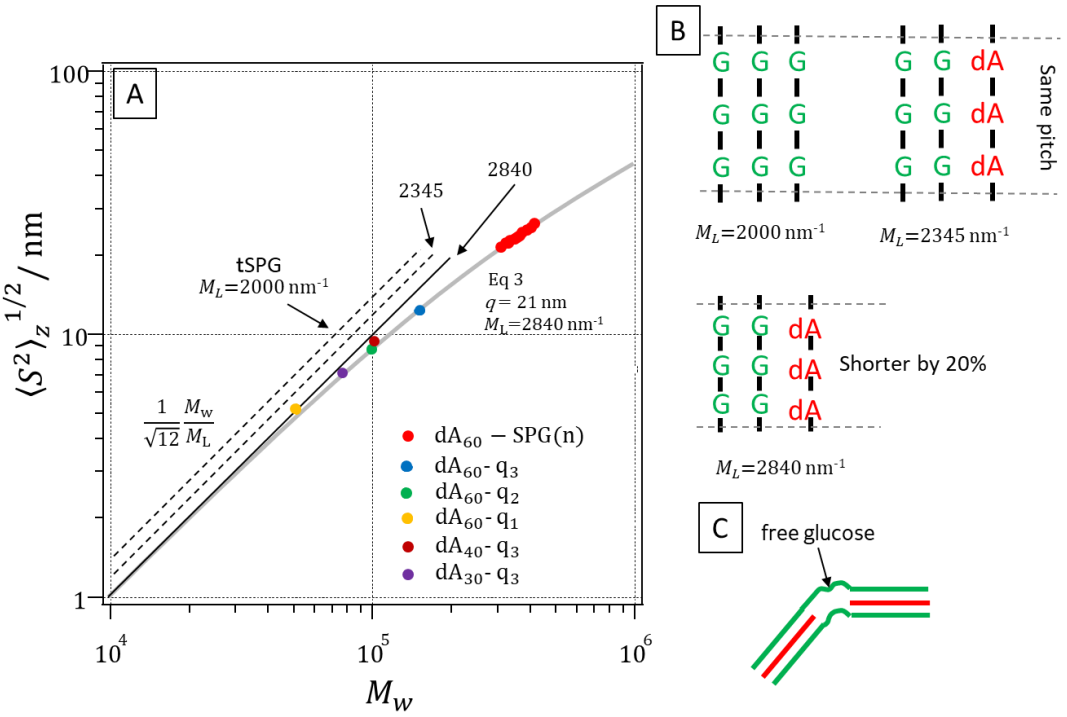

Figure 2-9. Double logarithmic plots of $\langle S^2 \rangle_z$ against M_w for all of the quantized dA$_X$-SPG complexes and dA$_{60}$-SPG(n), comparing with theoretical calculations from the rigid-rod with three different M_L and the Benoit-Doty equation with the best fitted parameters. In the right margin, B: schematic models of the main chain of the complex and tSPG, and C: presence of the free glucoses to explain a relatively small persistence length.

2-4 Conclusion

Supramolecular self-assembly can provide beautifully well-organized structures in a large scale, even up to 100 nm. However, this may not always be true when macromolecules are involved. Macromolecules inherently have distributions in length and structure and thus, when they form a supramolecular complex, the resultant structures may be kinetically trapped and frozen before reaching the most stable one. This causes distribution and diversity to a certain extent. Nature may avoid creating such diversity by the use of heterologous sequences in DNA and peptides. In this sense, it is surprising that homopolymers such as SPG and dA_X form a stoichiometrically defined complex with the best fitting length. In this paper, we have demonstrated that dA_{60} meticulously selects sSPG having 60, 120, or 180 main-chain glucoses from a large group containing different lengths of sSPG. In other words, the dA_{60}-SPG complex formation is a quantized phenomenon only occurring between dA_{60} and sSPG with a certain chain length. In terms of how dA_X chooses the right length, the mechanism behind this is still unknown. Presumably, they may exchange chains with each other to reach the minimum free energy without being kinetically trapped in intermediate states. As mentioned in the introduction, the SPG/DNA complexes have demonstrated excellent therapeutic efficacy in animal studies and the currently used complex has a relatively larger molecular weight of about 6×10^5 than the complex studied in this paper. The small complexes may show different pharmacokinetics due to their small size and can become the next new pipeline to deliver therapeutic oligonucleotides.

2-5 Reference

1. Norisuye, T.; Yanaki, T.; Fujita, H., Triple helix of a schizophyllum commune polysaccharide in aqueous solution. *Journal of Polymer Science: Polymer Physics Edition* **1980,** *18* (3), 547-558.

2. Kojima, T. T., K.; Yankai, T 1526909, 1989.

3. Synytsya, A.; Novak, M., Structural analysis of glucans. *Ann Transl Med* **2014,** *2* (2), 17.

4. Kono, H.; Kondo, N.; Hirabayashi, K.; Ogata, M.; Totani, K.; Ikematsu, S.; Osada, M., NMR spectroscopic structural characterization of a water-soluble β-(1→3, 1→6)-glucan from Aureobasidium pullulans. *Carbohydr Polym* **2017,** *174*, 876-886.

5. Ghareeb, H. O.; Malz, F.; Kilz, P.; Radke, W., Molar mass characterization of cellulose acetates over a wide range of high DS by size exclusion chromatography with multi-angle laser light scattering detection. *Carbohydrate Polymers* **2012,** *88*, 96-102.

6. Sakurai, K.; Mizu, M.; Shinkai, S., Polysaccharide – Polynucleotide Complexes. 2. Complementary Polynucleotide Mimic Behavior of the Natural Polysaccharide Schizophyllan in the Macromolecular Complex with Single-Stranded RNA and DNA. *Biomacromolecules* **2001,** *2* (3), 641-650.

7. Kashiwagi, Y.; Norisuye, T.; Fujita, H., Triple helix of Schizophyllum commune polysaccharide in dilute solution. 4. Light scattering and viscosity in dilute aqueous sodium hydroxide. *Macromolecules* **1981,** *14* (5), 1220-1225.

8. Fujita, H., In *Polymer Slutions*, Elsevier: Amsterdam, 1990; Vol. 9.

9. Benoit, H.; Doty, P., Light Scattering from Non-Gaussian Chains. *The Journal of Physical Chemistry* **1953,** *57* (9), 958-963.

10. Kaya, H., Scattering from cylinders with globular end-caps. *Journal of Applied Crystallography* **2004,** *37* (2), 223-230.

11. Cusack, S.; Miller, A.; Krijgsman, P. C.; Mellema, J. E., An investigation of the structure of alfalfa mosaic virus by small-angle neutron scattering. *J Mol Biol* **1981,** *145* (3), 525-39.

12. Sanada, Y.; Matsuzaki, T.; Mochizuki, S.; Okobira, T.; Uezu, K.; Sakurai, K., β-1,3-d-Glucan Schizophyllan/Poly(dA) Triple-Helical Complex in Dilute Solution. *The Journal of Physical Chemistry B* **2012,** *116* (1), 87-94.

13. Kono, H.; Kondo, N.; Hirabayashi, K.; Ogata, M.; Totani, K.; Ikematsu, S.; Osada, M., Two-dimensional NMR data of a water-soluble β-(1→3, 1→6)-glucan from Aureobasidium pullulans and schizophyllan from Schizophyllum commune. *Data Brief* **2017,** *15*, 382-388.

14. Yanaki, T.; Norisuye, T., Triple Helix and Random Coil of Scleroglucan in Dilute Solution. *Polymer Journal* **1983,** *15* (5), 389-396.

15. Sato, T.; Norisuye, T.; Fujita, H., Triple helix of Schizophyllum commune polysaccharide in dilute solution. 5. Light scattering and refractometry in mixtures of water and dimethyl sulfoxide. *Macromolecules* **1983,** *16* (2), 185-189.

16. Yanaki, T.; Norisuye, T.; Fujita, H., Triple Helix of Schizophyllum commune Polysaccharide in Dilute Solution. 3. Hydrodynamic Properties in Water. *Macromolecules* **1980,** *13* (6), 1462-1466.

17. Stokke, B. T.; Elgsaeter, A.; Brant, D. A.; Kitamura, S., Supercoiling in circular triple-helical polysaccharides. *Macromolecules* **1991,** *24* (23), 6349-6351.

18. Shimada, J.; Yamakawa, H., Moments for DNA topoisomers: The helical wormlike chain. *Biopolymers* **1988,** *27* (4), 657-673.

19. Miyoshi, K.; Uezu, K.; Sakurai, K.; Shinkai, S., Polysaccharide – Polynucleotide Complexes. Part 32. Structural Analysis of the Curdlan/Poly(cytidylic acid) Complex with Semiempirical Molecular Orbital Calculations. *Biomacromolecules* **2005,** *6* (3), 1540-1546.

20. Shi, X.; Macgregor, R. B., Jr., Effect of cesium on the volume of the helix-coil transition of dA.dT polymers and their ligand complexes. *Biophys Chem* **2007,** *130* (3), 93-101.

CHAPTER 3. Affinity Evaluation of SPG/DNA Complexes with Dectin-1

3-1 Purpose of this chapter

The objective is to show that SPG/DNA complexes can serve as an effective drug delivery system to human dectin-1. Previous studies have shown that these complexes carry drugs by targeting mouse-derived dectin-1, but there is little research on human dectin-1. For pharmaceutical applications, it is essential to study the behavior of complexes targeting human dectin-1. Therefore, our research focused specifically on evaluating the affinity between human dectin-1 and SPG/DNA complexes. This evaluation is intended to lay the groundwork for understanding the potential future therapeutic applicability of the complex in humans. We hope to contribute to new advances in the field of drug delivery by characterizing complexes that bind to human dectin-1 and exploring how they might work in real therapeutic scenarios.

3-2 Experimental Section

3-2-1 Materials and their characterization

SPG used in this experiment was S-3n, shown in the previous section. All DNA samples were synthesized by Gene Design Co., Ltd. (Osaka, Japan), and purified by high-performance liquid chromatography. Table 3-1 summarizes these DNA sequences. The six cDNAs for human Dectin-1 variants were obtained from three cell lines (CML-1, Mel15, and GC1) by Fujiwara et al. and we used their cDNA.[1]

Table 3-1. DNA sequences used in this thesis

Sample name	DNA sequence (5'→3')
dA_{40}	AAAAAAAAAAAAAAAAAAAAAAAAAAAAAAAAAAAAAAAA
s-dA_{40}	A^A^A^A^A^A^A^A^A^A^A^A^A^A^A^A^A^A^A^A^A^A^A^A^A^A^A^A^A^A^A^A^A^A^A^A^A^A^A^A[(a)]
YB-1-AS	A^C^T^G^G^G^G^C^C^G^G^C^T^G^C^G^G^C^A^G^C^T^G^C^G – s-dA_{40}
K-ras-AS	C^G^G^G^A^G^T^A^C^T^G^G^C^C^G^A^G^C^C^G^C^C^G^C^C – s-dA40
Alexa546-YB-1-AS	Alexa546-A^C^T^G^G^G^G^C^C^G^G^C^T^G^C^G^G^C^A^G^C^T^G^C^G – s-dA_{40}
K3	A^T^C^G^A^C^T^C^T^C^G^A^G^C^G^T^T^C^T^C – s-dA_{40}
FAM-YB-1-AS	FAM-A^C^T^G^G^G^G^C^C^G^G^C^T^G^C^G^G^C^A^G^C^T^G^C^G – s-dA_{40}

AS-YB-1	s-dA40– A^C^T^G^G^G^C^C^G^G^C^T^G^C^G^G^C^A^G^C^T^G^C ^G
K-ras-AS-YB-1	C^G^G^G^A^G^T^A^C^T^G^G^C^C^G^A^G^C^C^G^C^C^G^C ^C – s-dA40– A^C^T^G^G^G^C^C^G^G^C^T^G^C^G^G^C^A^G^C^T^G^C ^G

(a) ^ indicates phosphorothioate oligonucleotides.

3-2-2 Cell culture

The following cell lines and primary cells were used. PC-3 (human prostate cancer cell line), PC-9, A549 (human lung cancer cell line), HEK293 (human fetal kidney cell line), human peripheral blood mononuclear cells (PBMCs) derived from anonymous, healthy donors PBMCs were purchased from M&S TechnoSystems Inc. (Tokyo, Japan). PC-9, and PBMCs were cultured in RPMI 1640 medium, GlutaMAX™ (Life Technologies, Tokyo, Japan), PC-3, HEK293, and A549 was cultured in DMEM, and both were maintained in a 5% CO_2 atmosphere at 37 °C.

3-2-3 Preparation of SPG/DNA complexes

SPG was dissolved in 0.25N NaOH aq. for 1 h and the alkaline SPG solution was mixed with DNA samples in 330 mM NaH_2PO_4. At this time, the feeding molar ratio of [SPG]: [dA] was 1:4. After mixing, the mixture was stored at 4 °C for 24 h.

3-2-4 Flow cytometry and cell sorting

Fluorescence-conjugated anti-human Dectin-1 antibody and all other antibodies were purchased from Miltenyi Biotec K.K. The antibodies used for staining were against the following proteins. Dectin-1 (REA515), CD19 (LT19), CD14 (TÜK4), CD11c (REA618). Human PBMCs were stained for multicolor flow cytometry analysis using a standard method. In brief, cells were incubated with flow cytometry (FCM) buffer (PBS, 0.1% NaN_3, 2% fetal bovine serum) with the antibodies in the dark on ice for 10 min. Isotype control antibodies were used where appropriate to determine the background binding of antibodies and to set gates. Cell populations obtained by antibody staining were collected using a BD FACSMelody™ Cell Sorter (BD biosciences). BD FACSFlow sheath fluid (BD Biosciences) was used to operate all sorters and manufacturer's standard startup, cleaning and QC procedures were applied.

3-2-5 Stable transfectants of six Dectin-1 variants

pEBMulti-GFP-T2A-Puro vector (Wako Pure Chemical Industries, Ltd., Osaka, Japan)[1] expressing FLAG-tagged hDectin-1 variants was transfected into HEK293T cells (1×10^5 cells) using X-tremeGENE 9 DNA Transfection Reagent (Sigma, St. Louis, MO), in accordance with the manufacturer’s instructions. After transfection, these cells were cultured with 10 ng/mL puromycin (Invitrogen, Carlsbad, CA) for 2 weeks and successfully created transfectants were selected.

3-2-6 Transient expression of hDectin-1 variants with doxycycline

pEB Tet-On GFP-T2A-Puromycin vector[2] expressing FLAG-tagged hDectin-1 variants was transfected into PC-3. These cells were selected using the same method as in the previous section. After that, hDectin-1 was transiently expressed by adding 10 μg/mL doxycycline and culturing for 24. The cells were then washed twice with PBS and a fresh medium was added to stop new protein synthesis. The cells were then collected every 24 h, and the amount of expressed hDectin-1 variants was analyzed by western blotting. The half-life time of the variants was calculated using a sigmoid function.

3-2-7 Deglycosylation assay by PNGase F

Deglycosylation assay was performed with peptide-N-glycosidase F (PNGase F; New England Biolabs, Ipswich, MA), in accordance with the manufacturer's instructions. HEK293T cells expressing each Dectin-1 variant were lysed with lysis buffer containing 10 mM Tris-HCl (pH 7.9), 150 mM NaCl, 0.5% NP-40, and 1 mM PMSF. After centrifugation (14000rpm, 10 min at 4 ℃), each supernatant was immunoprecipitated with anti-Flag antibody and washed twice with lysis buffer by centrifugation. Immunoprecipitated samples were incubated with glycoprotein denaturing buffer at 100 ℃ for 10 min and cooled on ice for 10 s. GlycoBuffer, 10% NP-40 and PNGase F were added to the samples, which were then incubated at 37 ℃ for 1 h. The deglycosylated proteins were immunoprecipitated and immunoblotted with anti-Flag antibody.

3-2-8 Purification of wild and mutant the extracellular domain of Dectin-1 from HEK293T cells

The expression vector encoding wild and mutant the extracellular domain of Dectin-1 was transfected into HEK293T cells using X-tremeGENE 9 DNA Transfection Reagent (Sigma, St. Louis, MO). After incubation for 2 weeks with 10 ng/mL puromycin, the conditioned supernatants were collected. The extracellular domain of Dectin-1 with 6×His and Flag tag was purified by use of xTractor™ Buffer & Buffer Kits (Takara Bio, Shiga, Japan).

3-2-9 Interaction between the extracellular domain of hDectin-1 and SPG/DNA complexes determined with QCM

A 27 MHz QCM (AFFINIX QN l; INITIUM, Inc., Tokyo, Japan) was used for binding assays between the extracellular domain of hDectin-1 variants and SPG or SPG/DNA complexes. Anti 6×His antibody (Thermo Scientific, cat: MA1-21315) was immobilized on a gold substrate of the QCM sensor cell (INITIUM, Inc.). After blocking with 1% BSA in PBS for 1 h, the extracellular domain of Dectin-1 variants in PBS was added into the sensor cell and incubated for 1 h at room temperature. After washing with PBS, the sensor cell was filled with 500 μL of PBS containing 1 mM EDTA and added the samples and measured the frequency changes at 25 ℃.

3-2-10 Uptake of FITC-labeled SPG and Alexa546 and FAM-labeled SPG/YB-1 complexes

FITC-labeled SPG was synthesized by a previously reported method[3, 4] and Fluorescence-labeled SPG/YB-1 AS complexes were prepared by complexation

with Alexa546-labeled YB-1 AS and FAM-labeled-YB-1 AS. We prepared HEK293T cells which express Dectin-1 variants. The hDectin-1 transfectants (5 × 10^5 cells) were seeded in collagen-coated 6-well plates (IWAKI, Shizuoka, Japan, cat: 4810-010) and incubated for 24 h. FITC-labeled SPG (15 μg/ml) and Alexa546-labeled SPG/YB-1 AS (100 nM) were added to the medium and incubated for 1 h. After washing with PBS twice, an image of the cells was obtained with an EVOS® FL Imaging System (Thermo Scientific). For the analysis by use of a BZ-X800 (Keyence Corporation, Osaka, Japan), the cells were cultured at 3 × 10^5 cells/well in collagen-coated dishes (Nippi) for 24h, and then incubated with fluorescence-labeled SPG/YB-1-AS at 100 nM. After 1 h or 6h of incubation, the cells were stained by DAPI (Dojindo, Kumamoto, Japan) and LysoTracker® (Thermo Scientific) and then fixed with 10% paraformaldehyde for structured illumination microscopic image and 3D image. Fluorescence intensity was analyzed using the software installed in a BZ-X800.

3-2-11 Preparation of cell membrane components and Western blotting.

Whole cell lysates were prepared from 5 x 10^6 cells as previously described manner. [19] Cell membrane lysates then were obtained from 5 × 10^6 cells as well as cell lysate using a Minute Plasma Membrane Protein Isolation Kit (Invent Biotechnologies, Eden Prairie, MN, USA) according to the manufacturer's instructions. The same volume for both samples was transferred to a 15% polyacrylamide gel for SDS-PAGE, and then the transferred membrane was

immunoblotted with Flag antibody. Protein expression level was quantitated by use of Multi Gauge version 3.0 software (Fujifilm, Tokyo, Japan).

3-2-12 WST-8 assay

The hDectin-1 transfectants were seeded at 1.0×10^3 in a 96-well plate and incubated for 24 h at 37 °C under 5% CO_2. The complexes were added at a YB-1-AS concentration of 1.0 μM. After incubation for 72 h, the cellular growth was determined using Cell Counting Kit-8 (Dojindo, Kumamoto, Japan).

3-2-13 Analysis of hDectin-1 cDNA by RT-PCR

Total RNAs of the sample were obtained using the RNeasy Mini Kit (Qiagen, Hilden, Germany). To generate the cDNA, SuperScript® III RT (Invitrogen) was used. The multiple-PCR amplification method primers used in this study were as follows: forward: 5′ -ATGGAATATCATCCTGATTTAGAAAATTTG-3′ and reverse: 5′-CCATGGTACCCAGGACCACAG-3′. The 1st PCR primers were as follows: forward: 5′ -ATGGAATATCATCCTGATTTAGAAAATTTG-3′ and reverse: 5′ -TTACATTGAAAACTTCTTCTCACAAATACT-3′. The 2nd PCR primers were as follows: forward: 5′ - GTGATAGCTGTGGTCCTGGG-3′ and reverse: 5′ -GATGGGTTTTCTTGGGTAGCTGTGG-3′. When performing PCR, we used Ex Taq (Takara Bio, Shiga, Japan), according to the manufacturer's instructions. the PCR reaction conditions were as follows: 95 ℃ for 5 min, followed by 35 cycles of 95 ℃ for 15 s, 55 ℃ for 15 s and 72 ℃ for 60 s. The cDNA generated by 1st round PCR was purified, loaded into DNA chip, and assayed using a Bioanalyzer 2100 (Agilent Technologies)

3-2-14 Statistical analysis

All values are presented as mean ± standard deviation (SD). The statistical significance of differences between groups was determined using Student's t-test.

3-3 Results

3-3-1 Regarding Human Dectin-1 Variants

Both mouse and human Dectin-1 (hereinafter denoted with the prefix m or h for mouse or human, respectively. For example, mDectin-1, hDectin-1, hCRD, and hV-1) are composed of four parts, as shown in Figure 3-1: CRD, the transmembrane region, the stalk, and the N-terminal cytoplasmic tail.[5, 6] There are several variants due to alternative splicing and exon skipping of the Dectin-1 mRNA. Two variants (mV-1 and mV-2) are known in the mouse. mV-1 has all four parts, while mV-2 lacks the stalk region consisting of 46 amino acid residues.[6] Adachi and Yamaguchi have shown that Trp221, His223, and Tyr228 in exon 6 of mV-1 play important roles in the binding to β-1,3-glucan.[7, 8] Figure 3-2 shows the structure of the hDectin-1 mRNA (CLEC7A) and its alternative spliced variants, which is based on the work of Willment et al.[9] They reported that there are eight variants, of which only two variants (hV-1 and hV-2) have the complete CRD. These two variants are considered to bind more tightly to β-1,3-glucans than the others, and most of the preceding studies have focused on these two variants. At present, the biological roles of other variants are not clear. The amino acids required for β-1,3-glucan binding in hDectin-1 have not been identified. Given the high degree of homology between hDectin-1 and mDectin-1, with approximately 60% of the amino acid sequence identical, it is reasonable to expect that the same amino acids are involved in β-1,3-glucan binding in hDectin-1 as in mDectin-1. To confirm this speculation is one of the major aims of the study. The other difference between mDectin-1 and hDectin-

1 is the number and location of N-linked glycosylation sites. Since the amino acids sequence undergoing N-linked glycosylation is Asn-X-Ser/Thr,[10] both mV-1 and mV-2 have two N-linked glycosylation sites in their CRD. In contrast to mDectin-1, hDectin-1 has one N-linked glycosylation site in the stalk region. Therefore, hV-2 should not undergo N-linked glycosylation as illustrated in Figure 3-1.

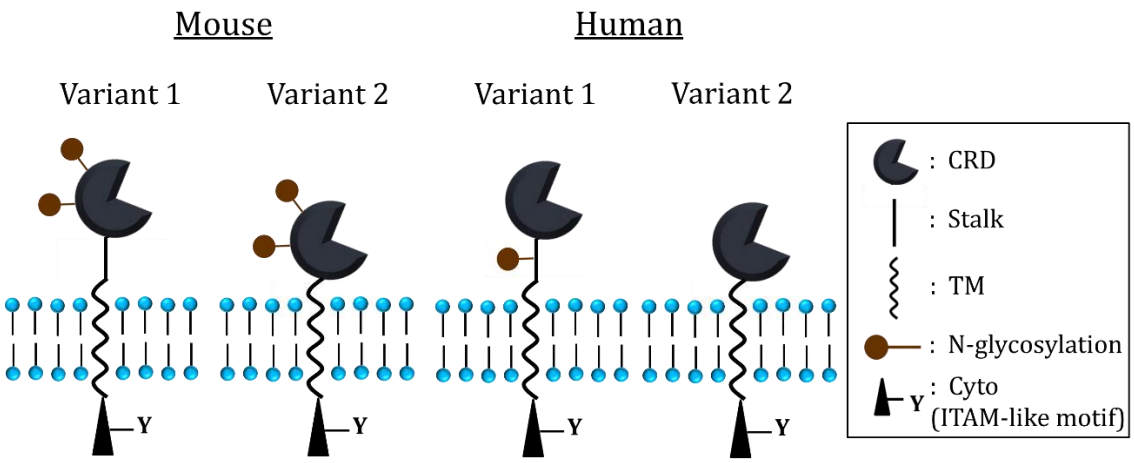

Figure 3-1 Schematical illustration of mouse and human Dectin-1s expressing on the cellular surface and their difference in the N-glycosylation site.

Willment et al[9] reported that two exon-skipping mutations can occur in hDectin-1 and these two exons are denoted as 2' and 4' in Figure 3-2. Among the eight variants, hV-7 does not skip 4' and hV-8 does not skip either 4' or 2'. In each variant, a new stop codon appears due to the frameshift caused by the absence of exon skipping. Fujiwara et al[1] examined the hDectin-1 variants extracted from chronic myelogenous leukemia-derived cells (CML-1) and confirmed the presence of the eight variants; however, there were several differences between the results in the two studies. These differences may be due to the different cell lines used in the analysis, where Willment et al used

NIH3T3 fibroblasts (ATCC no.TIB-71) and the HEK293T cell line. First, Willment's exon 4' was 86 bp, and Fujiwara's was 87 bp (to distinguish, we denote it as exon X). At this time, when we re-examined the previous data, we found that the number of bases was 87, not 86. Perhaps Fujiwara et al. had reported a miscounting error. Still, since the exact sequence of exon 4' has not been reported yet, it is difficult to confirm Willment's result and compare the two results (our exon X sequence is shown in S1 in List of Publications #5). Therefore, in this paper, we regard that Fujiwara' s hV-7 is similar to Willment's hV-7, but they are different because of the different base numbers. We denote Fujiwara's hV-7 as hV-A as illustrated in Figure 3-2. Secondary, Fujiwara found another exon that locates at the same position as exons 4' and X but has a different sequence from X (denoted Y). When the exon skipping does not occur at Y, the stop codon appears at the No 5 region. We denote this variant as hV-B and its structure is shown in Figure 3-2. We believe that this hV-B is first discovered as one of the human Decrin-1 variants. Third, Fujiwara could not find exon 2' and thus did not obtain hV-8 that does not skip exon 2'. We treat exons X and Y as new different exons in this study. Both hV-A and hV-B have transmembrane regions and thus their CRD may be expressed on the cell surface although they do not have the complete CRD without the key peptides of Trp222, His224, and Tyr229, as shown in Figure 3-2. The confirmation of the above-mentioned Fujiwara's results is one of the aims of this paper.

Mochizuki et al demonstrated that the SPG complexes and SPG itself bind to the complete mCRD using quartz crystal microbalance (QCM).[11] They prepared two mCRD mutants (rW221A and rH223A) and found that SPG/s-dA_X (again s-dA_X stands for phosphorothioate dA_X) maintained affinity toward the mutants, while original SPG and SPG/dA (natural phosphodiester) lost affinity completely. These results can be explained by the hypothesis that there seemed to be multiple binding sites in mCRD; the same site as SPG and SPG/dA_X, and an additional site (or sites) only for SPG/s-dA_X. In the additional sites, phosphate anion-specific electrostatic interactions may be mainly involved to create the attractive interaction. Fujiwara et al. transfected PC-3 cells (human prostate cancer cell line), which are known to express no hDectin-1 at all, with the corresponding genes to code hV-1, hV-2, hV-B, or hV-4. After the transfection, they examined binding to SPG or SPG/s-dA_X. As expected from the structure of CRD and the QCM results, only hV-1 and hV-2 transfected cells showed an affinity for SPG, but all cells showed a positive affinity for SPG/s-dA_X. They examined the YB-1 gene silencing for these cells after treating the cells with the SPG/DNA complex containing YB-1 antisense DNA. hV-1 and hV-2 transfected cells showed a significant silencing, while hV-B and hV-4 did not. QCM and transfection results do not seem to match, but the reason for this inconsistency is unclear. This is another motivation to start the present work. We decided to examine all the variants that are supposed expressed on the cell surface, which are hV-1, hV-2, hV-3, hV-4, hV-A, and hV-B.

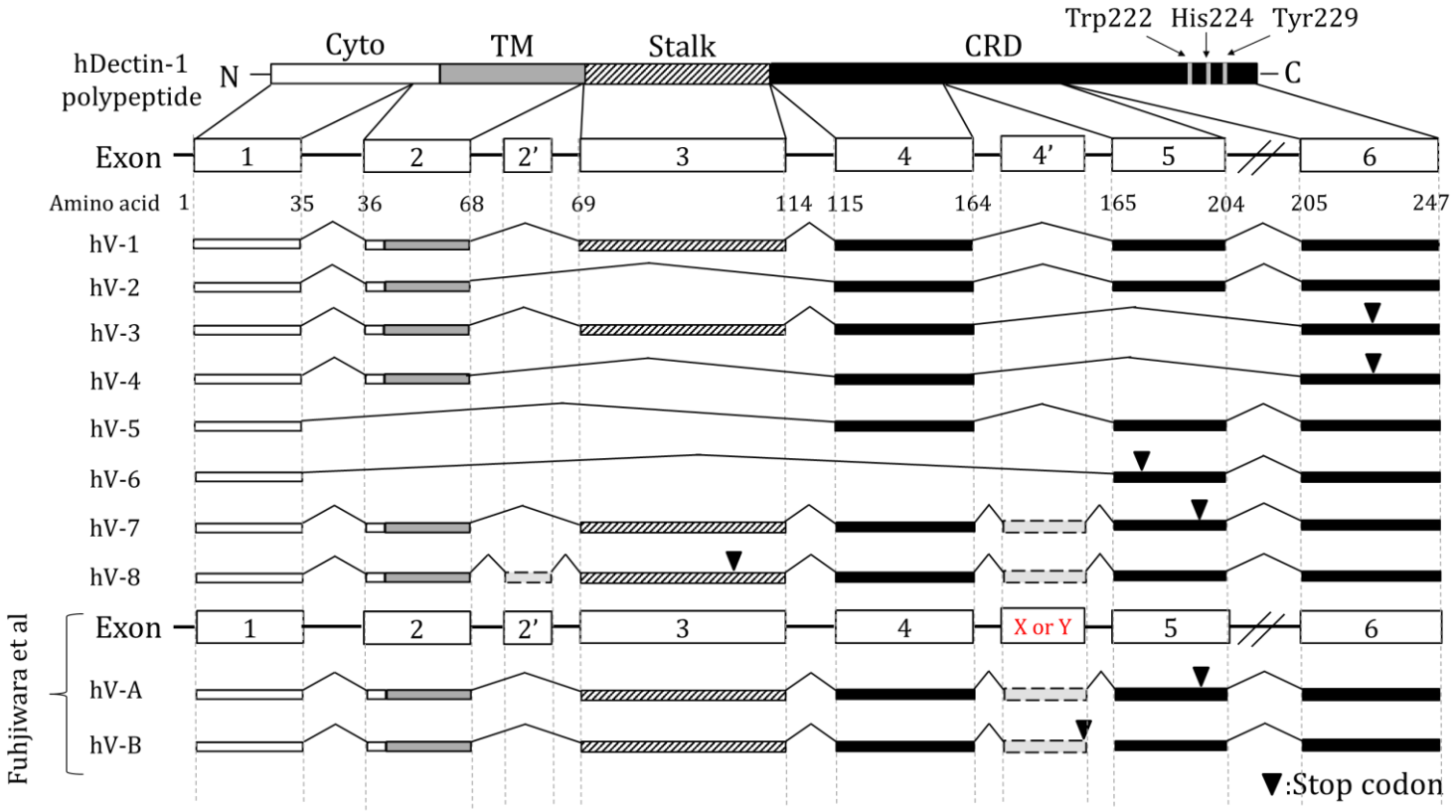

Figure 3-2. mRNA and peptide sequences of human Dectin-1s and their spliced isoforms. Eight exons and their corresponding residues in the protein are indicated by the numbered boxes and the peptide counting the numbers below the protein. The down arrows indicate the stop codon positions. The positions of three peptides: tryptophan 222, histidine 224, and tyrosine 229, which are crucial for binding β-1,3-glucans, are shown. Cyto, cytoplasmic tail; TM, transmembrane regions; CRD, carbohydrate recognition domain. Exon X and exon Y lead to exon skipping and the frameshift, resulting in creating an incomplete CRD, and we found that there are ten variants of hDectin-1, including two new V-A and V-B in addition to the eight variants.

3-3-2 Glycosylation of hDectin-1 variants: finding a new glycosylation site

hDectin-1 cDNAs were obtained from CML-1 and other cell lines by Fujiwara et al[1] and we used those. Six cDNAs corresponding to the six variants, hV-1, hV-2, hV-A, hV-3, hV-B, and hV-4, were prepared, and each was inserted into a plasmid DNA vector at the position after Flag coding region and the vectors were transfected into HEK293T cells. Their whole-cell lysates were analyzed by western blotting. After being stained with an anti-Flag antibody, the obtained image was presented in Figure 3-3-A. hV-1 showed three bands: the relatively clear top band, a faint middle one, and the bottom one. The bottom one showed a much lower molecular weight than expected from its sequence. Similar bottom bands were observed in hV-A and hV-3. These three variants have the stalk. Fujiwara et al and Kato et al observed the same bottom bands for the variants having the stalk (see Figure 5A and 3, respectively in their paper).[1, 12] We suppose that this low molecular weight band was created by enzymatic cleavage of a specific site. Therefore, we focused on these upper bands that express the full length Dectin-1. The top band in hV-1 shows a larger molecular weight than that calculated, while hV-2 shows the expected value of 27 kDa. As shown in the previous studies, the disagreement in the molecular weight in hV-1 is caused by N-glycosylation. Figure 3-3-B shows the Western blot results after de-glycosylated by PNGase F, compared with the untreated samples. hV-1 decreased the molecular weight, while hV-2 did not move, confirming that hV-1 is N-glycosylated, while hV-2 is not. This result is explained by the fact that the stalk site is modified by N-linked glycosylation in hDectin-1, as shown in

Figure 3-2. Note that we have confirmed the good reproducibility of the results that Fujiwara et al obtained for the same cells.

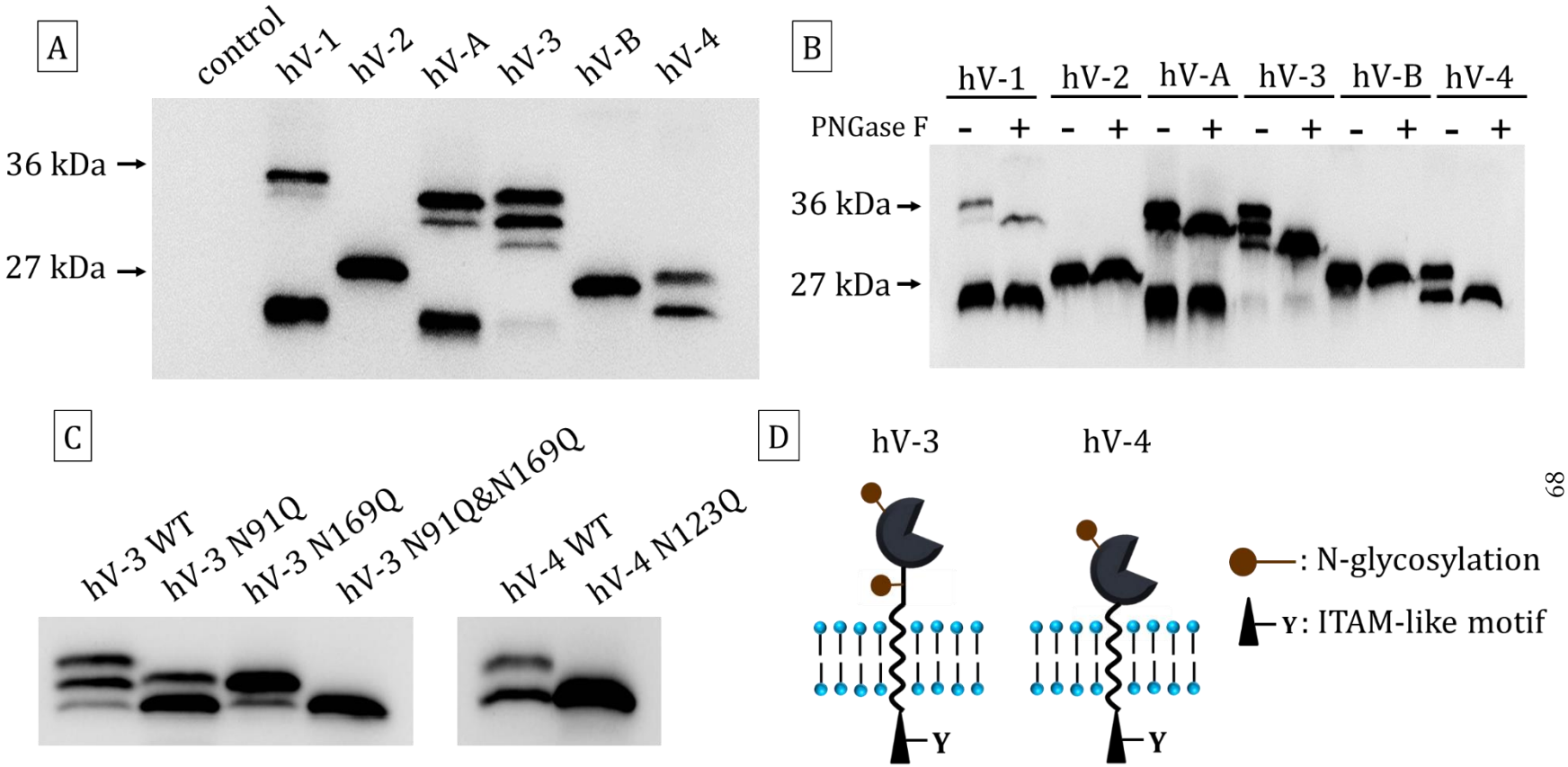

Figure 3-3. The western blotting before and after the de-glycosylation treatment for six hDectin-1 variants and their mutants. (A) western blotting assays (15% SDS-PEG) using anti-Flag antibody for the six hDectin-1 variants, (B) comparison before and after de-glycosylation with PNGase F, (C) Comparison of the hV-3 and hV-4 wild type and their respective mutants, (D) Models of glycosylated hV-3 and hV-4, note to compare Figure 3-1.

Neglecting the bottom band, hV-A gives two bands and hV-3 gives three bands. In the deglycosylation assay, the top band in hV-A and the top and middle two bands in hV-3 merged into the lower band. These results indicate that there were two glycosylation sites in hV-3, whereas there was only one in hV-A. With a similar discussion, hV-B has no glycosylation, and hV-4 has one. Note that hV-4 is glycosylated, but does not have the stalk, indicating that there is a new glycosylation site in the CRD of hV-4. As discussed in Figure 3-2, the frameshift due to skipping exon 5 has occurred in hV-4 and thus the amino acid sequence of its CRD should be different from hV-1 and hV-2. Since the same frameshift occurred in hV-3, hV-3 and hV-4 have the same CRD. Their peptide sequences suggest that Asn169 at hV-3 and Asn123 at hV-4 are glycosylated because they satisfy the peptide sequence requirement for the glycosylation (i.e., Asn-X-Ser/Thr).[10] To prove this, we created three mutants Asn91Gln (stalk) and Asn169Gln (CRD) in hV-3 and Asn123GLn (CRD) in hV-4 and carried out western blot (Figure 3-3-C). The mutants (N91Q&N169Q for hV-3 and N123Q for hV-4) showed only one band corresponding to the lower bands in Figure 3-3-B. Based on the results, we concluded that hV-3 and hV-4 have the structures shown in Figure 3-3-D. A new N-glycosylation site was first identified in the CRD region of hDectin-1 V-3 and V-4.

There is another issue that was not clear in the previous draft. The molecular weights of hV-A, hV-3, hV-B, and hV-4 did not match those calculated from their peptide sequence. These discrepancies may be attributed to the glycosylation. When we compared the molecular weights after the de-glycosylation, there is still a nonnegligible discrepancy. Except for N-glycosylation, there are various post-translational modifications of proteins, including phosphorylation, ubiquitination, nitrosylation, and so on.[13,14] We suppose that the discrepancy in the molecular weight may be caused by one or more of them.

3-3-3 QCM binding assay of the SPG complexes for different variants of hCRD: the presence of a new binding in human Dectin-1 that only binds the phosphorothioate SPG/s-dA, similarly to mouse.

hCRD can have four different amino acid sequences due to exon skipping. We created these four types of hCRDs bearing Flag and 6×His tag from the cDNAs of V-2, V-A, V-B, and V-4 described above (hereinafter denoted hCRD-V2, hCRD-VA, hCRD-VB, and hCRD-V4). After confirming the molecule weighs, we coated them on a QCM sensor surface and evaluate the affinity for SPG, SPG/dA_{40} and SPG/s-dA_{40} Figure 3-4 shows some of the results of QCM. As shown by Mochizuki et al for mCRD,[11] we found that hCRD-V2 shows almost the same affinity for SPG and SPG/dA_{40}, although slightly weaker for SPG/dA_{40}.[9] SPG/s-dA_{40} clearly showed a stronger binding than the others and this high affinity is maintained in the SPG complex having a hetero sequence (see Figure S4 in List of Publications #5). The naked dA_{40} showed a non-negligible decrease, suggesting that there may be involving non-specific binding to some extent, probably due to the hydrophobicity of the phosphorothioate. We carried out the same assay for hCRD-VA, hCRD-V4, and hCRD-VB (see Figure S5 in List of Publications #5). Both SPG and SPG/dA_{40} completely lost binding in all three variants, because these variants lost the key domain. On the contrary, SPG/s-dA_{40} still maintained the almost same affinity, although to a slightly weaker extent.

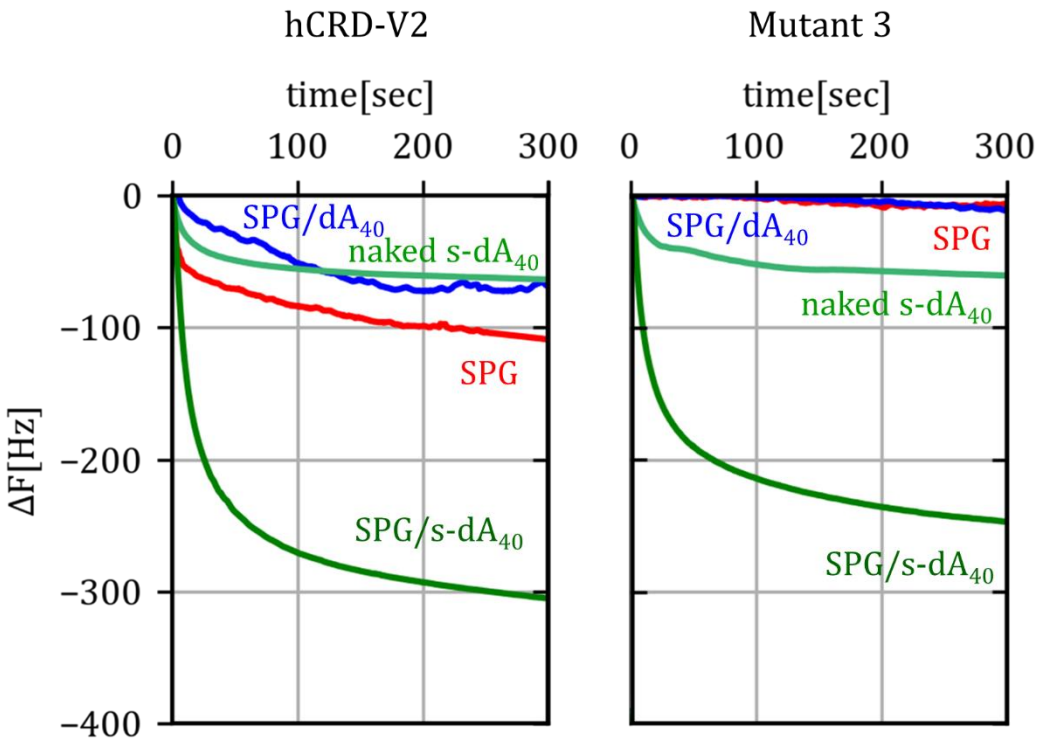

Figure 3-4. The hCRD binding assay with QCM for SPG, SPG/dA$_{40}$ and SPG/s-dA$_{40}$ for the wild type hDectin-1-V2 and mutant 3.

As mentioned in the introduction, Mochizuki et al[11] carried out a similar QCM assay for mCRD and found that SPG/s-dA$_{40}$ bind more strongly to mCRD than both SPG and SPG/dA$_{40}$. After they replaced the two key peptides (H223 and W221 in mCRD) with alanine, SPG and SPG/dA$_{40}$ lost affinity at all, but SPG/s-dA$_{40}$ maintained it. Based on these results, they concluded that there are multiple binding sites in mCRD; the same site as SPG and SPG/dA$_X$, and an additional site (or sites) only for SPG/s-dA$_X$. There is a high degree of homology between hDectin-1 and mDectin-1, and the peptide sequences of the β-1,3-glucan recognition domains of mV-1 and hV-1 are identical, although their numbers are different by one. In hDectin-1, Trp222, His224, and Tyr229 must be

the key peptides. However, these peptides are lacking in hCRD-VA, hCRD-V4, and hCRD-VB due to the stop codon and frameshift. This is the reason that binding with SPG was not observed in the QCM for them. The presence of binding between SPG/s-dA_{40} and hCRD-VA (also hCRD-V4 or hCRD-VB) supports Mochizuki's speculation that there is another binding site other than the key domain. Since electrostatic interactions are involved, they may contain cationic peptides, and some of the cationic peptides exposed on the surface of the protein are possible candidates but have not been identified at this time.

To confirm the key peptides in hDectin-1, we created seven mutants by changing the amino acids of W176, H178, and Y183 in hCRD-V2. We examined the affinity for SPG, SPG/dA_{40} and SPG/s-dA_{40} and the QCM frequency change for Mutant 3 is presented in Figure 3-4. Mutating any of the three peptides resulted in a loss of affinity for SPG and SPG/dA_{40}, similar to the findings of Mochizuki et al., but SPG/s-dA_{40} maintained its affinity, with the degree of affinity being $\Delta F(300)$ ~300 Hz. On the other hand, wild-type hCRD-V2 and SPG/s-dA_{40} exhibited $\Delta F(300)$ ~350 Hz. The $\Delta F(300)$ values did not vary significantly among the mutants. These results indicate that the 300 Hz decrease is associated with a new binding site, while the remaining 50 Hz can be attributed to the same binding site as SPG and SPG/dA40. It's important to note that SPG/s-dA40 is well recognized by all hDectin-1 variants even without the key peptides. (see Figure S5 in List of Publications #5)

3-3-4 Cellular uptake of SPG/YB-1-AS complexes by different hDectin-1 variants: all variants uptake the complex, while hV-1 and hV-2 uptake only SPG.

After preparing six different HEK293T cells expressing one of the six variants, we applied FITC-labeled SPG, Alexa546-labeled YB-1 AS, or the complex made from them, (hereinafter referred to as F-SPG, AlexYB-1, and SPG/AlexYB-1, respectively). After confirming that F-SPG was taken up by hV-1 and hV-2, and AlexYB-1 was interacting with none of them, we applied the complex to the cells (see Figure 3-5). Figure 3-6 compares the structured illumination microscopic (SIM) images for all cells. SIM is a microscopy technique that allows us to observe high particle localization accuracy, and the precise subcellular localization of various nanomaterials can be determined.[15] We can confirm that Alexa546 signal is inside the cells (see Panel B). The results show that SPG/AlexYB-1 is ingested by all variants, although there seemed to be differences in amount. The image analysis showed that the red areas in hV-1, hV-A, and hV-3 are higher than that of hV-2 and hV-4, and extremely low in hV-B. The order of cellular uptake from the microscopy observation does not match that of the binding affinity from QCM. QCM indicated that all four CRDs showed a similar affinity to the complex. Several possibilities can be considered to explain this. (1) Different variants express different amounts at the cell surface, and (2) there are differences in the stability of the variants.

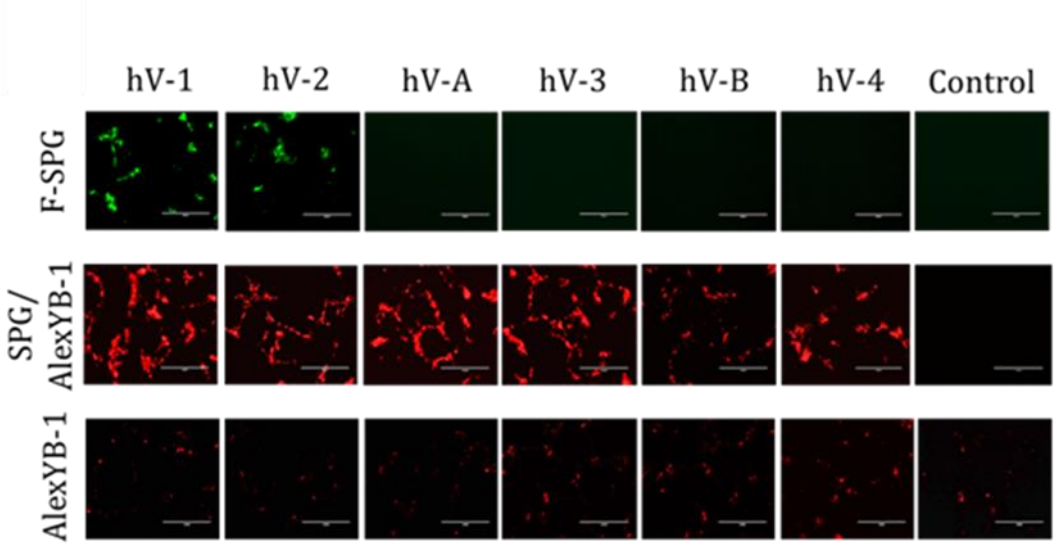

Figure 3-5. Uptake of SPG and SPG/YB-1 complexes after 1 h of incubation. The scale bar represents 100 µm. A: Fluorescence microscopy images of six hDectin-1 variants transfected HEK293T cells after treatment with F-SPG, SPG/AlexYB-1, and naked AlexYB-1. Control is HEK293T cells into which the empty vector was introduced.

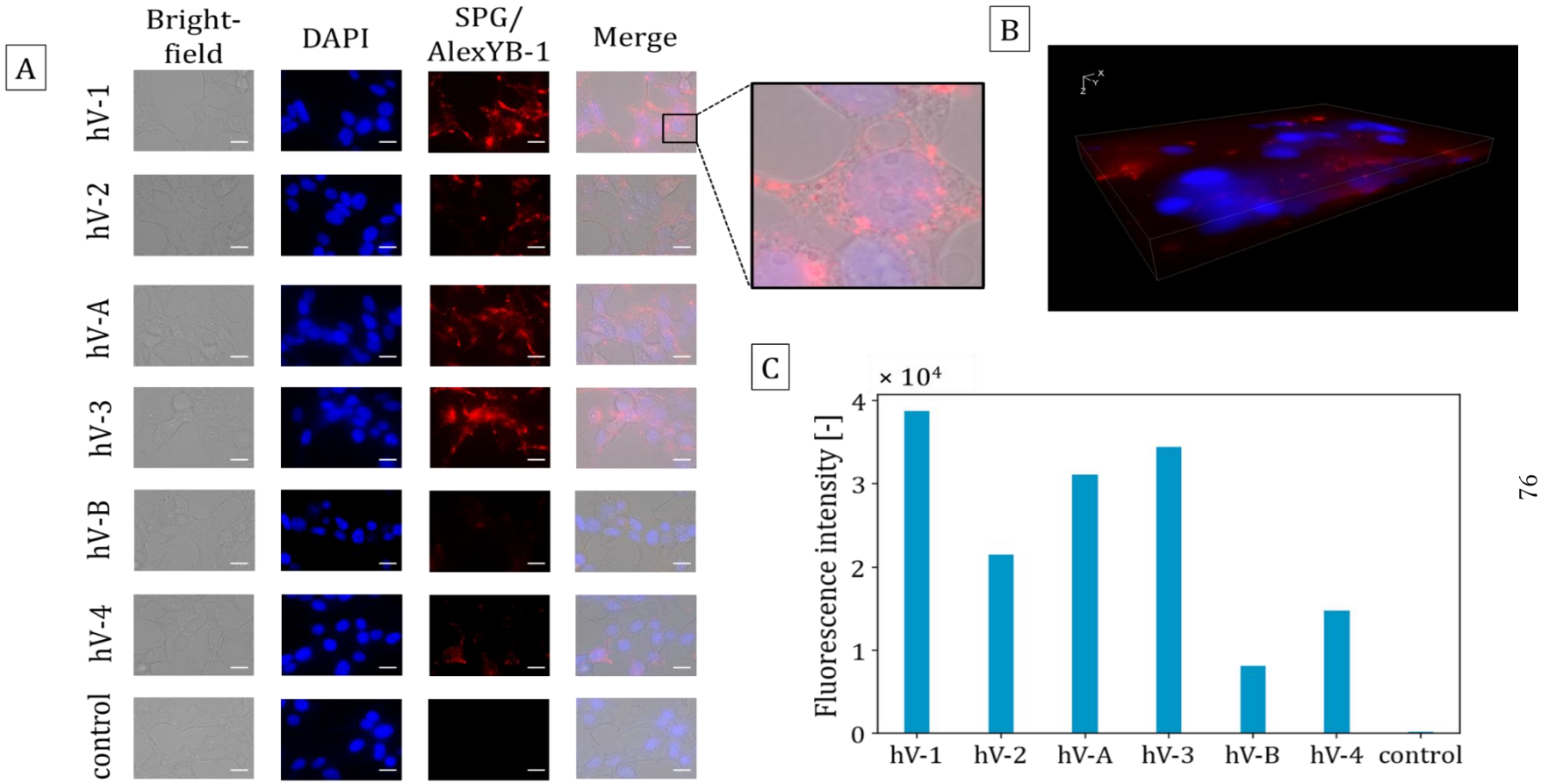

Figure 3-6. A: Cellular uptake of SPG/YB-1 AS complexes after 1 h of incubation, observed by structured illumination microscopy The scale bar represents 20 µm. The blue and red correspond to DAPI (nucleus) and Alexa546 (SPG/YB-1 AS). B: 3D images composed of Z-axis of HEK293T cells expressing hV-1. C: Fluorescence intensity derived from Alexa546 in the images.

3-3-5 Silencing of YB-1 and inhibition of cell growth by SPG/YB-1-AS complexes

We applied SPG/YB-1 AS complexes to HEK293T cells expressing each variant, and then examined the YB-1 expression and cell viability. Figure 3-7-A compares the results of the Western blotting of YB-1: hV-1, hV-2, hV-A, and hV-3 showed some reduction of YB-1, but not hV-B and hV-4. Among them, hV-1 showed the most significant efficacy. Figure 3-7-B compares the cell viability. Again, hV-1 showed the most significant efficacy, and the order is hV-1 > hV-3 > hV-A ≈ hV-2 > hV-4. Although data was not shown, no change in YB-1 expression or survival was observed in the cells not expressing Dectin-1, and no change in YB-1 expression occurred in naked YB-1 AS. Therefore, we can conclude that the decreases in the YB-1 expression and the viability can be ascribed to the efficacy of Dectin-1 mediated delivery of the complex of YB-1. Fujiwara et al carried out a similar assay using PC-3 instead of HEK293T and found the same results as the present results.[1] Comparing the order of the reduction efficacy in Figure 3-7 with that of the cellular uptake or with the binding at the QCM, the present result is more consistent with that of the cellular uptake than QCM.

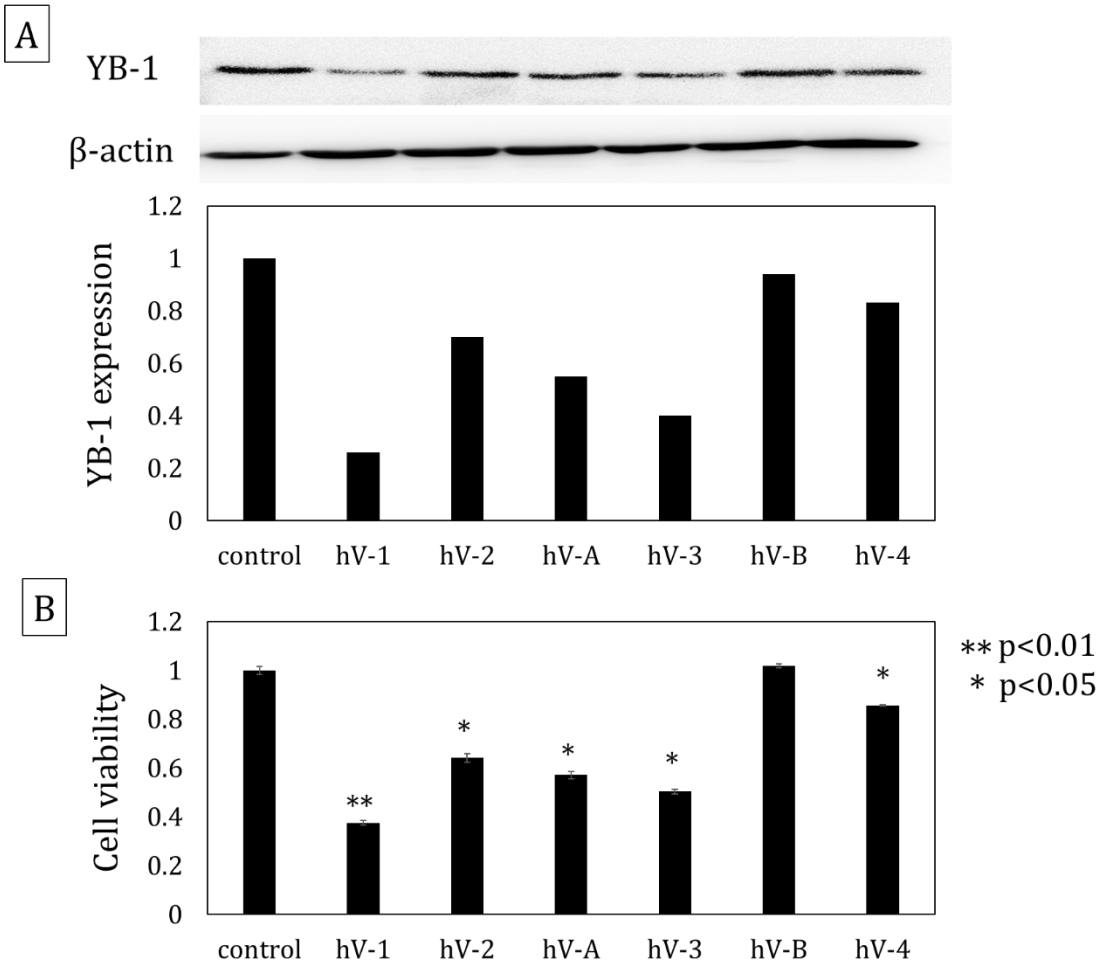

Figure 3-7. We applied SPG/YB-1 AS complex at a concentration of 1.0 μM to cells expressing Dectin-1. A: Analysis of the expression level of YB-1 by western blotting. β-Actin was used as an internal control. The expression level of control (transfected empty vector) is indicated as 1.0. B: The cell growth suppression in HEK293T cells transfecting six different Dectin-1 variants. Results are presented as mean ± SD (n = 3).

3-3-6 Membrane transport ratios of the variants and effects of N-linked glycosylation on the stability

Figure 3-8 compares the protein expression level for each variant at the plasma membrane and in the whole lysate. Here, the proteins expressed at the membrane were collected by centrifugation (see the experimental for detail). Since the proteins were obtained from the same number of cells, the expression levels can be calculated from the band intensities. The ratio of the amount of protein expressed in the membrane to the total was calculated, and the obtained numbers are shown under the gel image. (Table 3-2) hV-1 is close to 1.0, meaning that most proteins were transported to the membrane. Contrary to this, for hV-2 and hV-3, almost only half of the produced proteins have been transported to the membrane, respectively. For the others, only 20-30% of hV-A, hV-B, and hV-4 are transported. Carbohydrate modifications of proteins change their physical properties and/or function as specific recognition epitopes. Glycosylation also determines the transport pathway and destination in the cells.[16] In fact, Adachi et al. have reported that N-linked glycosylation of Dectin-1 increases the membrane transportation of Dectin-1.[12] The difference in the obtained values between hV-1 and hV-2 can be explained by the glycosylation, because more than 90% of hV-1 is glycosylated, while hV-2 is not at all. On the other hand, the correlation between the glycosylation and the transportation ratio is not clear for the other variants.

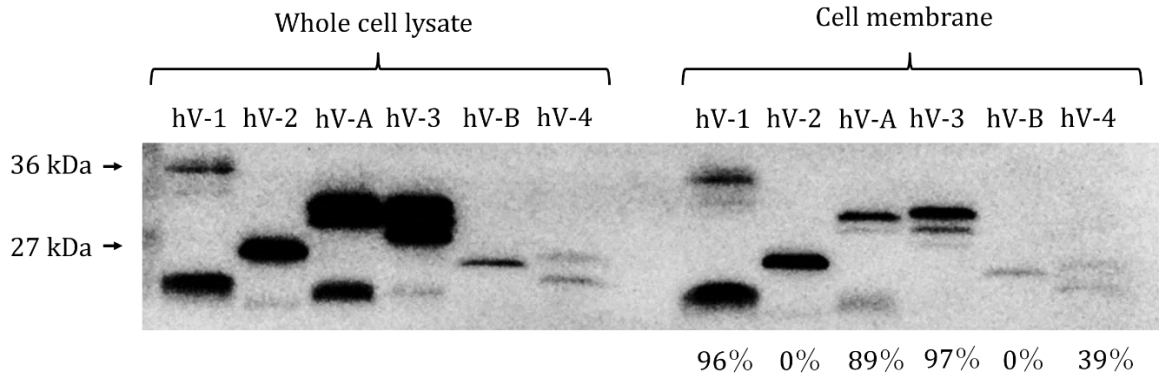

Figure 3-8. Membrane transport ratios of the protein for the six variants. After obtaining the cell membrane fractions of hDectin-1 expressing cells by using a membrane protein isolation kit, Western blotting was performed, comparing those from the whole cell lysate. The numbers under the image are the glycosylation ratios.

Table 3-2. Luminescence intensity ratio of variants

Sample	**hV-1**	**hV-2**	**hV-A**	**hV-3**	**hV-B**	**hV-4**
Fluorescence intensity ratio	1.07	0.57	0.33	0.46	0.21	0.31

Another role of glycosylation is to provide stability to the proteins.[17] We examined the stability of the variants by use of Tet-on system. Figure 3-9 shows the results of Western blotting and their analysis. The band intensity decreases with time. After normalized by the β-actin, the band intensities are plotted against time and the time courses were fitted by a sigmoidal function to evaluate the half-time (τ). The best-fitting curve and the obtained τ values are shown in the same figure. Note that there is a significant difference in the stability between hV-1 and hV-2. This difference could be due to the glycosylation. To confirm this, we prepared the mutated recombinant hV-1

(N91Q) at the glycosylation site at the stalk region and examined its stability. The value of τ was dramatically decreased from 70 to 19 h. For the other variants, hV-A, hV-3, and hV-4 were more stable than hV-B. As shown in Figure 3-3, the majority of the former four variants are glycosylated while hV-B has no glycosylation site.

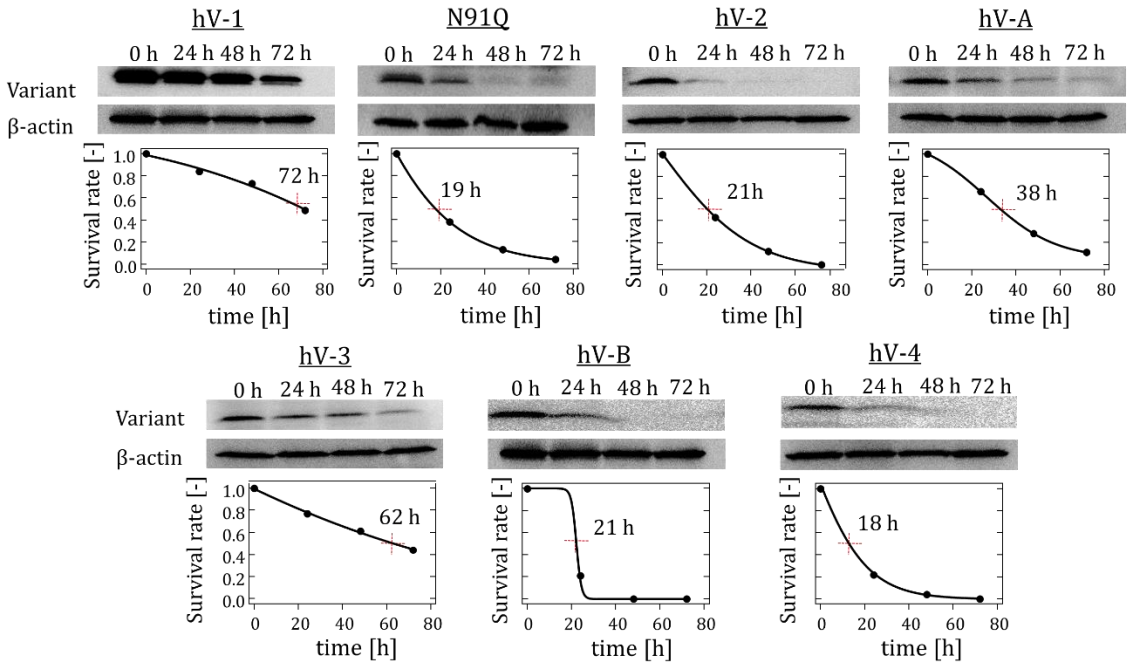

Figure 3-9. Relationship between protein stability and glycosylation. The time-course of the protein expression level was calculated from the band density of Western blotting and fitted by sigmoid function to evaluate the half-life time.

3-3-7 Identification of hDectin-1 variants gene expressing in cell lines and primary cells: hV-2 gene is expressed in PBMCs.

Figure 3-7 suggests that the efficiency of antisense therapy targeting Dectin-1 strongly depends on which variant is expressed on the cell surface. Therefore, it would be useful to have an accurate assay system that can identify the variant type for a given cell. As such a method, we used a cDNA multiple-PCR amplification method described in Figure 3-11. Exon 2 is indispensable for Dectin-1 variants to be expressed on the cell surface because Exon 2 codes the transmembrane region. Otherwise, the CRD would be in the cytosol. Therefore, as the initial screening, cDNA was produced by a reverse-transcription reaction using a primer having Exon 1 and 2. If no product is obtained in this process, the sample can be considered as having no genes capable of expressing Dectin-1 on the cell surface. If any product is obtained, we go to the 1st PCR to amplify the full length. For this product, we perform the 2nd PCR using the primer that amplifies the nested sequence from Exon 2 to Exon 6. The number of base pairs in the cDNA thus obtained should be different for each variant, and then it is possible to identify the type of variant. To test this protocol, we examined two types of human cell lines: PC-9 and A549. The former is known to express Dectin-1,[1] although we have not identified which type of variants are expressed, and the latter is known not to express Dectin-1 at all. Figure 3-11-B compares the gel electrophoresis images after the initial screening and the 1st PCR. As expected, PC-9 showed bands in both, while A549 did not at all. Figure 3-11-C shows the electrophoresis images, compared with the cDNA for six variants, indicating that PC-9 contains hV-2, hV-3, hV-B, and hV-4. Note that the

intensity of the bands in this experiment does not necessarily mean the high expression because of PCR amplification. We tested the other cell lines that have been known to express or not express Dectin-1 and the obtained results are consistent with each other.[1,9,18] (see Figure 3-10)

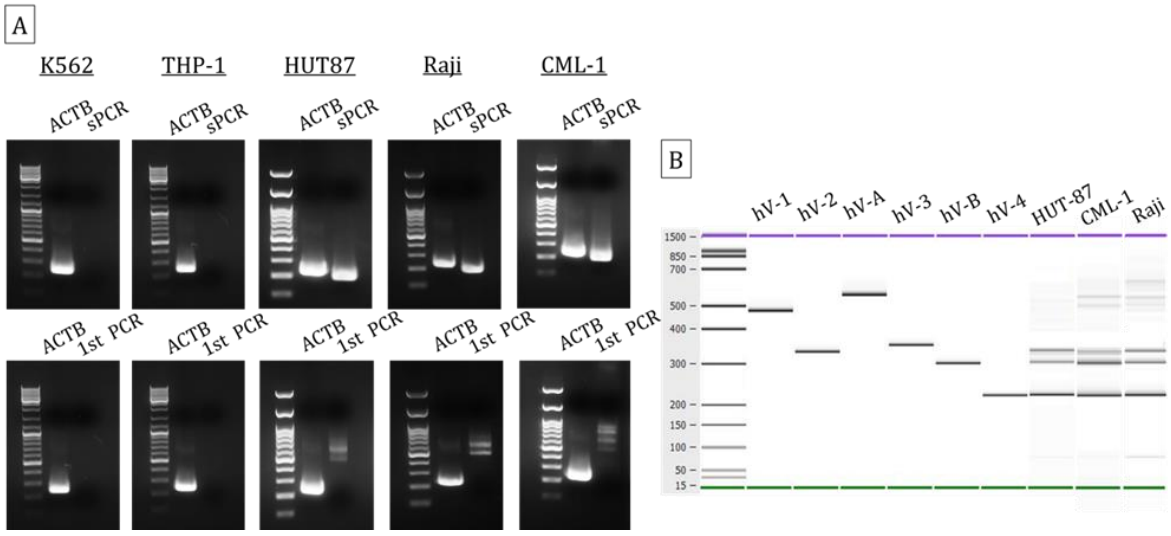

Figure 3-10. Human Dectin-1 variants expressed in cell lines were evaluated by PCR analysis. A: Dectin-1 mRNA in K562, THP-1, HUT87, Raji cells and CML-1 was investigated using sPCR and 1st round PCR. B: Bioanalyzer analysis of 2nd round PCR products.

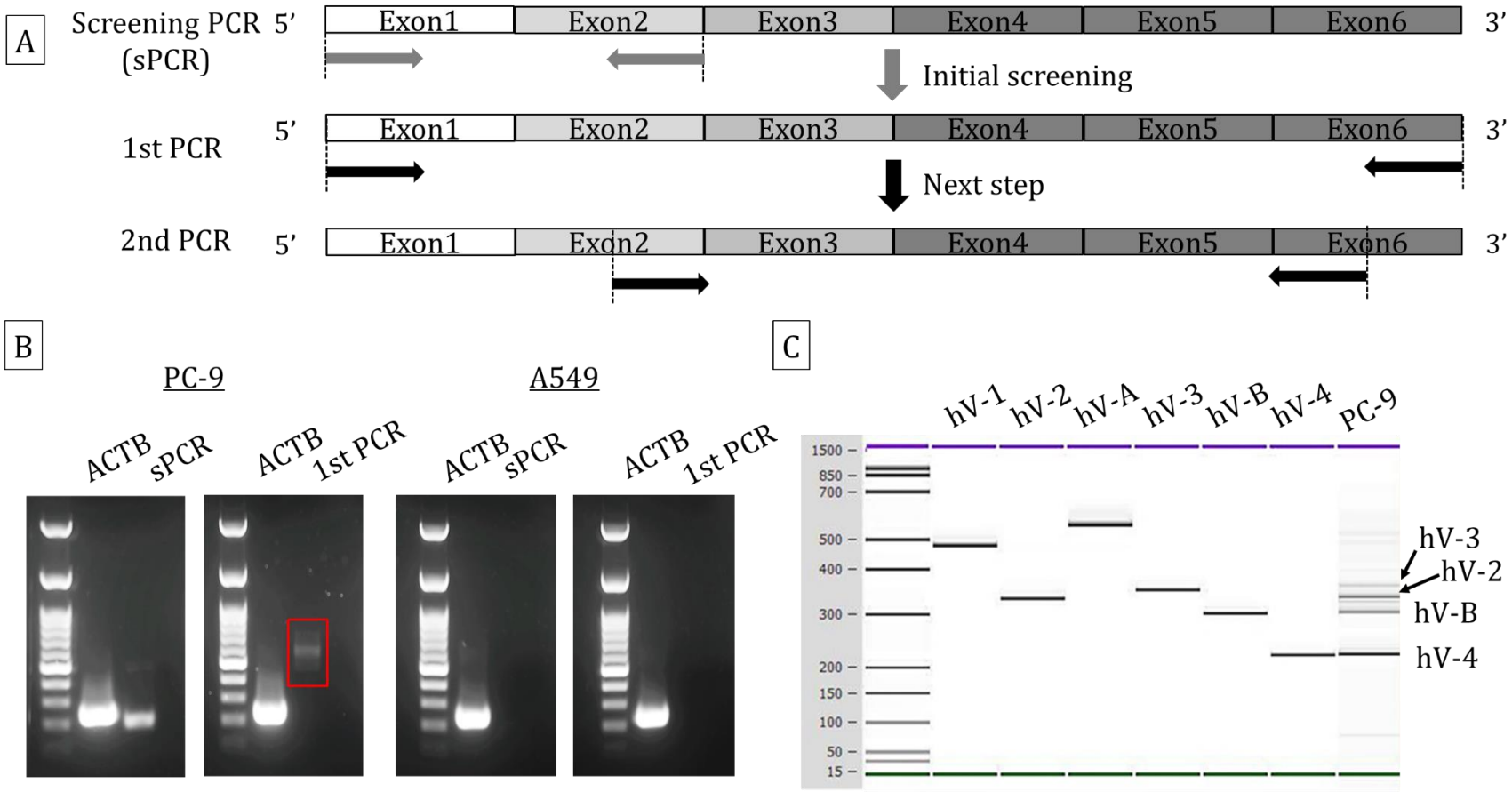

Figure 3-11. A new method to identify hDectin-1 variants and its demonstration for the positive and negative control cells: PC-9 and A549, respectively. A: a schematic presentation of the proposed multiple-PCR amplification, after the initial screening, B: comparison of the gel electrophoresis between PC-9 and A549, and C: the bands of the 2nd PCR cDNA obtained from PC-9 and its variant assignment in comparison with the references.

We examined human PBMCs using the above-mentioned method. Before that, we will examine which subsets in the PBMCs express hDectin-1, by following up on the results of Uno et al.[19] Figure 3-12-A and B shows the expression level of hDectin-1 in the samples evaluated by flow cytometry, indicating the presence of one cluster with Dectin-1 positive. Uno et al showed that monocytes (CD14 positive cells) and dendritic cells (CD11c positive cells) are the major populations in the Dectin-1 positive cells in PBMCs, and hDectin-1 was not expressed in B cells (CD19 positive cells).[19] We confirm that the same results are held in the present sample. Figure 3-12-D presents the gel electrophoresis images for PBMCs and its three populations. The result indicates that the monocytes and dendritic cells in this human PBMC express hV-2, hV-B, and hV-4、but not hV-1.

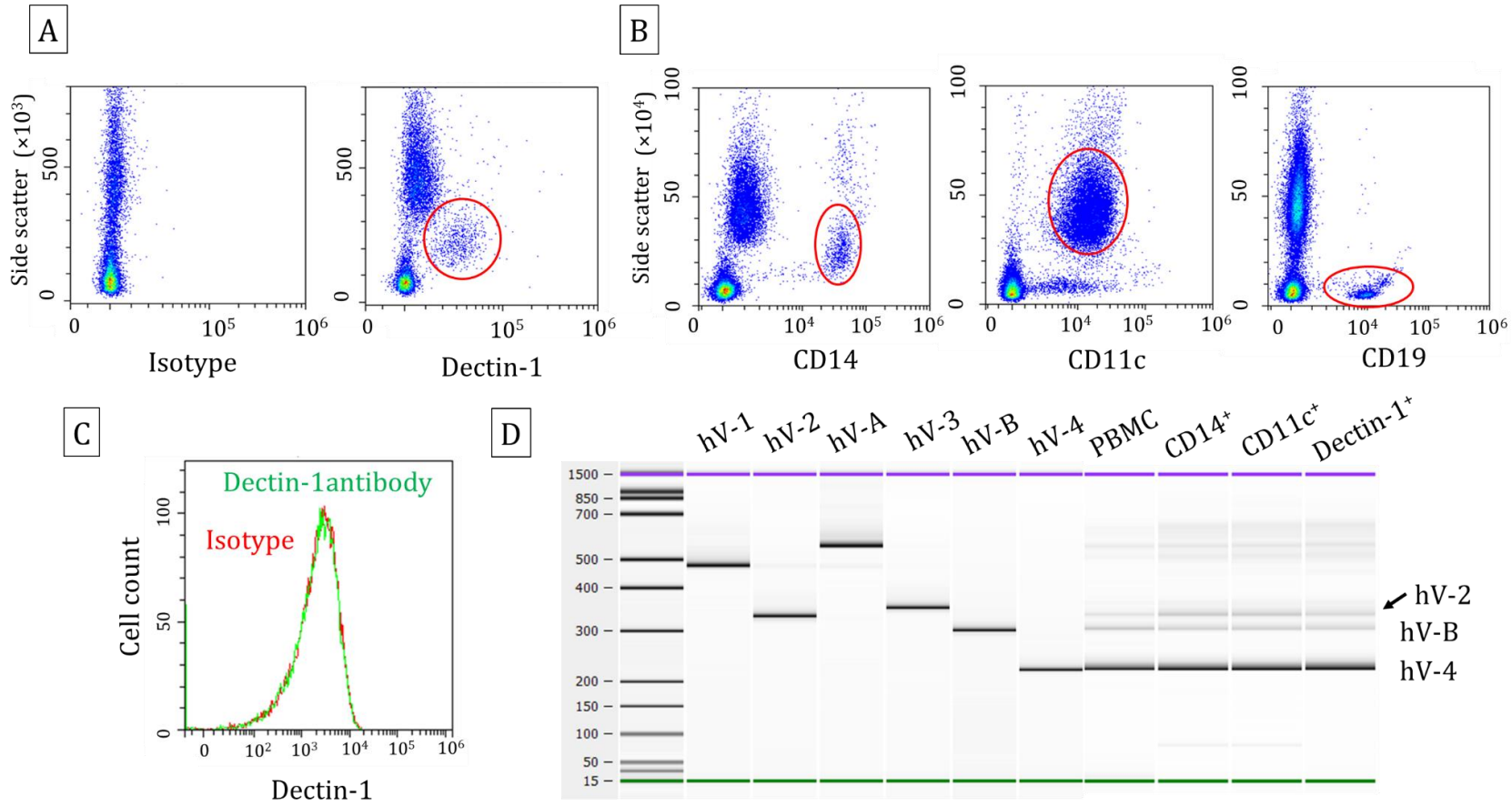

Figure 3-12. Dectin-1-expressing cells in a human PBMC. A: a cluster of cells was identified based on Dectin-1 and side scatter, B: CD14, CD11c, and CD19 positive clusters are present in PBMCs. These cell populations were fractionated by cell sorting and performed PCR analysis, C: Expression of Dectin-1 in CD19+ cells, D: Bioanalyzer analysis of 2nd PCR products with Agilent DNA chip.

3-3-8 Cellular uptake of SPG/DNA complexes by PBMC.

Our previous study showed that PC-9 takes up the SPG complexes but not A549, which is associated with hDectin-1-dependent uptake.[19] Uno et al showed that hDectin-1 is expressed in all subsets of monocytes as well as dendritic cell populations in humans, including conventional DCs and plasmacytoid DCs, except for B cells. The expression patterns in mice and humans are comparable, except for the expression in pDCs. They also demonstrated that the SPG/DNA complex was taken up by the hDectin-1-expressing cell population in human PBMCs, and their uptake was clearly increased in a dose-dependent manner.[19] To confirm their results, we examined intracellular uptake in monocytes and dendritic cells using SIM (Figure 3-13). As shown Figure 3-13, SIM has a higher resolution than conventional fluorescence microscopy; therefore, it can clearly measure for more detailed of the intracellular distribution of the SPG complexes. As far as we know, no preceding work has used microscopy to examine the uptake of the SPG complexes in terms of Dectin-1 expression.

We applied FAM-labeled SPG complexes (hereafter referred to as SPG/FAMYB-1) to PC-9, CD14, CD19, and CD11c positive cells. Figure 3-13-A and B shows the fluorescence observation results. We observed FAM signal except for CD19 positive cells, appearing to be present as small dots and diffused throughout the cell. The distribution suggests accumulation of SPG/FAMYB-1 in endosomes and migration into the cytoplasm. Given that a part of FAM signal co-localized with lysosome derived red fluorescence, it is assumed that most of the ingested

the SPG/DNA complexes moved into the cytoplasm. These results support the contention of Uno et al. that the SPG/DNA complex is taken up by monocytes and dendritic cells.

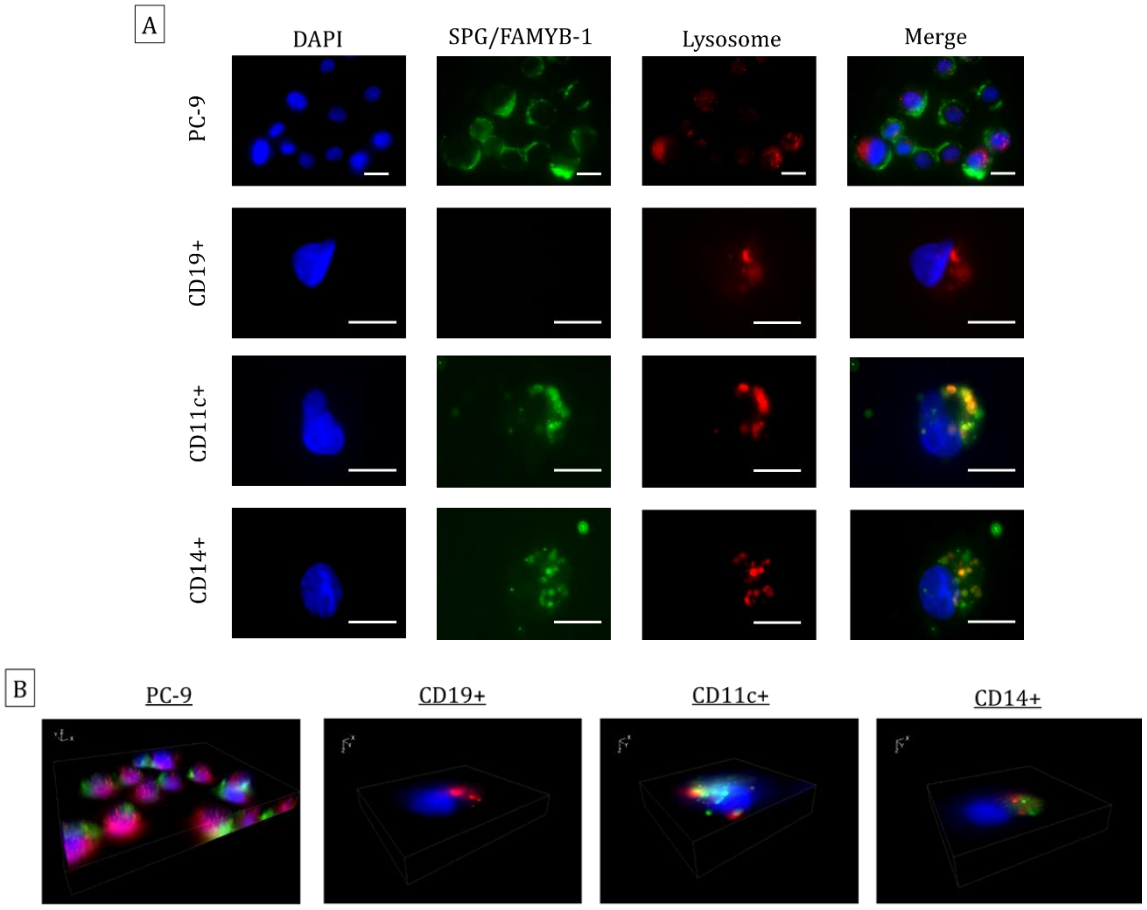

Figure 3-13. Intracellular distribution of FAM-labeled SPG/YB-1 AS after 6h of incubation. The scale bar represents 20 μm. A: Structured illumination microscopic images of PC-9, CD14, CD11c, and CD19 positive cells. The blue, green, and red indicate DAPI (nucleus), FAM (SPG/YB-1 AS), and lysosomes. B: 3D imaging of PC-9, CD14, CD11c, and CD19 positive cells.

3-4 Discussion

We used six hDectin-1 variants obtained by Fujiwara et al.[1] Among them, hV-A and hV-B are new variants. The difference between hV-A and hV-B is of difference in the Exon 4' sequence (see Figure 3-2). hV-B has the same sequence as A from 1 to 83 bp but has 4 additional bp attaching at 4, so the length is 87. We denoted these Exons as X and Y, respectively. In the previous paper, Fujiwara et al. reported the bp of exon4' as 86, but this is a calculation error; it is actually 87. However, we do not know X is the same as 4', because no sequence of 4' was reported. We found a new N-glycosylation site in hV-4 that locates at hCRD. The glycosylation is closely related to the membrane transport ratio of the variant and to the stability of the protein. We examined how the cellular uptake of SPG and SPG complexes differs depending on the type of variants. Similar to the previous results, SPG itself and SPG/dA complex (phosphodiester) were ingested by the hV-1 and hV-2 expressing cells, but SPG/s-dA complex (phosphorothioate) was ingested by all of the cells except for hV-B. In terms of the gene silencing efficacy, hV-1 > hV-3 > hV-A ≈ hV-2 >> hV-4. When we compare this order with that of the stability: hV-1 > hV-3 > hV-A > hV-2 ≈ hV-4, there is a good correlation. Again, the stability and the membrane transport ratio are closely related, and this trend can be explained by the level of the N-glycosylation. Therefore, we can conclude that the better targets for the SPG/s-dA complex are the cells expressing hV-1, hV-3, hV-A, and hV-2 because these variants are more likely transported to the cell membrane due to the N-glycosylation.

There are four different hCRD, instead of six, because hV-1 and hV-2, hV-3 and hV-4 are in the same sequence. We carried out an in-vitro binding assay between these four variants and SPG/s-dA complex, comparing with SPG and SPG/dA. Similar to mDectin-1, SPG and SPG/dA showed a certain affinity for only CRD-hV2 that have the complete CRD including the key peptides (see Figure 3-4). According to Adachi' work, these key peptides consist of the pattern-recognition binding pocket to capture the triple helix of SPG. The other variants lack this key domain due to the stop codon appearing before this key sequence; therefore, they did not show any affinity for SPG, and SPG/dA. In contrast, SPG/s-dA showed binding for all variants. CRD-hV2 was higher than the others by 50 Hz in $\Delta F(300)$. The other variants showed the same affinity, about 250 Hz at $\Delta F(300)$. It is still larger than that between CRD-hV2 and SPG (or SPG/dA). The mutation assay showed that there is an additional binding site (or sites) other than the key domain and its location is in front of the key domain. One may argue that this new binding may not be a specific pattern recognition type, but non-specific binding due to the hydrophobicity of phosphorothioate molecules. At present, we cannot completely rule out this argument, because naked s-dA_{40} showed the affinity of $\Delta F(300)$~ 50 Hz, which may be due to non-specific binding. However, it is difficult to find a reasonable explanation for why SPG/s-dA_{40} shows a much higher affinity than s-dA_{40}, considering that the hydrophobicity of s-dA_{40} is larger than SPG/s-dA_{40}. Nevertheless, the presence of attractive binding between hDectin-1 and SPG/s-dA_{40} is considered a great advantage for the targeting delivery of the SPG

complexes. Phosphorothioate nucleotides are considered ancient-type nucleotides because they contain sulfur, which might have been used by old life forms during the Precambrian era before oxygen was perpetually present in the atmosphere by photosynthetic plants.[20] Dectin-1 is highly homologous between species and appears to be a protein that has not changed much during evolution. Therefore, it would not be too speculative to assume that Dectin-1 retains an old memory of sulfur being the main constituent of nucleic acids. Further studies are needed to understand the exact mechanisms of this rather strong affinity between SPG/s-dA and hDectin-1.

N-linked glycosylation is widely found in cell surface receptors and its importance is well known. Glycosylation is crucial for protein stabilization, molecular folding, and intracellular transport, and sometimes regulates the expression and function of molecules at the cell surface.[16, 17] Kano et al. and other researchers reported that the glycosylation significantly affects the expression of hV-1 and hV-2 at the cell surface and even affects the binding of ligands and its anti-fungal effects with TLR2.[12, 21] However, the other minor variants have not been studied well. We found that hV-3 and hV-4 have a new glycosylation site in hCRD. Furthermore, hV-1, hV-A, hV-3, and hV-4 with this N-linked glycosylation tended to be more highly expressed on the cell surface and more stable than the other variants. Thus, it is clear that N-linked glycosylation is related to the up-take efficiency of the SPG/DNA complexes.

However, the original role of glycosylation in these minor variants is unknown. This issue requires further investigation in the future.

Developing techniques to deliver drugs only to target cells will lead to the discovery of important new therapies, such as givosiran and lumasiran, which were approved by the FDA in 2019 and 2020, respectively. Thus, drugs are increasingly being combined with DDS technology rather than drugs alone.[22] Givosiran is a conjugated siRNA that contains three molecules of N-acetylgalactosamine (GalNAc) at the 3' end of the sense chain. It binds to asialoglycoprotein receptor, enabling efficient and selective delivery of GalNAc-conjugated siRNA to the liver.[23] Other attempts to modify liver-targeting molecules such as cholesterol, tocopherol, antibodies, and aptamers to specifically deliver them to parenchymal cells have been actively pursued,[24] but their cellular targeting beyond the liver is still insufficient and none of them are yet ready for clinical use. Antigen-presenting cells, lung cancer cells, and in previous studies, clear cell renal cell carcinoma have also been reported to express Dectin-1.[25] Therefore, our proposed SPG/DNA complexes will be able to target an even wider range of cells and organs than conventional DDS techniques and will be useful.

3-5 Conclusion

In conclusion, we demonstrated that SPG/s-dA is recognized and internalized into cells by all hDectin-1 variants expressed on the cell surface. It is not known the binding site for SPG/s-dA and hCRD. However, QCM measurements confirmed that all hCRDs show a similar affinity for SPG/s-dA. On the other hand, the number of SPG complexes taken into the cells differed among the variants, resulting in gene repression effects by YB-1-AS in hV-1 hV-2 hV-A hV-3. This was attributed to the stability of the variant and its expression rate at the cell surface due to N-linked glycosylation. The abovementioned results indicate that hV-1, hV-2, hV-A, and hV-3 can be a good target to deliver therapeutic ODNs using the SPG/DNA complexes.

3-6 Reference

1. Fujiwara, N.; Izumi, H.; Kira, R.; Morimoto, Y.; Mochizuki, S.; Sakurai, K., Binding assay of human Dectin-1 variants to DNA/β-glucan complex for active-targeting delivery of antisense DNA. *Carbohydr Res* **2021,** *500*, 108219.

2. Koi, C.; Izumi, H.; Kurita, T.; Nguyen, T. T.; Murakami, M.; Yoshiura, Y.; Hachisuga, T.; Morimoto, Y., Lovastatin induced Kruppel like factor 2 (KLF2), Kruppel like factor 6 (KLF6) and Ras homolog family member B (RHOB) genes and preferentially led to viability reduction of Cisplatin-resistant cells. *Oncotarget* **2017,** *8* (63), 106429-106442.

3. Mizu, M.; Koumoto, K.; Anada, T.; Karinaga, R.; Kimura, T.; Nagasaki, T.; Shinkai, S.; Sakurai, K., Enhancement of the Antisense Effect of Polysaccharide-Polynucleotide Complexes by Preventing the Antisense Oligonucleotide from Binding to Proteins in the Culture Medium. *Bulletin of the Chemical Society of Japan* **2004,** *77*, 1101-1110.

4. Hasegawa, T.; Fujisawa, T.; Numata, M.; Umeda, M.; Matsumoto, T.; Kimura, T.; Okumura, S.; Sakurai, K.; Shinkai, S., Single-walled carbon nanotubes acquire a specific lectin-affinity through supramolecular wrapping with lactose-appended schizophyllan. *Chem Commun (Camb)* **2004,** (19), 2150-1.

5. Yokota, K.; Takashima, A.; Bergstresser, P. R.; Ariizumi, K., Identification of a human homologue of the dendritic cell-associated C-type lectin-1, dectin-1. *Gene* **2001,** *272* (1-2), 51-60.

6. Brown, G. D., Dectin-1: a signalling non-TLR pattern-recognition receptor. *Nat Rev Immunol* **2006,** *6* (1), 33-43.

7. Adachi, Y.; Ishii, T.; Ikeda, Y.; Hoshino, A.; Tamura, H.; Aketagawa, J.; Tanaka, S.; Ohno, N., Characterization of beta-glucan recognition site on C-type lectin, dectin 1. *Infect Immun* **2004,** *72* (7), 4159-71.

8. Dulal, H. P.; Adachi, Y.; Ohno, N.; Yamaguchi, Y., β-Glucan-induced cooperative oligomerization of Dectin-1 C-type lectin-like domain. *Glycobiology* **2018,** *28* (8), 612-623.

9. Willment, J. A.; Gordon, S.; Brown, G. D., Characterization of the human beta -glucan receptor and its alternatively spliced isoforms. *J Biol Chem* **2001,** *276* (47), 43818-23.

10. Marshall, R. D., The nature and metabolism of the carbohydrate-peptide linkages of glycoproteins. *Biochem Soc Symp* **1974,** (40), 17-26.

11. Mochizuki, S.; Morishita, H.; Adachi, Y.; Yamaguchi, Y.; Sakurai, K., Binding assay between murine Dectin-1 and β-glucan/DNA complex with quartz-crystal microbalance. *Carbohydr Res* **2014,** *391*, 1-8.

12. Kato, Y.; Adachi, Y.; Ohno, N., Contribution of N-Linked Oligosaccharides to the Expression and Functions of β-Glucan Receptor, Dectin-1. *Biological and Pharmaceutical Bulletin* **2006,** *29* (8), 1580-1586.

13. Lin, H.; Caroll, K. S., Introduction: Posttranslational Protein Modification. *Chem Rev* **2018,** *118* (3), 887-888.

14. Vu, L. D.; Gevaert, K.; De Smet, I., Protein Language: Post-Translational Modifications Talking to Each Other. *Trends Plant Sci* **2018,** *23* (12), 1068-1080.

15. Feiner-Gracia, N.; Pujals, S.; Delcanale, P.; Albertazzi, L., 15 - Advanced Optical Microscopy Techniques for the Investigation of Cell-Nanoparticle Interactions. In *Smart Nanoparticles for Biomedicine*, Ciofani, G., Ed. Elsevier: 2018; pp 219-236.

16. Helenius, A.; Aebi, M., Intracellular functions of N-linked glycans. *Science* **2001,** *291* (5512), 2364-9.

17. Helenius, A.; Aebi, M., Roles of N-linked glycans in the endoplasmic

reticulum. *Annu Rev Biochem* **2004,** *73*, 1019-49.

18. Willment, J. A.; Marshall, A. S.; Reid, D. M.; Williams, D. L.; Wong, S. Y.; Gordon, S.; Brown, G. D., The human beta-glucan receptor is widely expressed and functionally equivalent to murine Dectin-1 on primary cells. *Eur J Immunol* **2005,** *35* (5), 1539-47.

19. Uno, A.; Arima, K.; Shimazaki, M.; Ushida, M.; Amano, K.; Namikawa, R.; Sakurai, K., A novel β-glucan-oligonucleotide complex selectively delivers siRNA to APCs via Dectin-1. *J Control Release* **2021,** *338*, 792-803.

20. Wang, L.; Chen, S.; Xu, T.; Taghizadeh, K.; Wishnok, J. S.; Zhou, X.; You, D.; Deng, Z.; Dedon, P. C., Phosphorothioation of DNA in bacteria by dnd genes. *Nat Chem Biol* **2007,** *3* (11), 709-10.

21. Fischer, M.; Müller, J. P.; Spies-Weisshart, B.; Gräfe, C.; Kurzai, O.; Hünniger, K.; Hochhaus, A.; Scholl, S.; Schnetzke, U., Isoform localization of Dectin-1 regulates the signaling quality of anti-fungal immunity. *Eur J Immunol* **2017,** *47* (5), 848-859.

22. Roberts, T. C.; Langer, R.; Wood, M. J. A., Advances in oligonucleotide drug delivery. *Nature Reviews Drug Discovery* **2020,** *19* (10), 673-694.

23. Nair, J. K.; Willoughby, J. L. S.; Chan, A.; Charisse, K.; Alam, M. R.; Wang, Q.; Hoekstra, M.; Kandasamy, P.; Kel'in, A. V.; Milstein, S.; Taneja, N.; O'Shea, J.; Shaikh, S.; Zhang, L.; van der Sluis, R. J.; Jung, M. E.; Akinc, A.; Hutabarat, R.; Kuchimanchi, S.; Fitzgerald, K.; Zimmermann, T.; van Berkel, T. J. C.; Maier, M. A.; Rajeev, K. G.; Manoharan, M., Multivalent N-Acetylgalactosamine-Conjugated siRNA Localizes in Hepatocytes and Elicits Robust RNAi-Mediated Gene Silencing. *Journal of the American Chemical Society* **2014,** *136* (49), 16958-16961.

24. Zhang, X.; Ng, H. L. H.; Lu, A.; Lin, C.; Zhou, L.; Lin, G.; Zhang, Y.; Yang, Z.; Zhang, H., Drug delivery system targeting advanced hepatocellular

carcinoma: Current and future. *Nanomedicine: Nanotechnology, Biology and Medicine* **2016,** *12* (4), 853-869.

25. Xia, Y.; Liu, L.; Bai, Q.; Wang, J.; Xi, W.; Qu, Y.; Xiong, Y.; Long, Q.; Xu, J.; Guo, J., Dectin-1 predicts adverse postoperative prognosis of patients with clear cell renal cell carcinoma. *Sci Rep* **2016,** *6*, 32657.

CHAPTER 4.Dectin-1-expressing cell-specific drug delivery using SPG/DNA complexes

4-1 Purpose of this chapter

The objective of this study is to elucidate whether it is possible to deliver nucleic acid pharmaceuticals to cells expressing human Dectin-1 using complexes. Additionally, one of the goals is to verify whether the small molecular weight complexes newly identified in Chapter 2, which are said to possess different properties from their conventional counterparts, actually have pharmacological effects. Specifically, detailed in vitro studies were conducted to determine whether these complexes have the ability to specifically target dectin-1-expressing cells and effectively deliver the drug. These studies were designed to assess whether the complexes could properly bind to cell receptors and elicit the desired biological response. As a result, we hope to obtain important information to determine whether this new small molecule complex is suitable for use as a potential therapeutic agent. By evaluating both the pharmacological effects of the complexes and their ability to be delivered to cells, we can understand if these will be useful in the development of new drug delivery systems.

4-2 Experimental Section

4-2-1 Materials

In this experiment, S-3n was used. All phosphorothioated ODN (S-ODN) samples, including AS-ODN and CpG-ODN for YB-1-AS and K-ras-AS and K3-CpG, were synthesized by Gene Design Co., Ltd. (Osaka, Japan) and purified by high-performance liquid chromatography. Each sequence is summarized in Table 3-1.

4-2-2 Preparation of the YB-1-AS, K-ras-AS and K3-CpG/SPG complex

SPG was dissolved in 0.25 N aq. NaOH for 1 h, and the alkaline SPG solution was mixed with YB-1, K-ras-AS, AS-YB-1, K-ras-AS-YB-1 and K3-CpG in 330 mM NaH_2PO_4. The feeding molar ratio of [SPG]:[dA] was 1:4. After mixing, the complex was stored at 4 °C for 24 h.

4-2-3 Fractionation of the complex

The mixture was fractionated by collecting the eluate during an appropriate time range. We collected fractions corresponding to 24.3–24.6, 23.2–23.7, and 21.8–22.3 min for the S-SPG/YB-1-AS complex.

4-2-4 Cell culture

Two human lung cancer cell lines were used: PC-9 and A549. PC-9 cells were cultured in RPMI 1640 medium, GlutaMAX™ (Life Technologies, Tokyo, Japan), A549 cells were cultured in DMEM (Life Technologies, Tokyo, Japan). Both were maintained in a 5% CO_2 atmosphere at 37 °C. PC-9 cells were subjected to short

tandem repeat analysis by Takara Bio Ltd., which confirmed the absence of contamination by other cells and the status of the cells as PC-9 (lot: 6310PA-STR2017).

4-2-5 Uptake of Alexa546-labeled YB-1-AS/SPG complex

A fluorescence marker-attached complex of YB-1-AS/SPG was prepared by complexation with Alexa546-labeled YB-1-AS-ODN. PC-9 and A549 cells were seeded at 5.0×10^4 in 24-well plates and incubated for 24 h. The Alexa546-labeled YB-1-AS-ODN/SPG complex (100 nM) was added to the medium and incubated for 6 h. After washing with PBS three times, the cells were imaged with an EVOS® FL Imaging System (Thermo Scientific).

4-2-6 Western blot

PC-9 and A549 cells were seeded at 1.0×10^5 in a six-well plate and incubated for 24 h at 37 °C under 5% CO_2. The complexes were added at an AS-ODN concentration of 1.0 μM. After incubation for 36 h, the whole-cell lysates (10 μg) were transferred to a 10% or 15% polyacrylamide gel for SDS–PAGE, and then the transferred membrane was immunoblotted with antibodies. The following antibodies were used in this experiment: anti-K-ras (Sigma Aldrich; cat# WH0003845M1), anti-YB-1[6], and anti-β-actin (Sigma Aldrich; cat# A3854). The expression levels were quantified using Multi-Gauge Version 3.0 (Fujifilm, Tokyo, Japan).

4-2-7 WST-8 assay

PC-9 and A549 cells were seeded at 1.0×10^3 in a 96-well plate and incubated for 24 h at 37 °C under 5% CO_2. The complexes were added at an AS-ODN concentration of 1.0 or 0.4 μM. After incubation for 72 h, cellular growth was determined using Cell Counting Kit-8 (Dojindo, Kumamoto, Japan).

4-2-8 Cytokine assay

Mouse splenocytes were seeded at 1.0×10^6 cells in a 96-well plate and supplemented with CpG at 20 nM. After 24 h, the IL-6 concentrations in the culture medium were measured with a mouse IL-6 ELISA kit (Invitrogen).

4-2-9 Intracellular distribution of YB-1-AS after cellular uptake

Separation of the cell lysate into early endosomal and cytoplasmic components was performed using an endosome isolation kit (Biovision; cat# ED-028). A phenol-chloroform mixture was added to a cytoplasmic extract that had been pretreated with RNase H. YB-1-AS was purified by ethanol precipitation. Finally, after ligation between YB-1-AS and linker DNA (see Supplemental Table 1 in List of Publications #3) using T4 DNA ligase, the copy numbers of YB-1-AS in cytoplasmic components were determined by amplifying a part of YB-1-AS using PCR primers 1 and 2 (see Supplemental Table 1 in List of Publications #3). The quantitative PCR (qPCR) reaction conditions were as follows: 94 °C for 5 min and 40 cycles of 94 °C for 30 s, 62 °C for 30 s and 72 °C for 30 s.

4-2-10 Statistical analysis

All values are presented as the mean ± standard deviation (SD). The statistical significance of differences between groups was determined using Student's t test.

4-3 Results

4-3-1 Complex formation between YB-1-AS and single-stranded SPG

We prepared two sSPG samples with different M_w values of 1.9×10^5 and 8.7×10^4 named L-SPG and S-SPG, respectively. These were mixed with YB-1-AS to form complexes. (In all our previous related work, only L-SPG was used.) After mixing YB-1-AS and S-SPG (denoted S-SPG/YB-1-AS), we subjected the mixture to gel electrophoresis (Figure 4-1-A). This mixture showed three bands, which could be assigned to q1-YB-1-AS, q2-YB-1-AS, and q3-YB-1-AS, in this order from the bottom of the image. q2-YB-1-AS appeared to be the most abundant, while the number of complexes containing more than four YB-1-AS molecules was negligible. Figure 4-1-B presents a GPC chromatogram of S-SPG/YB-1-AS, showing that the chromatogram consists of three peaks and a relatively broad shoulder on the larger molecular weight side. These three peaks were assigned to q1-YB-1, q2-YB-1, and q3-YB-3 (in order of longer elution time) and q2-YB-1-AS was confirmed as the major component. Figure 4-1-B presents the chromatogram of L-SPG/YB-1-AS for comparison, showing that the major component of this mixture is complexes having more than three or four YB-1-AS molecules. As the molecular weight increased, the resolution of the GPC fractionation decreased. This explains why no clear peak separation was observed on the larger-molecular weight side. Figure 4-1-A and B indicates that when the M_w of sSPG decreased, the number of YB-1-AS molecules in the complex decreased and became isolated peaks, which would facilitate fractionation of the quantized complexes.

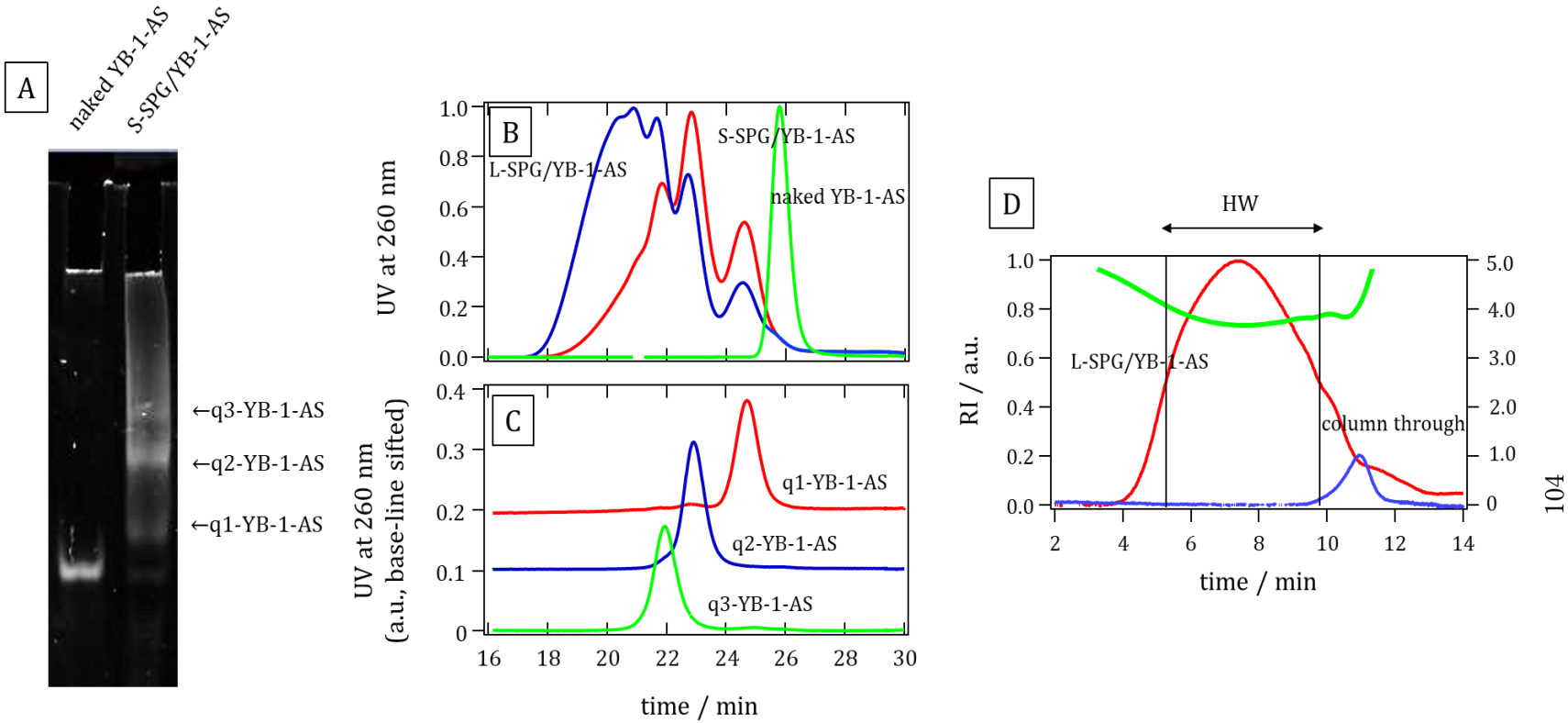

Figure 4-1. Proof of complex formation between S-SPG and YB-1-AS. A: Gel electrophoresis (using a 6.0% polyacrylamide gel). B: Comparison of the UV chromatograms between the L-SPG and S-SPG complexes. C: UV chromatograms for the quantized complexes q1-YB-1-AS, q2-YB-1-AS, and q3-YB-1-AS, where the baseline was shifted upward to facilitate easy comparison. D: Comparison of RI chromatograms between L-SPG/YB-1-AS and the column-through fraction and [mG]/[dA] of L-SPG/YB-1-AS calculated by UV and RI measurements.

We isolated q1-YB-1-AS, q2-YB-1-AS, and q3-YB-1-AS from S-SPG/YB-1-AS by taking an appropriate fraction (i.e., collecting eluents, for example, 24.3–24.6 min to obtain q1-YB-1-AS) from GPC. After fractionation, we carried out GPC for each sample; the resultant UV chromatograms are compared in Figure 4-1-C. Each sample shows a clear single peak that is almost symmetrical with respect to the elution time of the top of the peak. Although q1-YB-1 contained a small amount of q2-YB-1-AS, it was determined to contain less than 1 wt% of the peak area. The molecular weight of each sample was determined at the top of the peak by static light scattering; all of the results are summarized in Table 4-1. By subtracting the molecular weight of YB-1-AS from the measured M_{w} of the complex, the molecular weight of SPG that was bound in the complex was estimated, and then the number of main-chain glucoses was determined (the sixth and fifth columns in Table 4-1, respectively). We used YB-1-AS to bind sSPG, and from the stoichiometry of the complex, 80 main-chain glucoses were needed to bind one YB-1-AS chain in q1, 160 in q2, and 240 in q3. The number of glucoses in each complex was slightly larger than these values. This discrepancy may be due simply to (1) experimental error in determining the molecular weight, (2) unreacted glucoses at the end of the chain or (3) the sSPG chain adopting a hairpin form in the complex as illustrated in Figure 2-5. We do not have further data to explain this discrepancy, but the dA40 tail was almost completely bound to sSPG, while there was neither free YB-1-AS nor sSPG remaining in the solution of q1 and the other quantized complexes.

Table 4-1. Molecular characteristics of SPG and the complexes

Sample name	$10^{-4}M_w$	M_w/M_n(HW)	av.($\frac{[mG]}{[dA]}$) (HW)[b]	$10^{-4}M_w$sSPG	Number of mG	Free SPG (%)
L-SPG	18.7	1.54	-	-	-	-
S-SPG	8.68	1.22	-	-	-	-
L-SPG/YB-1-AS	54.1	1.48	3.7	33.5	1.54×10^3	7.0±0.1
q1- YB-1-AS	4.23	1.01	1.8	2.10	96	0[c]
q2- YB-1-AS	8.46	1.01	1.9	4.20	193	0[c]
q3- YB-1-AS	12.7	1.00	1.8	6.31	290	0[c]

a: HW: half-width.
b: Average value of [mG]/[dA] in the range of HW.
c: There is no free SPG because q-complexes are fractionated.

Contrary to quantized complexes such as q1-YB-1-AS and q2-YB-1-AS, we assume that the L-SPG/YB-1-AS mixture contains a certain amount of sSPG as an uncomplexed fraction after mixing, as well as the complex itself containing a renatured tSPG component, because an excess of sSPG was mixed with the AS-ODN to prevent free AS-ODN from remaining in the final mixture. The mixing ratio of these two components can be expressed in terms of [mG]/[dA], where [mG] and [dA] are the molar numbers of the main-chain glucose and of the dA tail of AS-ODN, respectively. The stoichiometric conditions are given by [mG]/[dA]=2.0, but we normally prepared the complex at a feeding mixing ratio of [mG]/[dA]=4.0. From our chromatographic analysis, we measured the UV absorbance (Abs) at 260 nm and the refractive index (RI) at 633 nm as a function of the elution time. Only dA_x absorbs UV light, and the RI is related to the concentration of the complex. Therefore, for each fraction, we can evaluate [mG]/[dA] as a function of the elution time. After integrating [mG]/[dA] over an appropriate elution time, we obtained the averaged [mG]/[dA] of the sample. Note that this value of [mG]/[dA] differs from the feeding [mG]/[dA]. The fourth

column in Table 4-1 shows the [mG]/[dA] value obtained. The quantized complexes showed [mG]/[dA]~2, which is expected from the stoichiometry; this value indicates that there is no renatured tSPG involved in the quantized complexes. In comparison, L-SPG/YB-1-AS showed [mG]/[dA] values that were almost twice as large. This means that (1) L-SPG/YB-1-AS contains some free uncomplexed sSPG because fractionation was performed or (2) some part of the complex is made from renatured tSPG. We reported that uncomplexed SPG can be separated from the complex using a cationic gel column (Bio–Rad; cat# 7324140).[1] In this method, SPG has no charge, while the complex has a negative charge due to DNA; therefore, the cationic gel absorbs only the complex, while the uncomplexed sSPG flows out as a column-through fraction.

Figure. 4-1-D compares the RI chromatograms for L-SPG/YB-1-AS and the uncomplexed SPG obtained using the cationic gel column (denoted as column-through). The uncomplexed SPG was present in the low-molecular weight region of 10.5 – 11.5 min, and the amount of uncomplexed SPG was approximately 7% of the total SPG. The [mG]/[dA] of L-SPG/YB-1-AS was determined in the range of the half-width (HW) of the main peak, as illustrated in the figure. The uncomplexed sSPG was present outside of the HW region, and thus, the obtained [mG]/[dA] did not count the uncomplexed sSPG. The obtained value of [mG]/[dA] was 3.7, which is much larger than that determined from the stoichiometry. This indicates that the L-SPG/YB-1-AS complex consists of both a dA/sSPG complex and renatured tSPG components, as shown

in Figure 1-2, leading to a large molecular weight and a broad molecular weight distribution. From the [mG]/[dA] value of L-SPG/YB-1-AS, almost half of the complex was made from renatured tSPG. To summarize the results in this section, the L-SPG/YB-1-AS mixture consisted of free uncomplexed sSPG and the L-SPG/YB-1-AS complex contained four to ten AS-ODNs and renatured tSPG. On the other hand, the q1-YB-1-AS solution contained only q1-YB-1-AS, and the complex did not have a renatured tSPG component.

4-3-2 Cellular uptake of Alexa546-labeled q1, q2, and q3/YB-1-AS complexes

To examine whether the quantized complexes can be recognized by Dectin-1, PC-9 and A549 cells were incubated with Alexa546-labeled complexes. Figure 4-2-A shows fluorescence microscopy images of PC-9 and A549 cells after 6 h of incubation. We observed red fluorescence derived from Alexa546 in PC-9 cells but not in A549 cells. We quantified the red areas and compared them, as shown in Figure 4-2-B. When we applied the complex with the coadministration of an excess amount of tSPG (20-fold more than the complex), the red fluorescence significantly decreased (Figure 4-2-C). These findings clearly show that the red area in Figure 4-2-A corresponds to the ingested (or cell-adsorbed) complexes. According to our previous study,[6] L-SPG/YB-1-AS can be taken up by PC-9 cells via Dectin-1, which was confirmed in the present study. Because A549 cells did not show any ingestion and the coadministration of tSPG dramatically decreased the ingestion of PC-9 cells, we can conclude that q1/q3-YB-1-AS are recognized by Dectin-1. There was no difference in fluorescence intensities, as shown in Figure 4-2-B; therefore, it can be assumed that all complexes have the same affinity for Dectin-1. These results indicate that quantized complexes can become a tool for delivering therapeutic ODNs to Dectin-1-expressing cells, similar to conventional SPG/DNA complexes.

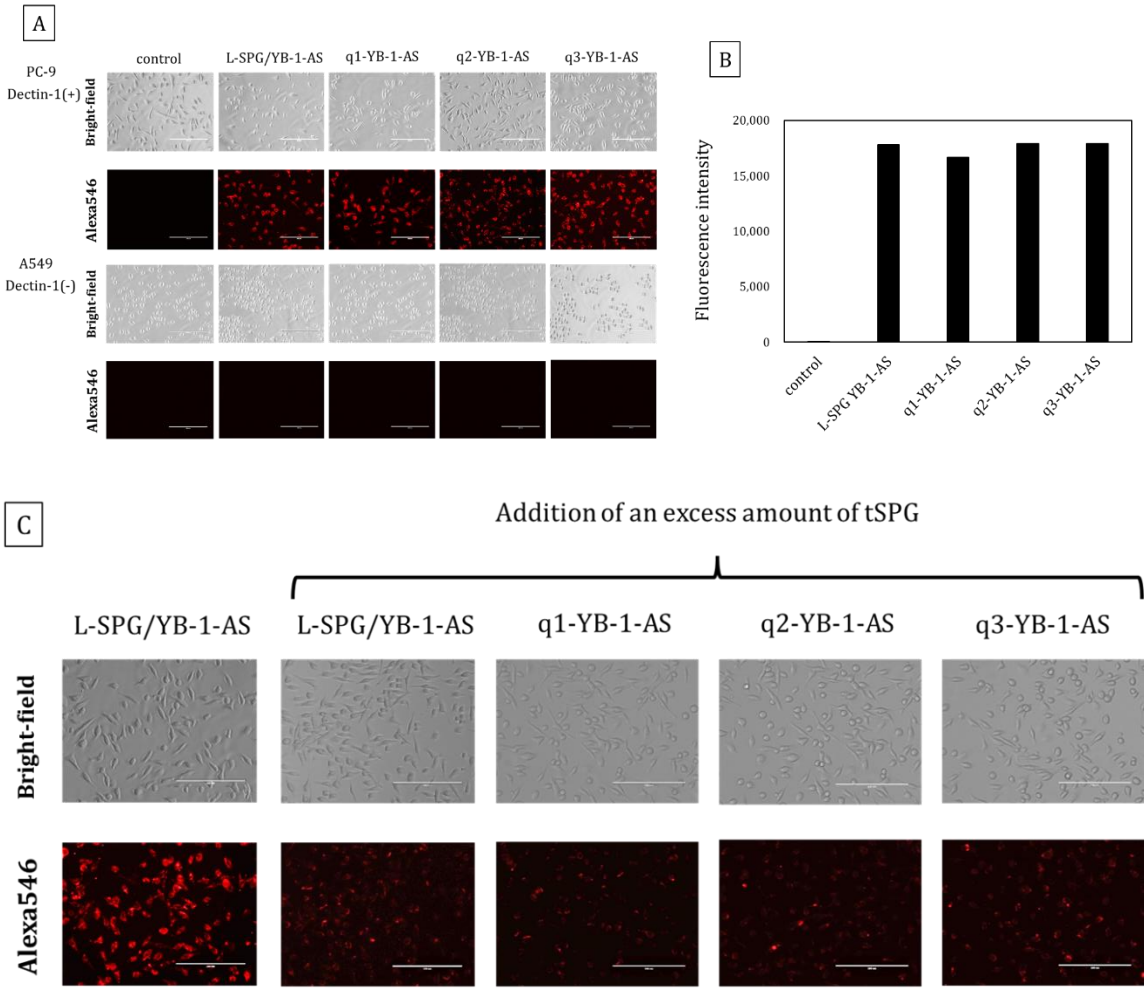

Figure 4-2. Cellular uptake of the SPG/YB-1-AS complex labeled with Alexa546 after 6 h of incubation. The scale bar represents 200 µm. A: Fluorescence microscopy images of PC-9 and A549 cells with the SPG/YB-1-AS complex labeled with Alexa546 (100 nM). B: Fluorescence intensity of Alexa546 in PC-9 cells. C: Complexes added to PC-9 cells with an excess amount of tSPG (2.0 µM).

4-3-3 In vitro anticancer efficacy of q1-YB-1-AS

Figure 4-4-A compares the Western blotting results of YB-1 expression after applying L-SPG/YB-1-AS, S-SPG/YB-1-AS, or q1-q3-YB-1-AS at the same AS-ODN dose in PC-9 (upper panel) and A549 (lower panel) cells. The level of q1-YB-AS protein expression in PC-9 cells reduced dramatically in the following order: q1-YB-1-AS > q2-YB-1-AS ≈ q3-YB-1-AS ≈ S-SPG/YB-1 > L-SPG/YB-1. On the other hand, A549 cells did not show an appreciable difference in any of the samples. The cell viabilities after administration of different doses were examined after 72 h of incubation (Figure 4-4-B). The results showed that q1 exhibited the most significant efficacy, and the cell viability reached less than 10% at the highest dose. All samples showed clear dose-dependent effects regarding the efficacy. The order of efficacy was as follows: q1-YB-1-AS >> q2-YB-1-AS ≈ q3-YB-1-AS > S-SPG/YB-1-AS ≈ L-SPG/YB-1-AS. This result is almost consistent with the Western blot results. 48 h after applying the complex, we imaged the cells (Figure 4-4-C). For L-SPG/YB-1-AS, the cells appeared normal, while they became almost spherical and showed a change in cell morphology after q1-YB-1-AS application. The present findings are consistent with previous results reporting that knockdown of the YB-1 gene caused apoptosis in cancer cells.[2-4] Cell viability and protein expression levels were examined for the SPG/K-ras-AS complex series after 72 h of incubation (Figure 4-3-A and B). The results shown in Figure 4-3 and 4-4 consistently indicate that the q1 complex most effectively inhibited protein expression and cell growth. The following explanations were proposed to explain the enhanced

efficacy: (1) the biodistribution of q1-YB-1-AS differs from that of L-SPG/YB-1-AS, with the former potentially rapidly entering the cytosol where the target mRNA is present, or (2) the structural difference between q1-YB-1-AS and L-SPG/YB-1-AS may increase the efficacy of the antisense sequence in q1-YB-1-AS.

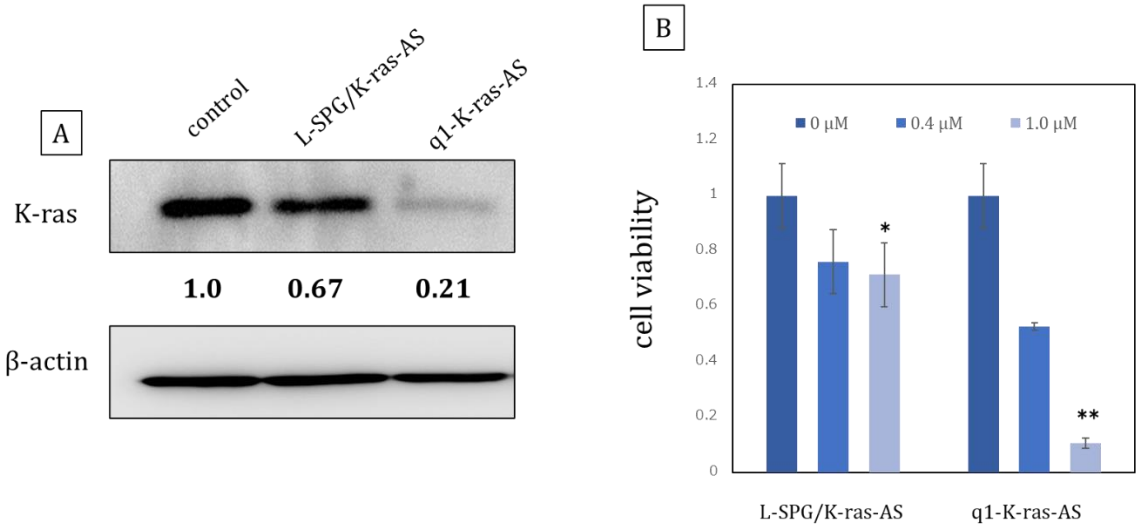

Figure 4-3. Anticancer efficacy of AS-ODNs other than YB-1-AS; K-ras-AS was used. A: The expression level of K-ras was determined by Western blotting. β-Actin was used as an internal control. B: Cell viability was determined 72 h after the addition of complexes. The results are presented as the mean ± S.D. (n = 3). *P < 0.05, **P < 0.01.

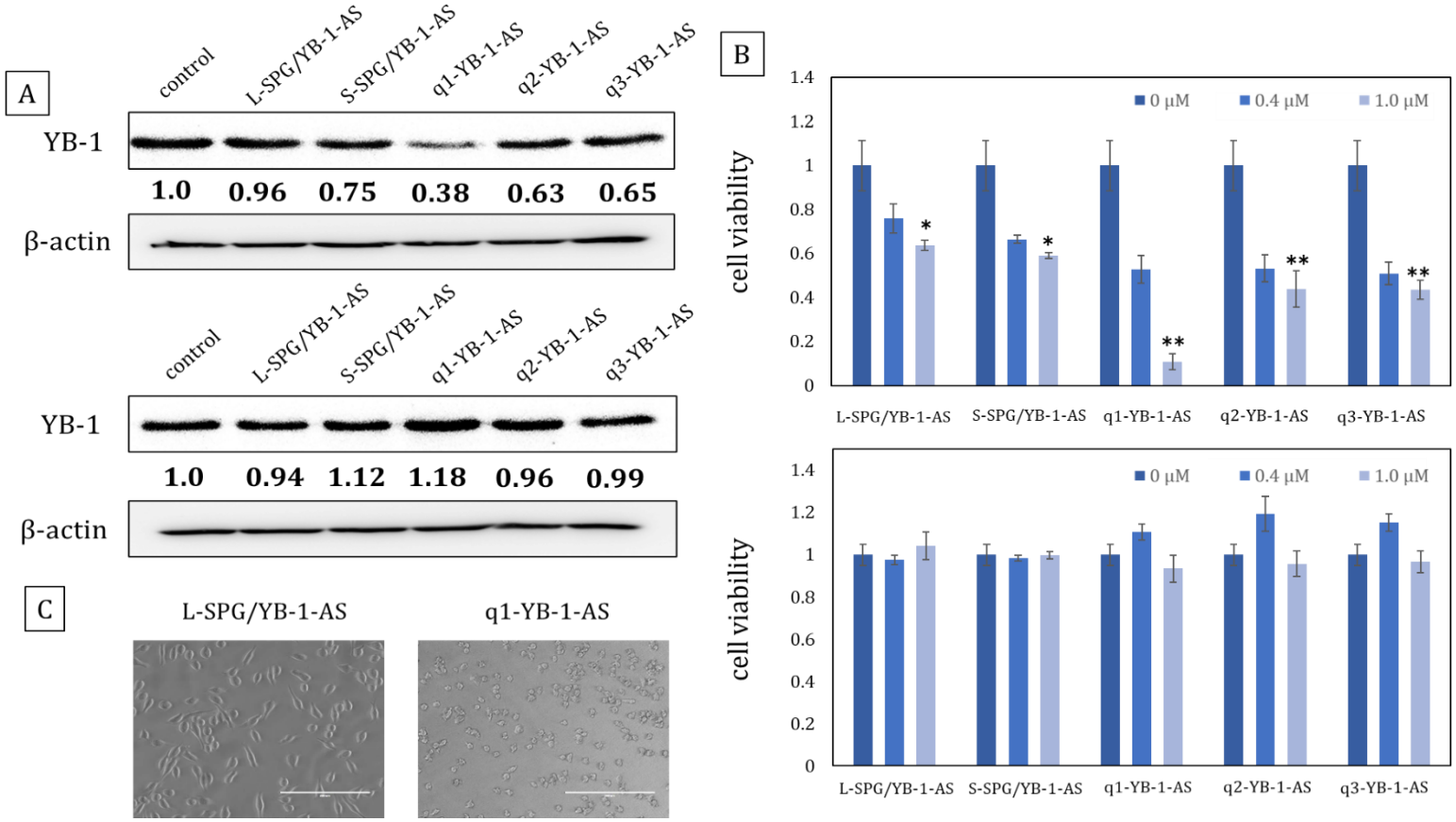

Figure 4-4. Comparison of anticancer efficacies between q1-YB-1-AS and L-SPG/YB-1-AS in vitro. A: Analysis of the expression level of the YB-1 protein by Western blotting. We used each complex at a concentration of 1.0 μM. β-Actin was used as an internal control. The expression level of the control (PBS treatment) is indicated as 1.0. B: PC-9 and A549 cells were treated with the complexes. After 72 h of incubation, cell viability was estimated. The cell viability at 0 μM (control) is indicated as 1.0. Results are presented as the mean ± S.D. (n = 3). *P < 0.05, **P < 0.01. C: Comparisons of cell morphology between q1-YB-1 and L-SPG/YB-1. PC-9 cells were treated with the complexes (1.0 μM), and after 48 h of incubation, images were obtained.

4-3-4 Immunostimulatory activity of q1-K3

There are two main types of CpG-ODNs: D and K-types.[5] D-types consist of one palindromic CpG motif with a phosphodiester (PO) backbone and phosphorothioated (PS) poly(G) tail and activate plasmacytoid DCs (pDCs) to produce IFN-α but cannot induce the maturation of pDCs or activate B cells.[7, 8] The D-types tend to form large aggregates due to intermolecular interactions associated with the G-quartet, while the K-types do not. Because of their larger size, the D-types are believed to remain in endosomes for longer than the K-types. Their longer stay in endosomes results in high IFN-a production.[8] On the other hand, K-types activate B cells to produce interleukin-6 (IL-6) and promote the maturation of pDCs. K-types cannot produce large amounts of IFN-α. [8, 9] The difference in the biological responses to D- and K-type CpG-ODNs may be due to the differences in biodistribution caused by their size differences, but not sequence differences. Kobiyama et al.[10] prepared the SPG complex with dA40-attached K3 by using L-SPG and found that this complex exhibited both K- and D-type properties, leading to IFN-α secretion and pDC maturation as well as IL-6 secretion. This dual response in L-SPG/K3 can also be ascribed to the differences in biodistribution caused by differences in size. Here, we investigated the IL-6 production associated with naked K3, L-SPG/K3, and q1-q3-K3 in a murine model (Figure 4-5). We confirmed the high production of IL-6 in L-SPG/K3 found in a previous study. Interestingly, q1-K3 and the other quantized complexes were inferior to L-SPG/K3 in terms of IL-6 production.

This experiment suggests that the biodistribution of the q1 complex may differ from that of the L-SPG complex.

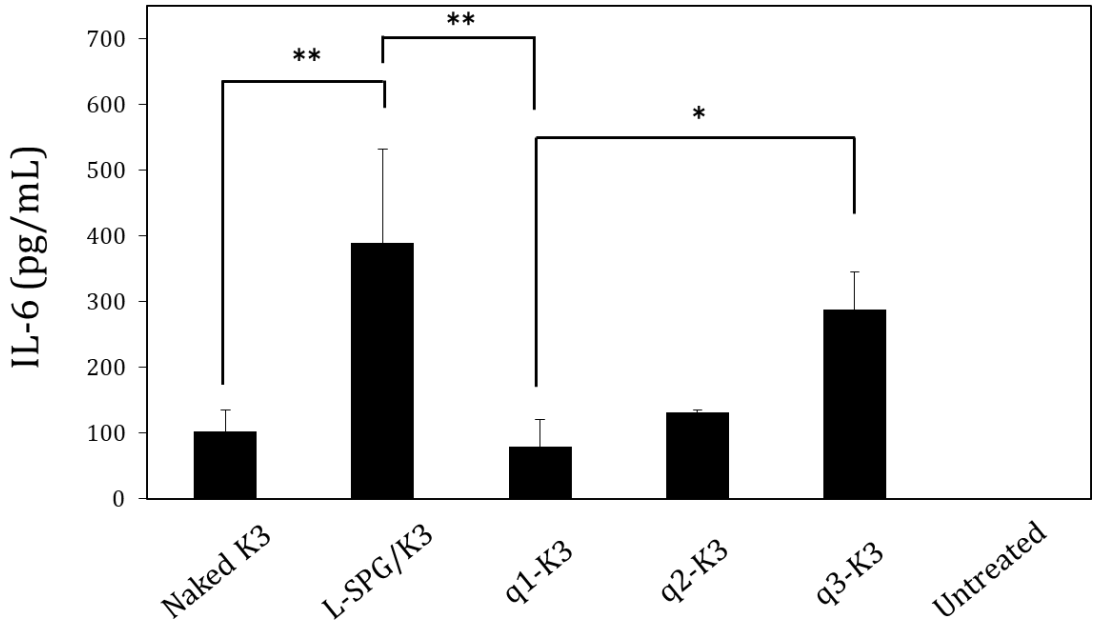

Figure 4-5. IL-6 release from mouse splenocytes by SPG/CpG complexes. All samples were added to splenocytes at a concentration of 20 nM. After 24 h of incubation, the presence of IL-6 in the culture media was measured by ELISA. *P < 0.05, **P < 0.01.

4-3-5 Intercellular distribution of YB-1-AS

The AS-ODN and CpG-ODN results suggest that the intracellular distribution of nucleic acid molecules differs between the q1 complex and the L-SPG complex. We compared the amount of YB-1-AS in the cytoplasm between the q1-YB-1-AS and L-SPG/YB-1-AS samples to confirm this hypothesis by using a combination of ligation and RT–PCR as illustrated in Figure 4-6-A. Figure 4-6-B shows the results, plotting the number of YB-1-AS as a function of the incubation time. This plot clearly shows that q1-YB-1-AS was associated with more YB-1-AS in the cytosol than L-SPG/YB-1-AS at all time points. YB-1-AS was detected after 30 min for both L-SPG/YB-1-AS and q1-YB-1-AS. The number of AS-ODNs in the cytosol peaked at 3 h and then gradually decreased to zero after 9 h for L-SPG/YB-1-AS, while the peak appeared at 1 h for q1-YB-1-AS and the number then remained constant at approximately 6.0×10^9. This plateau value was approximately three times higher than the maximum for L-SPG/YB-1-AS. Thus, it is clear that the intracellular biodistribution of YB-1-AS was completely different between the two complexes.

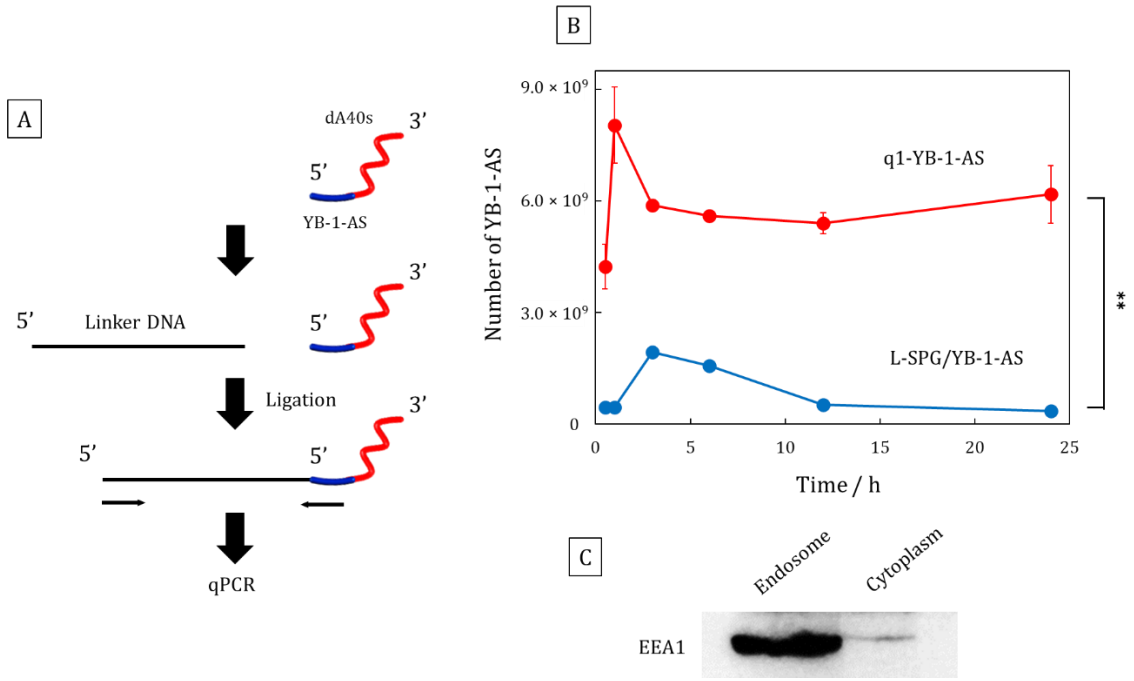

Figure 4-6. Intracellular distribution of L-SPG/YB-1-AS and q1-YB-1-AS A: Ligation reaction and qPCR were used to quantify the number of YB-1-AS. After isolating YB-1-AS, the linker DNA (for sequences, see the Supplementary Information) connected to the 5' end of the antisense sequence by a ligation reaction was amplified by qPCR. After amplification under the same conditions, the copy numbers of YB-1-AS were measured and plotted on the vertical axis in Panel B. B: Quantification of YB-1-AS in the cytosol. Red and blue represent q1-YB-1-AS and L-SPG/YB-1-AS, respectively. The results are presented as the mean ± S.D. (n = 2). **P < 0.01. C: Western blotting after separation of the endosomal and cytoplasmic fractions.

When we determined the number of YB-1-AS using the combination of ligation and qPCR, we separated the cell lysate into early endosomal and cytoplasmic fractions. We confirmed that the cytoplasmic components did not contain endosomes using the early endosomal marker EEA1,[11] as shown in Figure 30C. Therefore, the number of YB-1-AS determined for the endosomal and cytoplasmic fractions is quite reliable. In many previously papers, the intracellular distributions of AS-ODNs have been discussed based on results

obtained using fluorescence microscopy after the application of fluorescently labeled ODNs. In this method, there is no guarantee that the fluorescence marker is indeed attached to the DNA sequence. It is therefore possible that the observation is instead based on a marker-labeled fragment of DNA that has moved from the endosomes after the enzymatic degradation of DNA. It should thus be noted that the fluorescence does not necessarily reflect ODN localization.

4-3-6 Construction of a simultaneous delivery system for YB-1-AS and K-ras-AS using q1-complex.

As shown in Table 3-1, we synthesized three different ODNs with phosphothiolated dA40 at the center and different combinations of K-ras-AS and YB-1-AS at the 3' or 5' end. In this context, two complexes were prepared using KSY (K-ras-AS at the 5' end and YB-1-AS at the 3' end, and in Table 3-1 as K-ras-AS-YB-1.) with two sSPG samples of different molecular weights (molecular weight = 1.56×10^5 and 1.60×10^4). PAGE and GPC-MALS measurements were performed to determine if they formed a complex. Figure 4-7-A compares the gel electrophoresis patterns of Naked KSY, the q1 complex (q1-KSY), and the conventional complex (L-SPG/KSY). q1-KSY shows two bands corresponding to q1 and q2. L-SPG/KSY is composed of large molecular weight fractions L-SPG/KSY is composed of large molecular weight fractions, but contains small amounts of q1 and q2. Figure 4-7-B compares the gel permeation chromatograms of the three samples and shows that q1 is the major component of q1-KSY, while L-SPG/KSY is a mixture of various molecular weights. This result is the same as with dA60.

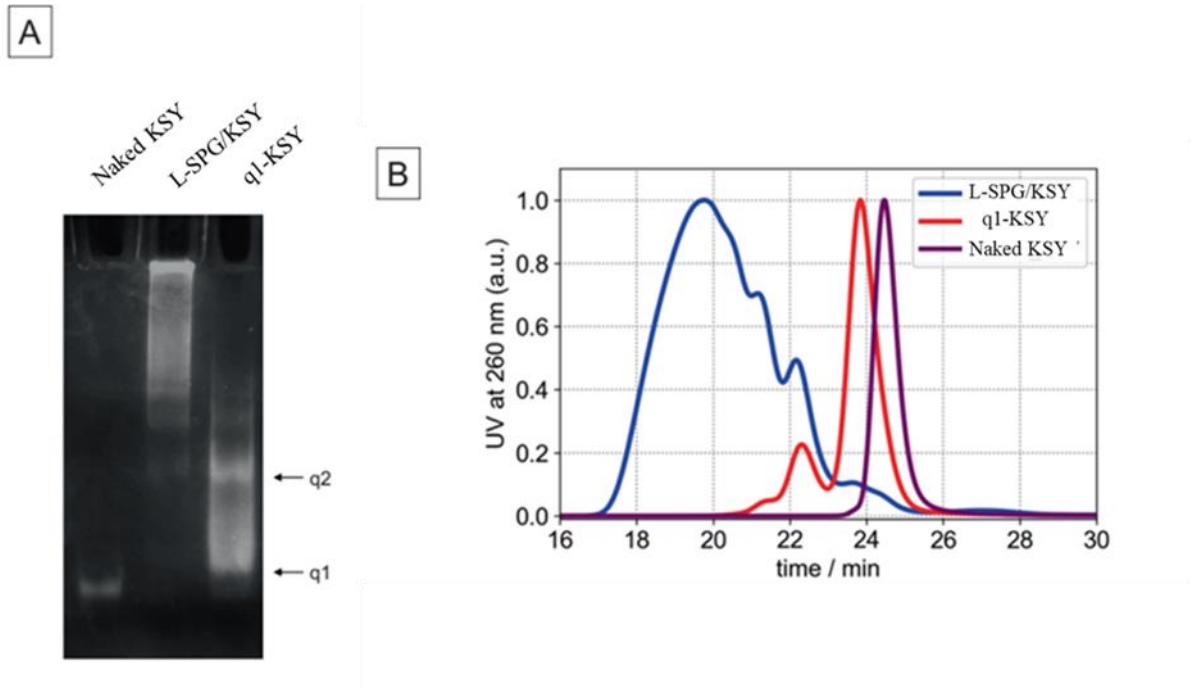

Figure 4-7. Complex formation of L-SPG/KSY and q1-KSY. A: Gel electrophoresis (using a 6.0% polyacrylamide gel) to show the presence of the q1 and q2 complexes. B: Comparison of the UV chromatograms between L-SPG/KSY and q1-KSY as well as Naked_KSY.

The following in vitro studies were performed to examine the pharmacological effects of these complexes. Figure 4-8 compares the inhibitory effects of L-SPG and q1 complexes on YB-1 and K-ras gene expression when applied to PC-9 cells. q1-SY showed 45% expression rate of YB-1 protein and L-SPG complex showed about 70%. K-ras expression rate was reduced to 30% with q1-KS. The silencing effect was better for the q1-complex than for the L-SPG complex, which is consistent with the previous results and supports that the q1-complex is more effective than the conventional complex. when AS-YB-1 and AS-K-ras were applied simultaneously, q1-KSY showed a significant decrease in YB-1 expression YB-1 when AS-YB-1 and AS-K-ras were applied simultaneously, q1-

KSY showed a similar effect to q1-SY with respect to YB-1 expression. It was also able to suppress the expression of K-ras. Notably, q1-KSY was more effective than the L-SPG complex for both YB-1 and K-ras expression. These results indicate that the q1-complex can be used to efficiently deliver two antisense nucleic acids into the cell.

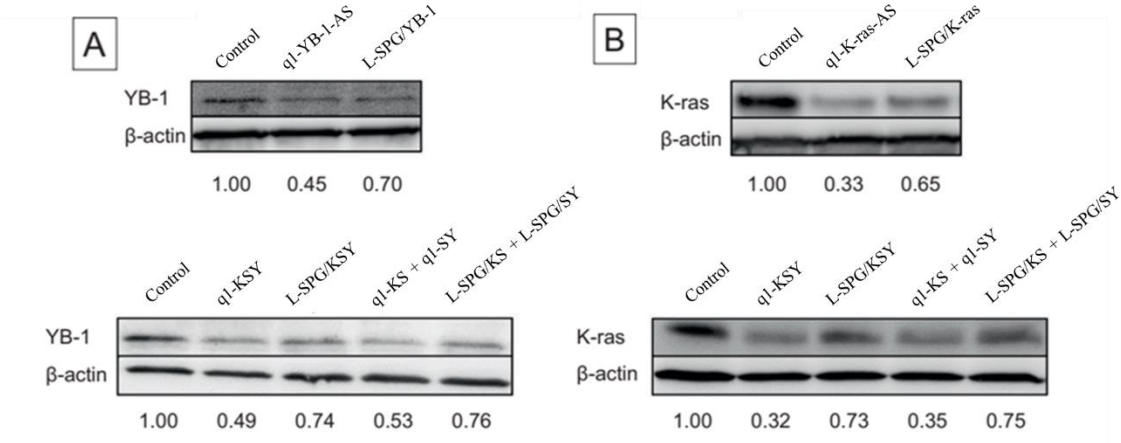

Figure 4-8. Comparison of anticancer efficacies of the L-SPG and q1 complexes made from three different ODNs. A,B: Western blot analysis was performed to determine the levels of YB-1 and K-ras after treatment with SPG/AS-ODN complexes. β-actin was used as an internal control. The expression level of control is indicated as 1.0.

4-4 Discussion

In this study, we compared the functions of the L-SPG complex and quantized complexes as carriers of therapeutic ODNs. The quantized complexes were recognized by Dectin-1 in almost the same manner as the L-SPG complex and taken up into cells. In addition, the gene silencing and immune response of the q1 complex were investigated. High gene silencing was achieved for q1-YB-1-AS and q1-K-ras-AS, while IL-6 secretion of q1-K3 was much lower than that of L-SPG/K3. Finally, we examined the subcellular distribution of YB-1-AS for the L-SPG complex and q1 complex. The results showed that the q1 complex could deliver more YB-1-AS molecules to the cytoplasm than the L-SPG complex.

Based on our obtained results, we assume that q1-YB-1-AS escapes from the endocytotic pathway in endosomes earlier than L-SPG complexes do, as schematically illustrated in Figure 4-9. After L-SPG/YB-1-AS is recognized by Dectin-1, it moves to the endosomes by endocytosis,[12] from which it does not appear to be able to transfer. Particular peptide sequences or cationic modifications are usually used to escape endosomes, but this complex does not have such modifications. However, as shown in Figure 4-9, the low-molecular weight complexes clearly escaped into the cytoplasm. Although we do not know the precise reason for this, we think that a small molecular size increases the diffusion coefficient and facilitates the transfer from endosomes to the cytoplasm. This causes the q1 complex to achieve high gene silencing for AS-

ODNs, which target mRNAs in the cytoplasm, while this is less effective for CpG-ODN, which targets TLR9 in endosomes.

Many carbohydrate receptors, including the asialoglycoprotein receptor for galactose and the hyaluronic receptor for endocytosis of hyaluronic acid, are known to be re-expressed on the cell surface by recycling.[13, 14] In general, the concentration of cellularly ingested substances in endosomes is determined by the balance between uptake and degradation in lysosomes. This role of the balance between uptake and degradation suggests that, for L-SPG/YB-1-AS, degradation is higher than uptake after 9 h. The decrease in uptake after 9 h may be due to decreased Dectin-1 recycling. The reason for the decrease in Dectin-1 is thought to be that the Dectin-1 used for uptake reaches the lysosomes with the complex, where it is degraded, resulting in no recycling. On the other hand, the quantized complexes escape from the endosomes before reaching the lysosomes. As a result, Dectin-1 does not reach the lysosomes and may be rapidly recycled to the cell surface. Therefore, the number of Dectin-1 molecules on the cell surface is always maintained at a high level, and the quantized complexes continue to be taken up even after 9 h. This can explain the behavior of YB-1-AS after 9 h, as shown in Figure 4-9. However, this explanation remains speculative, and further studies are necessary to understand the precise mechanism of uptake of the quantized complexes and its high efficacy.

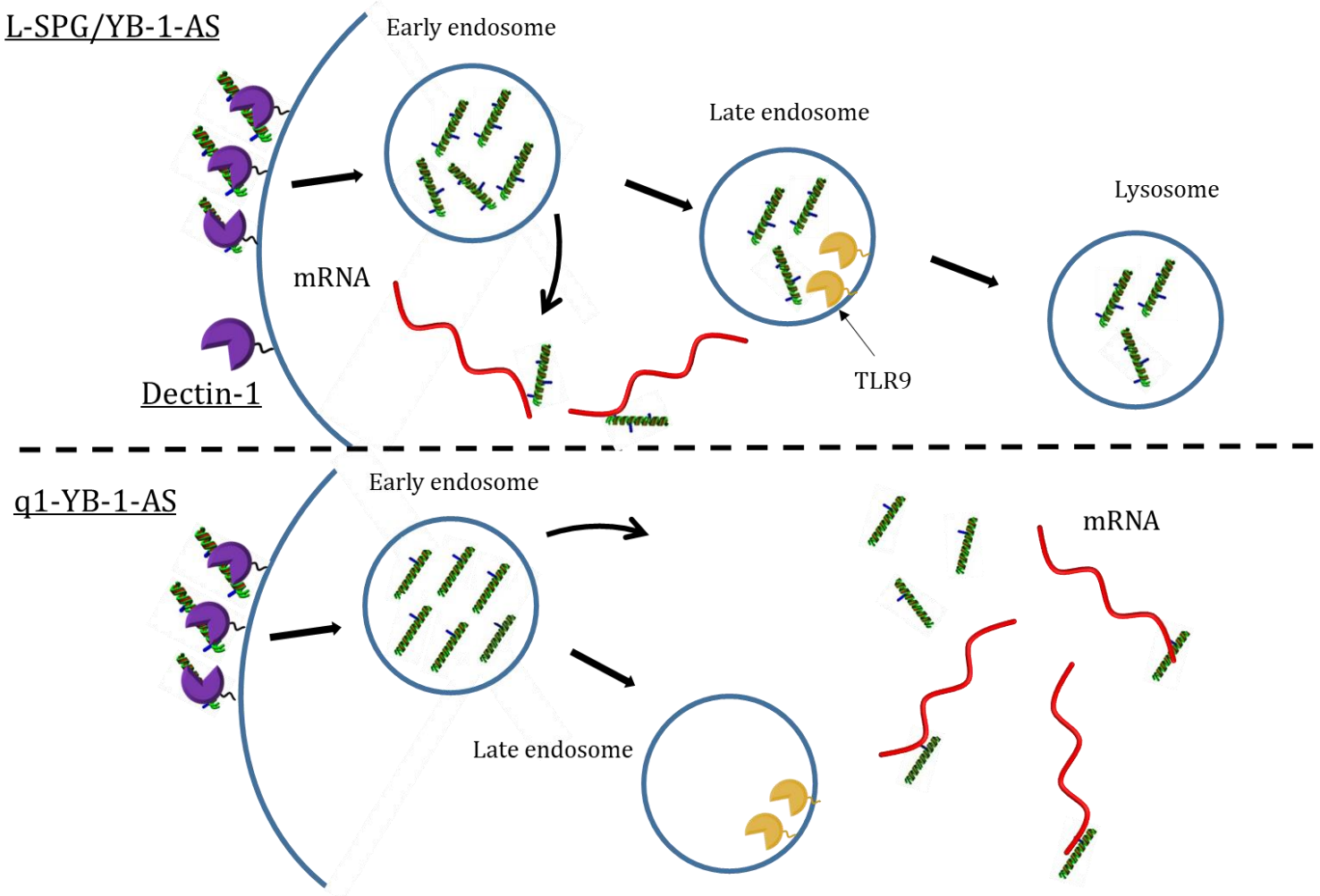

Figure 4-9. A proposed model for endosomal escape to explain why the q1 complex was more effective for AS-ODN but less effective for CpG-ODN. SPG/YB-1-AS complexes are internalized via Dectin-1-mediated endocytosis and carried to endosomes. L-SPG/YB-1-AS is large, impeding its escape from endosomes. In contrast, q1-YB-1-AS can easily escape from endosomes due to its small size.

4-5 Conclusion

Quantized complexes were found to have completely different physical properties from the conventional L-SPG complexes. These differences include the monodisperse vs. polydisperse nature and the absence of denatured tSPG in the quantized complexes while accounting for almost half of the L-SPG complexes. Despite thier large differences, both complexes can be taken up into cells by human Dectin-1. In terms of the antisense efficacy, q1-YB-1-AS and q1-K-ras-AS outperformed the conventional L-SPG complexes. In contrast, q1-K3 was inferior to L-SPG/K3 in this regard because of their different biodistributions. These results can be due to the rapid endosomal escape due to the small size of the q1 complex. These findings suggest that the q1 complex can be a new carrier for AS-ODN delivery to cells expressing Dectin-1, and q1 may also be more effective than the L-SPG complex in vivo.

4-6 Reference

1. Sanada, Y.; Matsuzaki, T.; Mochizuki, S.; Okobira, T.; Uezu, K.; Sakurai, K., β-1,3-D-glucan schizophyllan/poly(dA) triple-helical complex in dilute solution. *J Phys Chem B* **2012,** *116* (1), 87-94.

2. Basaki, Y.; Taguchi, K.-i.; Izumi, H.; Murakami, Y.; Kubo, T.; Hosoi, F.; Watari, K.; Nakano, K.; Kawaguchi, H.; Ohno, S.; Kohno, K.; Ono, M.; Kuwano, M., Y-box binding protein-1 (YB-1) promotes cell cycle progression through CDC6-dependent pathway in human cancer cells. *European Journal of Cancer* **2010,** *46* (5), 954-965.

3. Kohno, K.; Izumi, H.; Uchiumi, T.; Ashizuka, M.; Kuwano, M., The pleiotropic functions of the Y-box-binding protein, YB-1. *Bioessays* **2003,** *25* (7), 691-8.

4. Kuwano, M.; Oda, Y.; Izumi, H.; Yang, S. J.; Uchiumi, T.; Iwamoto, Y.; Toi, M.; Fujii, T.; Yamana, H.; Kinoshita, H.; Kamura, T.; Tsuneyoshi, M.; Yasumoto, K.; Kohno, K., The role of nuclear Y-box binding protein 1 as a global marker in drug resistance. *Mol Cancer Ther* **2004,** *3* (11), 1485-92.

5. Vollmer, J.; Krieg, A. M., Immunotherapeutic applications of CpG oligodeoxynucleotide TLR9 agonists. *Adv Drug Deliv Rev* **2009,** *61* (3), 195-204.

6. Izumi, H.; Nagao, S.; Mochizuki, S.; Fujiwara, N.; Sakurai, K.; Morimoto, Y., Optimal sequence of antisense DNA to silence YB-1 in lung cancer by use of a novel polysaccharide drug delivery system. *Int J Oncol* **2016,** *48* (6), 2472-2478.

7. Krug, A.; Rothenfusser, S.; Hornung, V.; Jahrsdörfer, B.; Blackwell, S.; Ballas, Z. K.; Endres, S.; Krieg, A. M.; Hartmann, G., Identification of CpG oligonucleotide sequences with high induction of IFN-alpha/beta in plasmacytoid dendritic cells. *Eur J Immunol* **2001,** *31* (7), 2154-63.

8. Verthelyi, D.; Ishii, K. J.; Gursel, M.; Takeshita, F.; Klinman, D. M., Human peripheral blood cells differentially recognize and respond to two distinct CPG motifs. *J Immunol* **2001,** *166* (4), 2372-7.

9. Hartmann, G.; Krieg, A. M., Mechanism and function of a newly identified CpG DNA motif in human primary B cells. *J Immunol* **2000,** *164* (2), 944-53.

10. Kobiyama, K.; Aoshi, T.; Narita, H.; Kuroda, E.; Hayashi, M.; Tetsutani, K.; Koyama, S.; Mochizuki, S.; Sakurai, K.; Katakai, Y.; Yasutomi, Y.; Saijo, S.; Iwakura, Y.; Akira, S.; Coban, C.; Ishii, K. J., Nonagonistic Dectin-1 ligand transforms CpG into a multitask nanoparticulate TLR9 agonist. *Proc Natl Acad Sci U S A* **2014,** *111* (8), 3086-91.

11. Stenmark, H.; Aasland, R.; Toh, B. H.; D'Arrigo, A., Endosomal localization of the autoantigen EEA1 is mediated by a zinc-binding FYVE finger. *J Biol Chem* **1996,** *271* (39), 24048-54.

12. Fujiwara, N.; Izumi, H.; Morimoto, Y.; Sakurai, K.; Mochizuki, S., Complex consisting of antisense DNA and β-glucan promotes internalization into cell through Dectin-1 and hybridizes with target mRNA in cytosol. *Cancer Gene Ther* **2019,** *26* (1-2), 32-40.

13. Ashwell, G.; Harford, J., Carbohydrate-specific receptors of the liver. *Annu Rev Biochem* **1982,** *51*, 531-54.

14. Raja, R. H.; McGary, C. T.; Weigel, P. H., Affinity and distribution of surface and intracellular hyaluronic acid receptors in isolated rat liver endothelial cells. *J Biol Chem* **1988,** *263* (32), 16661-8.

CHAPTER 5. SUMMARY

In this thesis, the structure and pharmacological effects of the complex in solution were investigated for the creation of the SPG/DNA complex-based drug delivery carrier specific for Dectin-1-expressing cells and its clinical application in humans.

The first chapter describes the status and challenges of modern drug development. Advances in technology, increasing digital information, and global communication are transforming society, requiring the pharmaceutical industry to respond rapidly to new diseases and improve treatments. Data science and AI are changing drug development, but challenges remain, such as disparities in access and high development costs. Small molecule drugs act on specific targets and offer new options for cancer treatment, for example, but managing the risk of side effects and the lack of effective treatments for specific diseases are challenges. Nucleic acid drugs are based on RNA or DNA and have the potential to push the boundaries of conventional therapies, but also present unique challenges such as cell membrane barriers and biological instability. DDS technologies are being developed to address these issues. He stated that this field involves multidimensional challenges and requires in-depth research from basic research to clinical trials.

In Chapter 2, the importance of research in DDS technology is based on the fact that the structure of nanoparticles (especially shape and size) significantly

affects the distribution of the drug in the body and its behavior in the cell. Evidence to date indicates that the physical properties of nanoparticles significantly affect the efficiency and efficacy of DDS. Therefore, in order to optimize the pharmacological effects of the SPG/DNA complexes and realize their full potential, it is essential to understand the exact structure of these complexes. To achieve this goal, we attempted to elucidate the structure of polysaccharide-nucleic acid complexes in solution using light scattering. As a result, we revealed the existence of a new type of complex without molecular weight distribution, which is different from conventional complexes.

Chapter 3 is to show that SPG/DNA complexes can function as an effective drug delivery system using human-derived dectin-1. Previous studies have shown that these complexes can target mouse-derived dectin-1 to carry drugs, but studies on human-derived dectin-1 are scarce. For pharmaceutical applications, it is essential to study the behavior of complexes that target human dectin-1. Therefore, the study focused specifically on evaluating the affinity of human dectin-1 for polysaccharide-nucleic acid complexes. The results showed that the complex showed affinity for human Dectin-1 as well as mouse Dectin-1. This indicates that the drug delivery technology by the complex may be applicable to humans.

In Chapter 4, the goal is to determine whether the complexes can be used to deliver nucleic acid drugs to cells expressing human dectin-1. Another goal is to

verify whether the small molecular weight complexes newly identified in Chapter 2 have properties different from those of conventional ones and whether they have pharmacological effects. Specifically, we attempted to determine whether these complexes can specifically target Dectin-1-expressing cells and effectively deliver the drug by in vitro testing. The results showed that while conventional complexes could deliver drugs specifically to Dectin-1-expressing cells, the newly discovered small molecule complexes were more efficient in delivering drugs into the cells. This has the potential to lead to the development of new DDSs that are more selective and faster-acting in terms of nucleic acid drug delivery.

Through this study, we have suggested that SPG/DNA complexes provide an effective drug delivery mechanism that targets specific cellular receptors and that this is a promising approach for future therapeutic drug development. Furthermore, the discovery of small molecular weight complexes represents a new direction in nucleic acid drug delivery and will encourage further research in this area.

Acknowledgments

The research embodied in this dissertation was meticulously conducted at the Sakurai Laboratory, a division of the Department of Chemistry and Biochemistry, University of Kitakyushu. This scholarly endeavor was a part of my doctoral course from 2018 to 2024. It is with the deepest appreciation that I extend my sincere thanks to Professor Kazuo Sakurai for his unparalleled guidance and wisdom during this time. Additionally, in the field of biotechnology-related research, our objectives were achieved under the distinguished tutelage of Associate Professor Hiroto Izumi and Professor Yoshiyuki Adachi. I am also indebted to my fellow laboratory members - Shogo Sasaki, Yuki Hata, Takuya Matsunaga, and Motoko Tanaka - for their substantial support and collaboration. The experimental procedures were conducted using the sophisticated equipment available at the Department of Department of Occupational Pneumology, Institute of Industrial Ecological Sciences at the University of Occupational and Environmental Health and the Measurement and Analysis Center at The University of Kitakyushu. The SAXS measurements also were performed at SPring-8 BL40B2.

In addition, this thesis was proofread with the help of Chat GPT and the grammar correction feature of DeepL.

March 2024

Kazuki Sumiya

List of Publications

This thesis has been published in the following papers.

1. Sumiya K, Matsunaga T, Tanaka M, Mochizuki S, Sakurai K. Oligo-DNA Stoichiometrically Binds β-1,3-Glucan with the Best Fit Length. *Biomacromolecules*.2020;21(12):4823-4834. Copyright (2020) American Chemical Society

2. Sumiya K, Izumi H, Mochizuki S, Sakurai K. Enhanced in-vitro efficacy of antisense delivery by use of low-molecular weight polysaccharide/DNA complex. *Chem Lett*. 2021; 50:1191–3.

3. Sumiya, K., Izumi, H., Matsunaga, T. et al. Delivery of therapeutic oligonucleotides targeting Dectin-1 using quantized complexes. *Polym J* 54, 591–601 (2022).

4. Hata, Y., Sumiya, K., Izumi, H. et al. Antisense DNA cocktail therapy using short ß-1,3-glucan/oligonucleotide complexes. *Polym J* 55, 283–288 (2023).

5. Sumiya K, Izumi H, Adachi Y, Mochizuki S, Sakurai K. Binding assay of human Dectin-1 variants for DNA/ β-glucan complex for active-targeting delivery of antisense DNA: Part II. *Carbohydr Res*. 2023;523:108731.